Investigation of Supercritical Water Processing of Biomass: Study of High Pressure Separation

---

A Dissertation Presented to

The Faculty of the Graduate School at

The University of Missouri-Columbia

In Partial Fulfillment of the Requirements for the Degree

Doctor of Philosophy

---

by

Reza Espanani

Prof. William A. Jacoby, Dissertation Supervisor

May, 2016

The undersigned, appointed by the dean of the Graduate School, have examined the dissertation entitled

Investigation of Supercritical Water Process of Biomass: Study of High Pressure Separation

Presented by Reza Espanani

A candidate for the degree of Doctor of Philosophy,
and hereby certify that, in their opinion, it is worthy of acceptance.

_____

Professor William Jacoby, Bioengineering - Joint Appointment in Chemical Engineering

_____

Professor James Lee, Bioengineering

_____

Professor Shramik Sengupta, Bioengineering

_____

Professor Paul Chan, Chemical Engineering

DEDICATION

I would like to dedicate this dissertation to my wife, Dr. Atri Ariapad, and my son, Ryan, for their encouragement. They have had to put up with long days of research, and for that I am most grateful. They are my pillars of strength and my biggest supporters.

ACKNOWLEDGEMENTS

I would like to thank my advisor, Dr. William Jacoby, for his expert guidance and continuous encouragement throughout the course of this study and in preparation of the thesis. I would like to acknowledge the encouragement, advice and support of Dr. James Lee, Dr. Shramik Sengupta, and Dr. Paul Chan as members of the advisory committee.

I would also like to thank Mr. Gordon Ellison of the Agricultural Engineering machine shop. Without his skills at manufacturing our equipment, I would not be able to perform any of this research. I would also like to thank Mr. Lakdas Fernando for his assistance with sample analysis using the GC in his lab. I wish to thank Ms. Linda Little and Ms. Stacy Osterthun for their helps and supports.

I would like to thank my colleagues and fellow graduate students Andrew Miller, Nikolas Wilkinson, Malithi Wickramathilaka, Doug Hendry, Allen Busick and Di Zhu for their help during experimental planning and execution.

Most of all, I would like to thank my family, my parents and parents-in-law for their support and encouragement throughout my doctoral studies.

TABLE OF CONTENTS

LIST OF FIGURES

LIST OF TABLES

LIST OF ABBREVIATIONS AND SYMBOLS

Most of these abbreviations are defined in the text, but provided here for quick reference.

Abbreviation	Meaning
AADP	Average Absolute Deviation of pressure
AADy	Average Absolute Deviation of vapor phase mole fraction
BPR	Back-Pressure Regulator
CEOS	Cubic Equation Of State
CRC	Carbon Recycling Center
EOS	Equation Of State
HDS	High-pressure, Density-driven Separator
HEPS	High-pressure Equilibrium Phase Separator
HRSG	Heat Recovery Steam Generation
HV	Huron-Vidal
IPCC	International Panel on Climate Change
LHV	Low Heat Value
MHV	Modified Huron-Vidal
NOAA	National Oceanic and Atmospheric Administration
NRF	Non-Random Factor
NRTL	Non-Random Two Liquid
OF	objective function
PDU	Process Development Unit
PR	Peng-Robinson
PRSV	Peng-Robinson-Stryjek-Vera
PSA	Pressure-Swing Adsorption
PVT	Pressure-Volume-Temperature
SCW	Supercritical Water

SCWG	Supercritical Water Gasification
SCWO	Supercritical Water Oxidation
SRK	Soave-Redlich-Kwong
TSA	Thermal-Swing Adsorption
VdW	Van der Waals
VLE	Vapor-Liquid Equilibrium/Equilibria
VLLE	Vapor-Liquid-Liquid Equilibrium/Equilibria
WS	Wong-Sandler

Symbol	**Meaning**
a	activity, molecular attraction parameter
A	Helmholtz free energy
Ar	Archimedes number
b	volume parameter
C_P	heat capacity at constant pressure
C_V	heat capacity at constant volume
D	diffusion coefficient
Es	Espanani number
f	fugacity
g	acceleration of gravity
G	Gibbs free energy
G^{ex}	excess Gibbs energy
Gr	Grashof number
H	enthalpy, Hessian matrix
ig	ideal gas
k_{ij}	interaction parameter

K_W	dissociation constant
L	length of the inlet tube
m	number of components
$\dot{m}$	mass flow rate
mix	mixture
n	number of moles
NP	number of experimental points
n_t	total mole
P	pressure
P_B	bubble point pressure
P_C	critical pressure
Q	volumetric flow rate, heat transfer rate
R	gas constant
Re	Reynolds number
s	molar entropy
S	total entropy, separation efficiency
sat	saturation
T	temperature
T_C	critical temperature
U	total internal energy, velocity
V	total volume
v	molar volume
W	work
x, y	mole fraction
Z	compressibility factor
°	standard state

ρ	density
μ	dynamic viscosity
ϕ	fugacity coefficient
μ_i	chemical potential
π	number of phases
γ	activity coefficient
ω	acentric factor
α	non-randomness factor, step length
∇f	gradient vector
σ	standard deviation

ABSTRACT

This dissertation includes two sections. In the first section, a thermodynamic model is presented for vapor-liquid equilibrium calculation of low boiling point components. In the second section, separation of N_2/CO_2 mixture is investigated by a high-pressure, density-driven separator.

Vapor-liquid equilibrium (VLE) of low boiling point components occurs at low-temperature and usually at high pressure. A proper method for computing the fugacity coefficient is to use a cubic equation of state with mixing rules. However, empirical mixing rules include one adjustable parameter and cannot predict VLE of some mixtures accurately. An alternative that could be used for non-ideal mixtures is the Wong-Sandler mixing rule, which is derived based on the excess Gibbs free energy (G^{ex}). In this research, VLE of light gaseous mixtures was calculated at low temperatures and medium to high pressures using the Peng-Robinson equation of state (PR EOS), the Wong-Sandler mixing rule, and the nonrandom two-liquid (NRTL) equation as a G^{ex} model. This introduces an additional adjustable parameter. Assuming the adjustable parameters as a function of temperature, the results show that this thermodynamic model is an appropriate method to predict VLE of low boiling point materials at wide range of temperatures.

A mixture of 85% nitrogen and 15% carbon dioxide (N_2/CO_2) is separable at ambient temperature on a continuous basis. A high-pressure, density-driven separator (HDS) was designed and fabricated to explore the process. The effect of the fluid variables, including pressure and mixture flow rate, was assessed on a separation efficiency metric. An important design parameter, the length of the HDS, was also evaluated in the experimental design. Essentially perfect separation is observed over a wide-range of conditions. Separation efficiency is correlated with two dimensionless

groups. The first is the Archimedes number. It is a ratio of buoyant force to viscous force. The second dimensionless group is defined in this work. The Espanani number is the ratio of the pressure force to the viscous force. Excellent correlation between separation efficiency and the product of the Archimedes number and the Espanani number is observed. This observation informs both process and equipment design.

CHAPTER ONE

1

Introduction

1.1. Biomass

Since the Industrial Revolution in the seventeenth century and the invention of the steam turbine, fossil fuels (oil, natural gas and coal) have been the most important energy resources of human societies for more than two centuries. However, limited fossil energy sources, climate change and environmental problems, as well as fluctuations in energy prices are new challenges; so the governments have been forced to move from fossil energy sources to renewable and sustainable energy sources [1.1]. Figure 1.1 shows the renewable energy consumption in the United States since 2000. It seems that biomass energy consumption is continually increased after 2002 and produces most of sustainable energy.

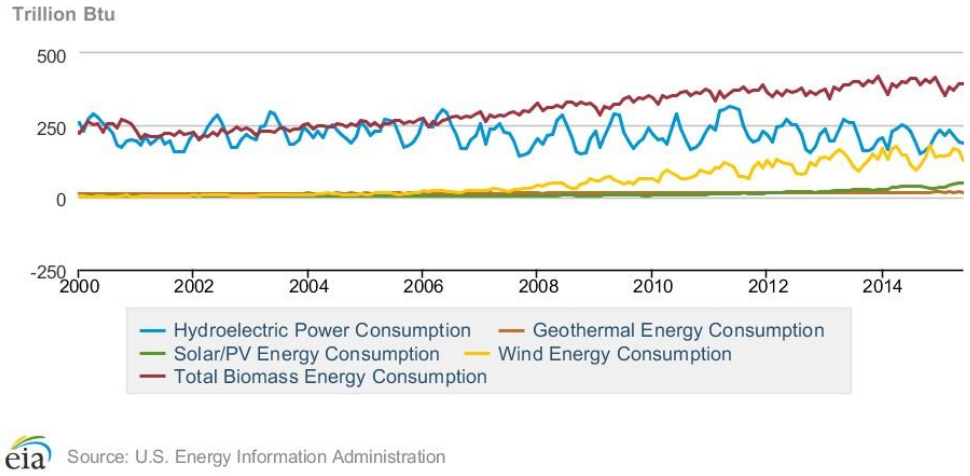

Figure 1.1. U.S. renewable energy consumption by source [1.2].

Biomass is a stored source of solar energy. Plants collect solar energy by the process of photosynthesis. During the photosynthesis, carbon dioxide is captured and converted to plant materials mainly in the form of cellulose, hemi-cellulose and lignin (figure 1.2).

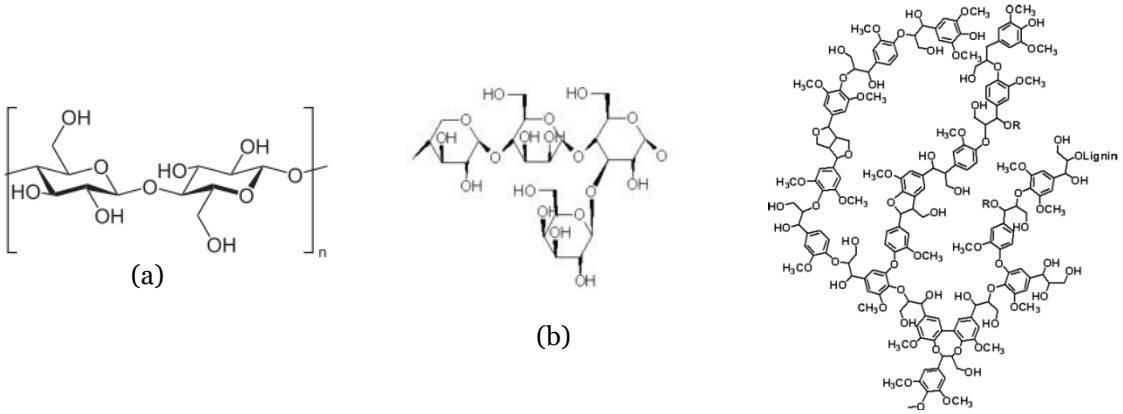

Figure 1.2. Plant materials: (a) cellulose; (b) hemi-cellulose; (c) lignin.

Biomass includes crop residues, forest and wood process residues, animal wastes including human sewage, municipal solid waste, food processing wastes, purpose grown energy crops and short rotation forests [1.1]. It is estimated that the amount of carbon in biomass produced in the world is 104.9 billion ton per year [1.3]. The advantages of biomass energy are [1.1]:

- Biomass is renewable, abundant and can be produced everywhere.
- Biomass energy can be converted to useful thermal energy, electricity and fuels for power.
- Biomass production is labor intensive, so it increases rural employment in developing countries.

There are different chemical processes for energy production using biomass. They can be divided to two main groups [1.4]: (a) thermo-chemical conversion, and (b) Bio-

chemical/biological conversion. Thermo-chemical conversion includes three different processes as described the following:

Combustion: The burning of biomass in air is a process that converts the chemical energy stored in biomass to heat. The temperature range of output gases produced by traditional combustion of biomass is about 800–1000 °C. Combustion is an exothermic process.

Gasification: Conventional gasification is a chemical process that converts biomass into a combustible gas mixture, such as carbon monoxide and hydrogen, by the partial oxidation of biomass at high temperatures (800–900 °C). The gaseous mixture can be consumed as a fuel in gas turbines [1.5]. Gasification is an endothermic process.

Pyrolysis: Pyrolysis takes place when in the absence of air, the biomass is converted to solid, liquid, and gaseous products at around 500 °C [1.5]. Pyrolysis is an endothermic process.

Recently, a new technology which uses supercritical water (SCW) is developing for oxidation and gasification of biomass. In supercritical water, oxygen is infinitely miscible and organic materials become soluble. Therefore, a homogeneous mixture reduces the mass transport limitations that results a low residence time and high efficiency of the reaction [1.6].

1.2. Supercritical water

Figures 1.3 and 1.4 show the diagrams of PVT of pure water. Figure 1.3 illustrates that the volume of liquid water and vapor at pressure of 221 bar (22.1 MPa) and temperature of 374 °C are the same. In thermodynamics, this point is called the critical point of water and placed at the end of the vapor-liquid equilibrium curve (figure 1.4).

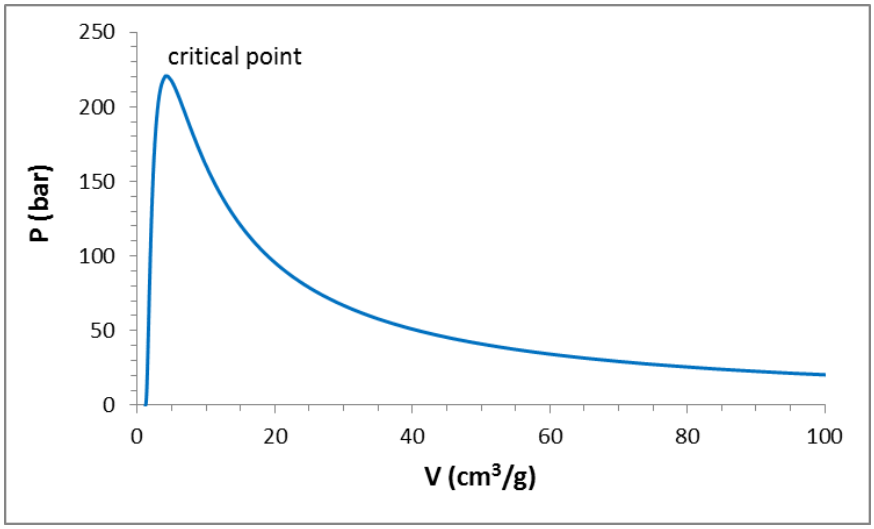

Figure 1.3. The diagram of pressure vs volume for water.

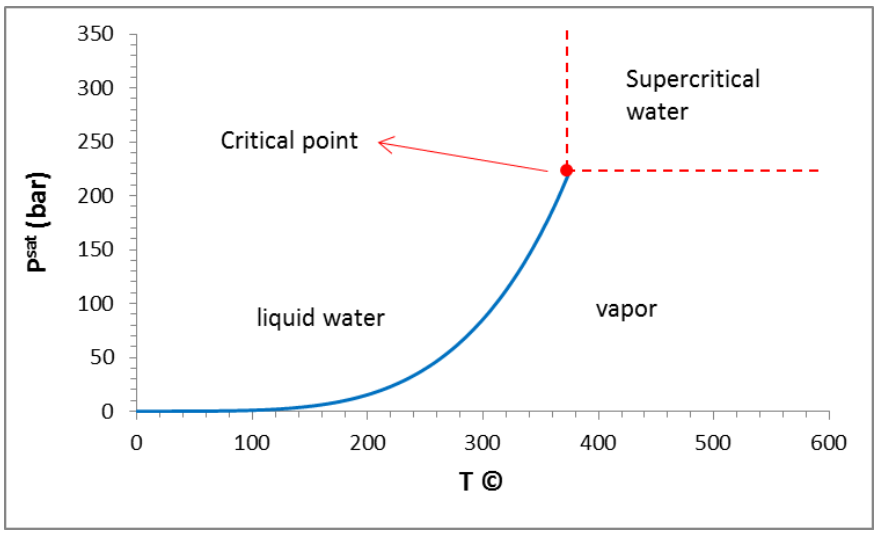

Figure 1.4. The diagram of water vapor pressure at different temperature.

At the critical point, phase boundaries vanish and only one phase exists. So, the heat of vaporization will be zero. Water above its critical point (P>221 bar and T>374 °C) is called supercritical water where distinct liquid and gas phases do not exist. The thermodynamic properties of supercritical water have been compared with liquid and vapor states in table 1.1 which is intermediate between gaseous and liquid states [1.7]. Figure 1.5 demonstrates the changes of some properties of pure water against temperature [1.8].

Table 1.1. Thermophysical properties of pure water at different states [1.7].

Property	Liquid	Supercritical	Gas
T (°C)	25	400	150
P (MPa)	10	30	0.1
ρ (kg/m^3)	999	353	0.52
μ (Pa.s)	90×10^{-5}	4.5×10^{-5}	1×10^{-5}
D (m^2/s)	$\approx1\times10^{-9}$	$\approx1\times10^{-8}$	$\approx1\times10^{-5}$

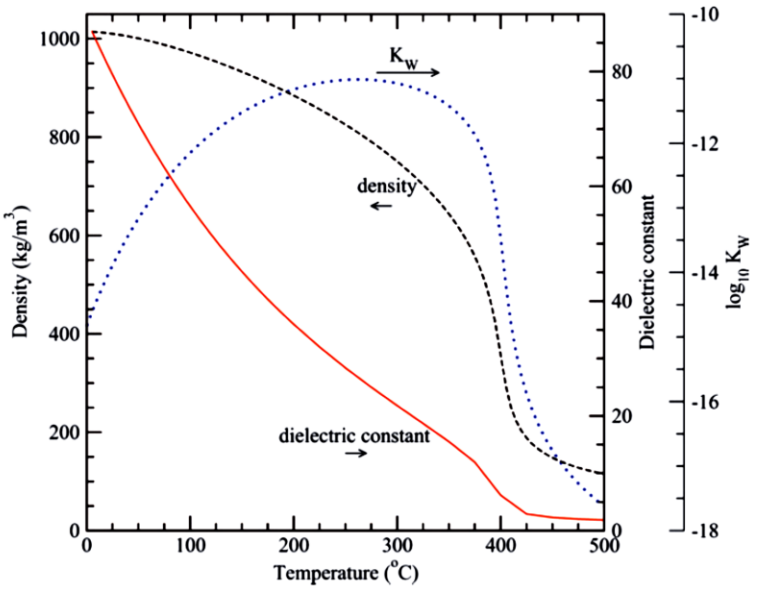

Figure 1.5. Diagram of density, static dielectric constant and ion dissociation constant (K_W) of water vs temperature at 30 MPa [1.8].

When temperature of water rises, the hydrogen bonds of water are weakened. Thus, the structure and properties of water change dramatically. Liquid water has a high dielectric constant (78.5) at 25 °C and is able to dissolve polar compounds very well. However, water is a poor solvent for nonpolar materials such as hydrocarbons. Compared to liquid water, supercritical water has a very low dielectric constant (1.2 at 24 MPa and 500 °C). Consequently, it can dissolve nonpolar compounds; while it is a poor solvent for salts. For instance, the solubility of benzene in water is very low (0.07 wt% at ambient temperature). But it is soluble in supercritical water in all proportions [1.7].

The density of supercritical water can change continuously from high (liquid-like) to low (gas-like) when the temperature and pressure are changed. According to figure 1.5, the density of supercritical water is 0.3 g/cm^3 and can be easily decreased to 0.1 g/cm^3 by increasing the temperature or by decreasing the pressure near the critical temperature [1.7].

When temperature is increased, the viscosity of water is reduced. At 25 °C, liquid water has a viscosity of 0.001 Pa.s, while the viscosity of supercritical water is very low, for example 3.06×10^{-5} Pa.s at 500 °C and 250 bar. So, supercritical water is a very good medium for very fast reactions due to high diffusion coefficient resulted by low viscosity [1.7].

1.3. Supercritical water gasification of biomass

Supercritical water gasification (SCWG) is a novel technique for generating syngas. This reaction takes place in the absence of oxygen. In SCWG process, the main reactions are [1.9]:

$$[C, H, O, N] + H_2O \rightarrow CO + H_2 + H_2O + NH_3 + N_2 \quad (1\text{-}1)$$

$$CO + H_2O \rightarrow CO_2 + H_2 \quad (1\text{-}2)$$

$$CO + 3H_2 \rightarrow CH_4 + H_2O \quad (1\text{-}3)$$

where [C, H, O, N] is biomass consisting of carbon, hydrogen, oxygen, and nitrogen atoms. The final gaseous product from SCWG includes fuel gas which is a mixture of H_2, CH_4. The product composition and the yields of gas, liquid, and char highly depend on the experimental conditions. The main factors are the feed composition, the water content, the reaction temperature, the heating rate, and the final temperature [1.7]. The advantages of SCWG process are [1.9]:

- Wet waste biomass can be rapidly converted to a fuel gas mixture containing hydrogen and methane.
- The drying of waste biomass with a high moisture content is not necessary.
- Environmentally friendly water is used as the gasification reagent.
- Water itself decomposes to hydrogen and the hydrogen yield is increased.

1.4. Supercritical water oxidation of biomass

Supercritical water oxidation (SCWO) is defined as the oxidation of organic pollutants with an oxidizing agent (oxygen, air, hydrogen peroxide . . .) in a homogeneous supercritical medium [1.10]. SCWO of biomass is an exothermic reaction as below:

$$[C, H, O, N] + O_2 \rightarrow CO_2 + H_2O + NH_3 + N_2 \quad (1\text{-}4)$$

where [C, H, O, N] is biomass. The products of oxidation using SCW are harmless compounds such as carbon dioxide, water, nitrogen, and/or ammonia. SCWO process

can also be used for the treatment of many kinds of wastes with high moisture contents [1.9]. In addition, this process converts nitrogen compounds in waste biomass to nitrogen (or ammonia) without producing any toxic NO_x [1.11]. The reason is that oxidation in SCW has fast kinetics and occurs at lower temperature compared to conventional combustion and able to destroy more than 99% of the organic compounds in a few minutes or less [1.10]. So, this technology is considered an environmentally friendly technique without toxic products.

1.5. Process Development Unit for SCWO of biomass

At the Carbon Recycling Center (CRC), we have designed and developed a Process Development Unit (PDU) for SCWO process [1.6]. The PDU has been utilized for oxidation of sludge and animal wastes, as well as propanol, motor oil and food waste in the recent experiments. Figure 1.6 shows a schematic of the PDU.

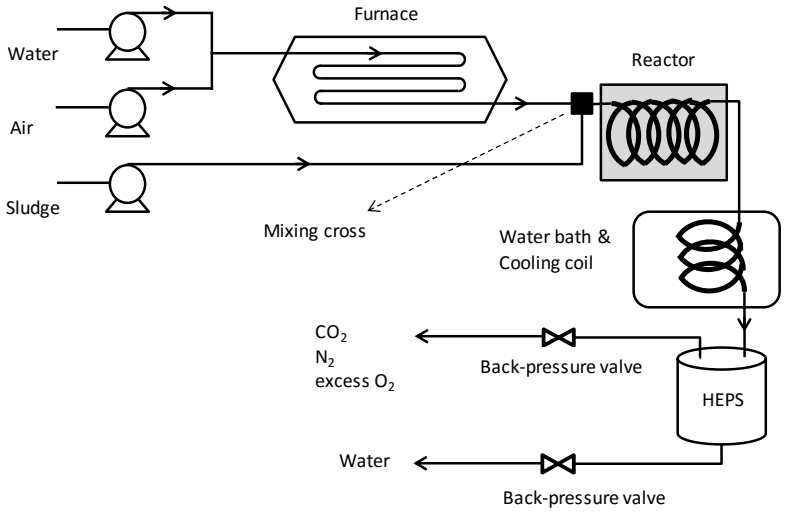

Figure 1.6. Schematic of the PDU [1.6].

The fabricated apparatus consists of a tubular reactor built from 305 cm of stainless steel 316 and covered with fiberglass insulation in order to minimize heat loss. Operation of the PDU at steady-state is briefly described as the following:

The compressed air (equal to, or in excess of, the amount required for full oxidation) and water are pumped to the furnace for preheating at pressure of 24.1-28.9 MPa. When temperature of the mixture reaches to 500-600 °C in the mixing cross (mixture of SCW and air), the simulant stream is entered to the mixing cross at ambient temperature. Consequently, temperature of the mixture in the mixing cross will be 400-475 °C, indicating that the entire mixture is supercritical. Then, the mixture is delivered to the reactor starting the operation at SCWO conditions. Downstream of the reactor, the gaseous products are cooled to ambient temperature at process pressure using a water/ice bath; therefore, vapor is condensed. Subsequently, a High-pressure Equilibrium Phase Separator (HEPS) separates liquid water from other gases (mixture of CO_2, N_2 and non-reacted O_2).

Investigation of upstream of the PDU and effective parameters on SCWO process have been reported in reference [1.6]. Here, we will focused on downstream of the process for separation of gas mixture in this dissertation.

1.6. Importance of separation of CO_2 from flue gas

Global warming threatens the environment and humanity in the 21st century. Figure 1.7 illustrates temperature anomalies based on data from the National Oceanic and Atmospheric Administration (NOAA). Global temperature has been above the average temperature of the 20th century continually for past 35 years. In 2014, anomaly

has reached 0.74 °C. The trend reveals that global temperature will rise 2 °C relative to the 20th century average by the end of this century [1.12].

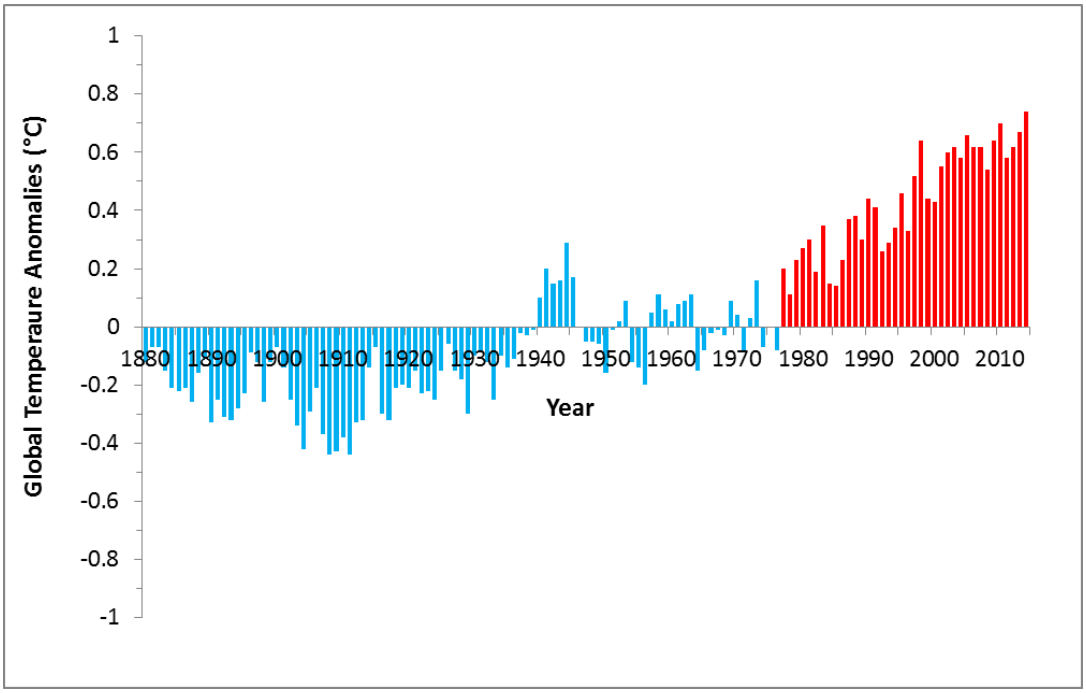

Figure 1.7. Annual global anomalies from 1880 to 2014 [1.12].

Global warming is caused by greenhouse gases such as CO_2, CH_4, NO_x, and SO_x. CO_2 makes up about 80% (by mass) of greenhouse gas emitted by human activities [1.13]. Therefore, CO_2 emission plays a significant role in global warming. CO_2 concentration in the atmosphere has increased from 280 ppm at the beginning of the industrial revolution, to 380 ppm today [1.14]. The International Panel on Climate Change (IPCC) predicts it will reach 570 ppm by the end of the century [1.15].

Combustion of coal, oil, and natural gas emits CO_2. Therefore, separation of CO_2 from flue gas is an important tool to limit global warming. SCWO presents unique opportunities for high-pressure CO_2 separation.

1.7. Outline of the dissertation

In *chapter 2*, we will review separation methods for gas mixture, especially separation of CO_2. Then, for thermodynamic modeling, we focus on mixing rules based on excess free energy.

Chapter 3 is about thermodynamic principles of phase equilibria, especially vapor-liquid equilibrium (VLE).

In *chapter 4*, thermodynamic modeling of VLE for low boiling point gases will be carried out using ϕ-ϕ approach and PR-WS-NRTL model.

Chapter 5 provides experimental method for separation of N_2/CO_2 mixture at high pressure and ambient temperature and effective parameters of separation.

In *chapter 6*, we will present a concept for energy recovery from outlet high-pressure gases.

CHAPTER TWO

2

Literature Review

2.1. Gas separation techniques

Conventional separations of CO_2 in flue gas are based on the molecular, thermodynamic and transport properties of gaseous components in the mixture. The main separation processes include [2.1]:

- Chemical reaction
- Absorption
- Adsorption
- Permeation through a membrane
- Gas hydrate formation
- Phase creation (by heat transfer, shaft work or throttling)

2.1.1. Chemical reaction

If methane is added to the flue gas, its reaction with CO_2 produces syngas (a mixture of H_2 and CO). Thus CO_2 is consumed, but both reactants (CO_2 and CH_4) are thermodynamically stable. The reaction needs a catalyst with considerable activation energy [2.2].

2.1.2. Absorption

Amine-based absorption removes acid gases from the flue gas. Figure 2.1 illustrates a diagram of a typical absorption process for the separation of CO_2 and other acid gases from natural gas using amine-solvent. In this process, the flue gas contacts aqueous solutions of molecules such as monoethanolamine or diethanolamine. The amine functional group takes part in a reversible reaction with CO_2 to form a carbamate. The sorbent is regenerated from the saturated solution by heating and releasing CO_2. Ammonia and alkali salt carbonates can be also used as the solvent in chemical absorption technology. Wide deployment of the technology has not occurred due to high solvent circulation rate, energy intensive regeneration, and corrosion [2.1, 2.3-2.5].

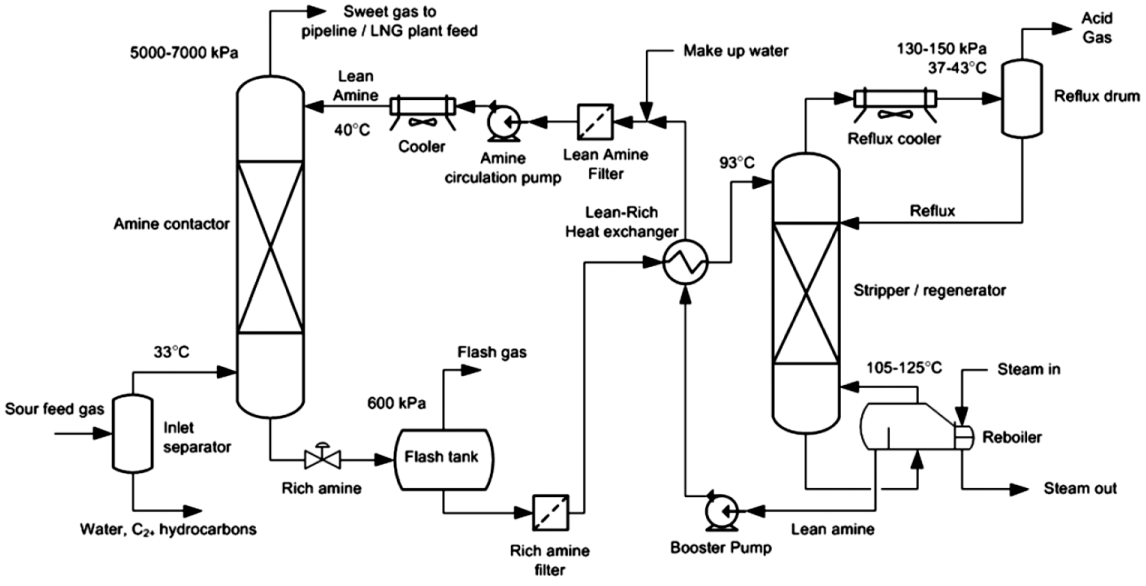

Figure 2.1. Schematic of a typical chemical absorption process using amine-solvent [2.6, 2.7].

Figure 2.2 shows a schematic of a typical physical absorption system. When the CO_2 partial pressure in a gaseous mixture is greater than 10 bar, a solvent such as methanol and dimethylether polyethylene glycol may be used for physical absorption of CO_2 [2.8].

Depressurizing the solvent-rich stream regenerates the pure sorbent; therefore the physical absorption technology requires less energy for regeneration than the chemical absorption process. However, a high solvent circulation rate is required because of low absorption of CO_2 by the solvent [2.1].

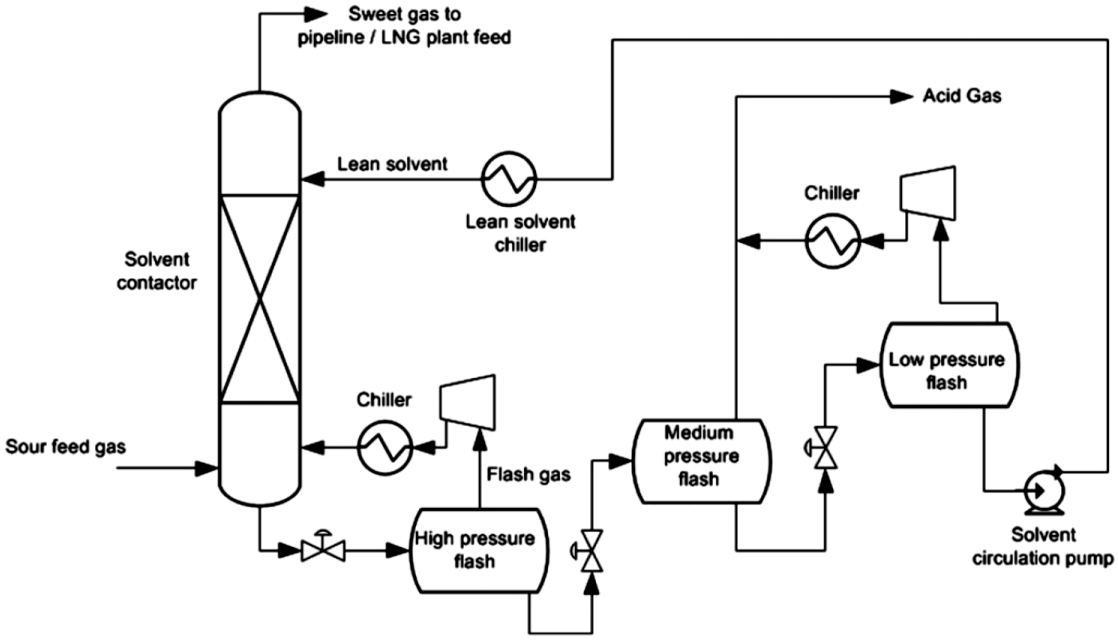

Figure 2.2. Schematic of a typical physical absorption system [2.1].

2.1.3. Adsorption

Carbon dioxide can be adsorbed on porous solid adsorbents such as zeolite, activated carbon, and molecular sieve. Regeneration is driven by temperature changes in thermal-swing adsorption (TSA), or pressure changes in pressure-swing adsorption (PSA) [2.1]. This process is shown in figure 2.3. In practice, the limited adsorption

capacity of available adsorbents leads to large bed size, which effects the rate of and energy required for thermal- or pressure-swing regeneration [2.1, 2.5, 2.9].

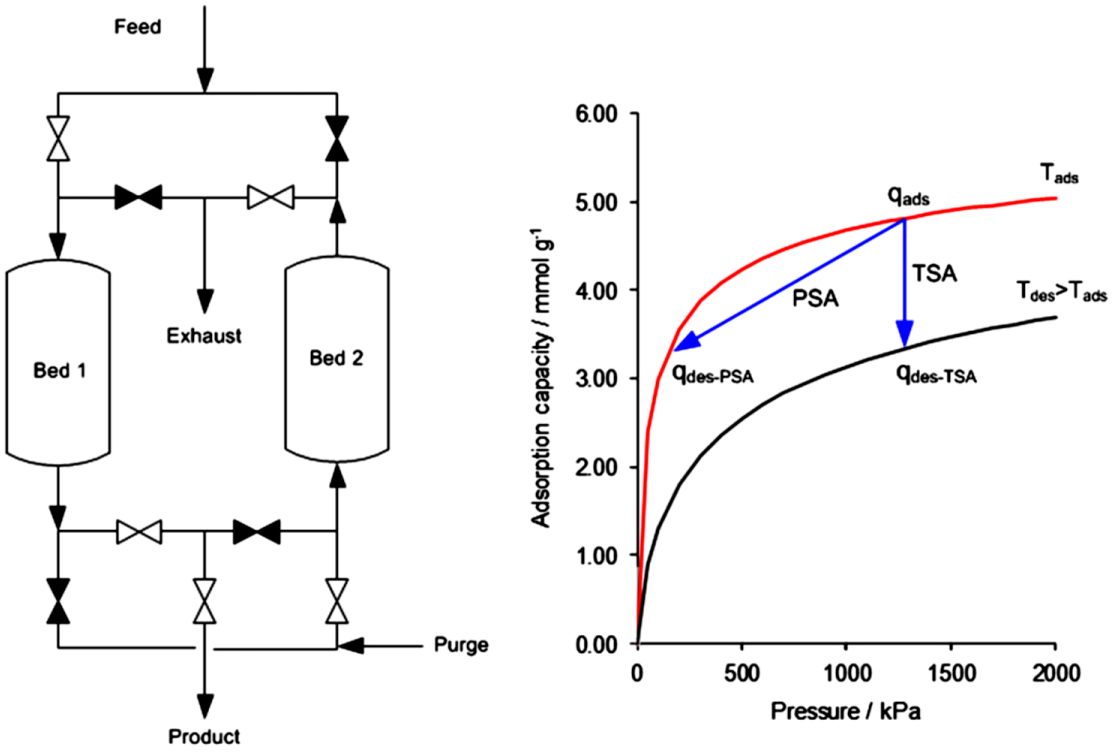

Figure 2.3. Diagram of a two-bed cyclic adsorption system with PSA and TSA cycles shown on isotherms for CO_2 adsorption on a carbon molecular sieve Takeda MSC 3K-171 [2.10].

2.1.4. Permeation through a membrane

Separation of gaseous mixtures using membrane technology is also under development (Figure 2.4). The mechanism of membrane separation is a partial pressure gradient (driving force) between the feed and the permeate sides. Polymeric, inorganic

and mixed matrix membranes are used. Advantages include lack of phase change, no solvent requirements, and low thermal energy requirements. However, utility is limited by low removal rates of CO_2, insufficient purity of permeate, and large membrane area requirements [2.1, 2.9, 2.11].

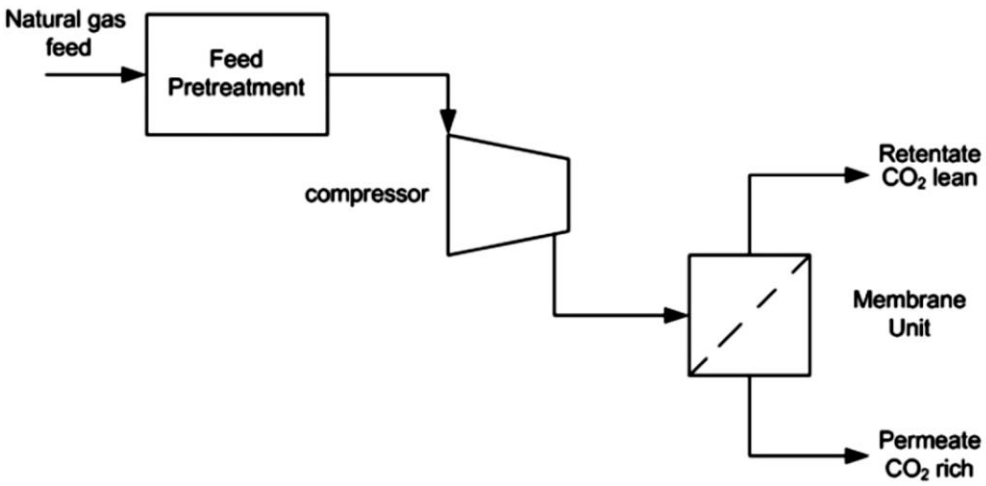

Figure 2.4. Separation of CO_2 from natural gas using a single-stage membrane [2.1].

2.1.5. Gas hydrate formation

Gas hydrates are formed by hydrogen-bonded water molecules at specific pressures and temperatures. They are non-stoichiometric crystalline compounds that create cages to trap small molecules such as CO_2 or CH_4 (figure 2.5). High storage capacity and selectivity are the most important advantages of gas hydrates. However, the high energy requirements and process precision required for gas hydrate formation remain barriers to commercial implementation [2.1, 2.12-2.14].

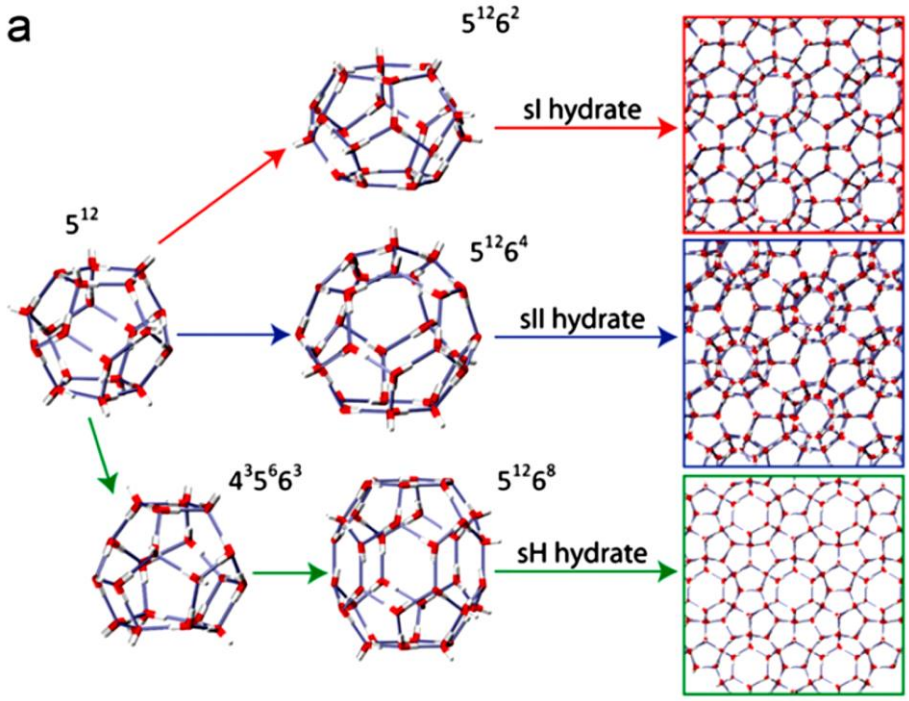

Figure 2.5. Basic hydrate cage structures [2.15].

2.1.6. Phase creation

This method consists of the partial vaporization or partial condensation of components with different volatility from a feed mixture. If the volatility differences among components of the mixture are large, just one stage is enough for separation of components. However, for mixtures such as N_2-CH_4 which the volatility differences are not sufficiently large, a distillation process involving multiple vapor-liquid contact stages maybe required [2.1]. Figure 2.6 shows the McCabe-Thiele diagram for calculation of the number of ideal equilibrium stages for separation of N_2-CH_4 mixture. Using the VLE data, the relative volatility is 7 at 2757 kPa [2.1].

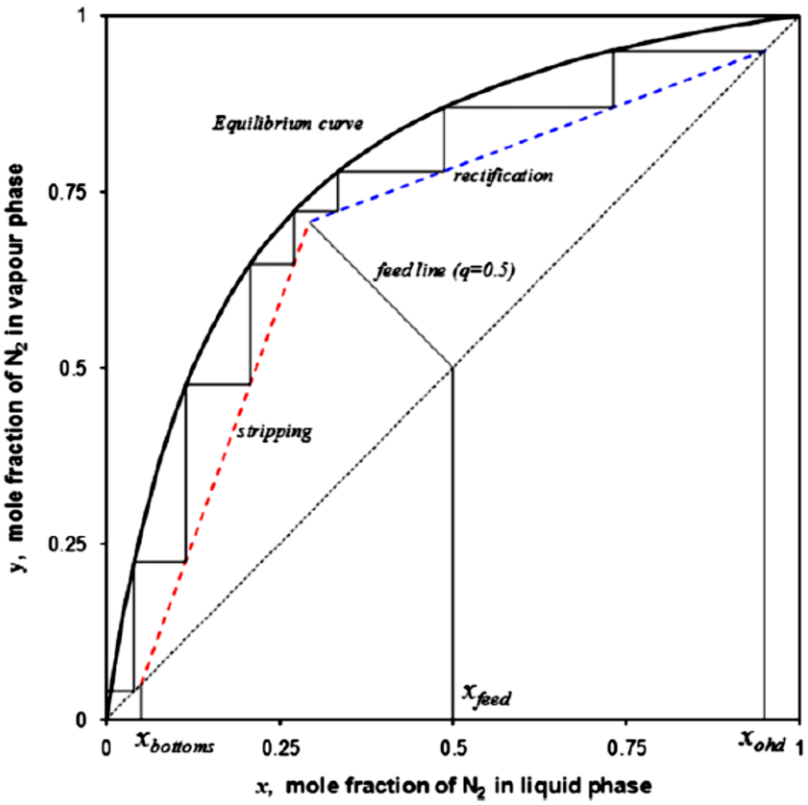

Figure 2.6. McCabe-Thiele diagram for N_2-CH_4 mixture [2.1].

2.2. Vapor-liquid equilibria of low boiling point gaseous mixture

The study of vapor-liquid equilibria of low boiling point gaseous mixture are applied to many chemical processes such as the oil and gas industries including gas-transfer pipelines under high pressure and gas separation processes. Recently, due to the role of greenhouse gases in increasing global temperature, there has been a growing interest to develop technologies for the separation of flue gases produced by combustion. In addition, supercritical water gasification of biomass or steam reforming of organic materials produces mixtures of syngas, methane and carbon dioxide [2.16, 2.17]. Therefore, the accurate thermodynamic models of the VLE of mixtures such as (CH_4 + CO_2) are important for processes designed to separate CO_2 from the mixture.

2.2.1. Van der Waals mixing rule

The use of a cubic equation of state (CEOS) requires a mixing rule to obtain the parameters of a mixture for a VLE calculation. The Van der Waals (VdW) mixing rule is an example and will be explained in chapter 3. It has one adjustable parameter. Computational results can be found in reference [2.18] for many systems using the Soave-Redlich-Kwong (SRK) and Peng-Robinson (PR) EOSs.

2.2.2. Mixing rules based on excess free energy

Other methods for VLE calculations involve mixing rules based on excess free energy. These include Huron-Vidal (HV) [2.19, 2.20], modified Huron-Vidal (MHV1 and MHV2) [2.21-2.23], and Wong-Sandler (WS) [2.24, 2.25]. These methods are able to predict VLE of mixtures more accurately than the VdW mixing rule. In recent years, researchers have paid much attention to the WS mixing rule because of its accuracy for phase equilibrium prediction of non-ideal and strongly non-ideal mixtures [2.26-2.48].

In the WS mixing rule, the excess Helmholtz free energy at infinite pressure is approximated by the excess Gibbs free energy at zero pressure. The literatures suggest different G^{ex} models according to physical properties of mixtures. Orbey *et al.* [2.26] used the NRTL and van Laar for phase equilibrium calculation of CO_2 in water, alcohols and n-alkanes mixtures. They compared the results of the WS, MHV2 and Orbey-Sandler mixing rules for these systems. Alvarado and Sandler [2.27] show that the excess enthalpies of highly non-ideal mixtures can be predicted using the WS mixing rule and the NRTL and UNIQUAC models at low and high pressures. Salinas *et al.* [2.28] calculated the viscosity of liquid polar binary mixtures using the Eyring's theory and the WS mixing rule, and van Laar model. Haghtalab and Espanani [2.29] modified the

NRTL-NRF model based on the volume fraction and computed the VLE of polymer solutions using the WS mixing rule. Ohta *et al.* [2.30] compared the results of liquid-liquid equilibria of ternary systems such as (water + methanol + alkyl ether) and (water + alcohol + 1,1-difluoroethane) using the WS mixing rule and MHV1. They also considered the NRTL and UNIQUAC equations as G^{ex} model. Wang and Wong [2.31] investigated the phase behavior of the (n-hexane + water) system using the VdW, HVM2 and WS mixing rules and the NRTL model and calculated the critical points in a wide range of pressures. Valderrama and Zavaleta [2.32] obtained a generalized binary interaction parameter in the WS mixing rule and predicted phase equilibrium for (CO_2 + n-alkanols) mixtures using the van Laar model. Lopez and Cardona [2.33] used the WS mixing rule and NRTL model for phase equilibrium calculations of (CO_2 + n-alkanes) systems. Theveneau *et al.* [2.34] investigated the (H_2S + n-heptane) binary mixture at different temperatures and pressures and calculated VLE of this system using the WS mixing rule involving the NRTL model. Lim *et al.* [2.35] and Seong *et al.* [2.36] measured the VLE data for (1,1-difluoroethane + n-butane) and (Propane + n-Butane) systems, respectively, and computed the phase equilibria using the WS mixing rule and NRTL model. Lee and Lin [2.37] predicted VLE of organic mixtures using the WS mixing rule and determined the activity coefficient from the COSMO-SAC model for the phase equilibrium calculation. Lazzus [2.38] estimated the solid-vapor equilibria for (CO_2 + biomolecule) systems using the WS mixing rule and the van Laar model. Ye *et al.* [2.39] carried out VLE and vapor-liquid-liquid equilibria (VLLE) calculation for (water + methanol + dimethyl ether + CO_2) quaternary system using the WS mixing rule and the group contribution activity models. Salinas *et al.* [2.40] calculated CO_2 solubility in ionic liquids using the SRK EOS and PR EOS involving the WS mixing rule and the UNIQUAC model. Wyczesany [2.41] investigated the VLLE of ternary systems containing water at low and high pressures using the WS mixing rule and NRTL model. Cho *et al.* [2.42],

Quevedo *et al.* [2.43], Pereira *et al.* [2.44] and Brandalize *et al.* [2.45] obtained phase equilibrium data for different systems containing CO_2 and modeled the results using the WS mixing rule. Although adjustable parameters has been considered independent of temperature in most research, they can also be a function of temperature [2.26, 2.33, 2.34, 2.39, 2.46-2.48] to compute phase equilibria. The work cited above is summarized in table 2.1, which also includes the current study reported in the following chapters.

Table 2.1. Various thermodynamic models for phase equilibria calculation cited in papers.

Component	System	EOS	G^{ex}	Mixing rule	Ref.
CO_2/water, CO_2/alcohols, CO_2/n-alkanes	VLE	PRSV*	NRTL, van Laar	WS, MHV2, Orbey-Sandler	[2.26]
CO_2/ethanol, ethane /methanol, CO_2/methanol, propane/ methanol, tetrahydrofuran/ n,n-dimethylformamide, cyclohexane/ dimethylformamide, benzene/cyclohexane, cyclopentane/ tetrachloroethylene, tetrahydrofuran/ cyclohexane	VLE	PRSV	NRTL, UNIQUAC	WS	[2.27]
Cyclohexane/ethanol, methanol/ethanol, acetone/cyclohexane, acetone/toluene, water/ methanol, water/ethanol, water/1-propanol		PRSV	van Laar	WS	[2.28]
PIB/n-pentane, PIB/n-hexane, PS/benzene, PS/2-butanone, PE/chlorobenzene, PE/toluene, PVAc/benzene, PPG/water, PPG/n-hexane, PEG/water	VLE	PRSV	FH-NRTL-NRF	WS	[2.29]
Water/methanol/alkyl ether, water/alcohol/1,1-difluoroethane	LLE	PRSV	NRTL, UNIQUAC	WS, MHV2	[2.30]
n-hexane/water	LLE	PRSV	NRTL	VdW, HVM2, WS	[2.31]

CO_2/n-alkanols	VLE	PR	van Laar	WS	[2.32]
CO_2/n-alkanes	VLE	PRSV	NRTL	WS	[2.33]
H_2S/n-heptane	VLE	PR	NRTL	WS	[2.34]
1,1-difluoroethane/n-butane	VLE	PR, CSD	NRTL	WS	[2.35]
Propane/n-butane	VLE	PR	NRTL	WS	[2.36]
Pentane/hexane, hexane/octane, octane/heptane, methane/ethane, propane/ethane, methane/hexane, pentane/1-butanol, pentane/2-butanol, pentane/ethanol, acetone/hexane, ethanol/water, 2-propanol/water	VLE	PR	COSMO-SAC	WS	[2.37]
CO_2/biomolecule	SVE	PR	van Laar	WS	[2.38]
Water/methanol/dimethyl ether/CO_2	VLE, VLLE	PR	UNIFAC-PSRK, UNIFAC-Lby	WS	[2.39]
CO_2/ionic Liquids		SRK, PR	UNIQUAC	WS	[2.40]
ternary systems containing water	VLLE	SRK, PR	NRTL, UNIFAC	WS	[2.41]
CO_2/methyl iodide	VLE	PR	NRTL, UNIQUAC	WS	[2.42]
CO_2 /ethanol/nonane, CO_2/ethanol/decane	VLE	PR	NRTL	WS	[2.43]
(CO_2 + 1-pentanol), (CO_2 + 1-hexanol)	VLE, LLE, VLLE	SRK, PR	NRTL	VdW, WS	[2.44]
CO_2/ethyl oleate, CO_2/ethyl stearate	VLE, LLE, VLLE	PR	NRTL	VdW, WS	[2.45]
ionic liquids/gas systems	VLE	PRSV	van Laar	WS	[2.46]
CO_2/1,1,1,2,3,3,3-heptafluoropropane	VLE	PR	NRTL	WS	[2.47]
butan-2-ol/water, 2-butoxyethanol/water, methanol/cyclohexane, methanol/butane	LLE	PR	UNIQUAC, COSMO-SAC	MHV1, WS	[2.48]
N_2/CO_2, CH_4/CO_2, CH_4/ethylene, N_2/isobutane, N_2/propane, N_2/propylene, H_2/N_2	VLE	PR	NRTL	WS	This work

* Peng-Robinson-Stryjek-Vera

ꦏꦺꦴꦏꦺꦴꦏꦺꦴ
ꦏꦺꦴꦏꦺꦴ
ꦏꦺꦴ
✵

CHAPTER THREE

3

Thermodynamic Principles for Vapor Liquid Equilibrium[1]

3.1. Fundamental Equations of thermodynamics

The Fundamental Equation of thermodynamics is a combined statement of the first and second laws of thermodynamics for open simple systems. Equation 3-1 is termed the energy representation of the Fundamental Equation as differential form.

$$dU = TdS - PdV + \sum_{i=1}^{m} \left(\frac{\partial U}{\partial n_i}\right)_{S,V,n_j} dn_i \qquad (3-1)$$

Where U, S, V, and P are, respectively, total internal energy, total entropy, total volume, and pressure of the system. Also, n_i is the number of moles of the ith component and m is the number of components in the system. U is called the potential function. Other potential functions can be defined as the following:

Enthalpy: $H = U + PV$ $(3-2)$

Helmholtz free energy: $A = U - TS$ $(3-3)$

Gibbs free energy: $G = H - TS$ $(3-4)$

Substitution the potential functions for dU (equation 3-1), we can obtain other the Fundamental Equations.

[1] It has been used from references [3.1-3.3] for preparation of this section.

$$dH = TdS + VdP + \sum_{i=1}^{m} \left(\frac{\partial H}{\partial n_i}\right)_{S,P,n_j} dn_i \qquad (3-5)$$

$$dA = -SdT - PdV + \sum_{i=1}^{m} \left(\frac{\partial A}{\partial n_i}\right)_{T,V,n_j} dn_i \qquad (3-6)$$

$$dG = -SdT + VdP + \sum_{i=1}^{m} \left(\frac{\partial G}{\partial n_i}\right)_{T,P,n_j} dn_i \qquad (3-7)$$

Using the Fundamental Equations, we may define an intensive quantity called chemical potential, μ_i.

$$\mu_i = \left(\frac{\partial U}{\partial n_i}\right)_{S,V,n_j} = \left(\frac{\partial H}{\partial n_i}\right)_{S,P,n_j} = \left(\frac{\partial A}{\partial n_i}\right)_{T,V,n_j} = \left(\frac{\partial G}{\partial n_i}\right)_{T,P,n_j} \qquad (3-8)$$

Therefore, there are four expressions for the chemical potential. Since the independent variables T and P are chosen for defining partial molar quantities, the chemical potential is the partial molar Gibbs energy, but it is not the partial molar internal energy, enthalpy, or Helmholtz energy.

3.2. Phase equilibrium

A heterogeneous closed system with two or more phases may be considered (figure 3.1). We can suppose that each phase is an open system within the overall closed system. It is also assumed that the heterogeneous system is in a state of internal equilibrium.

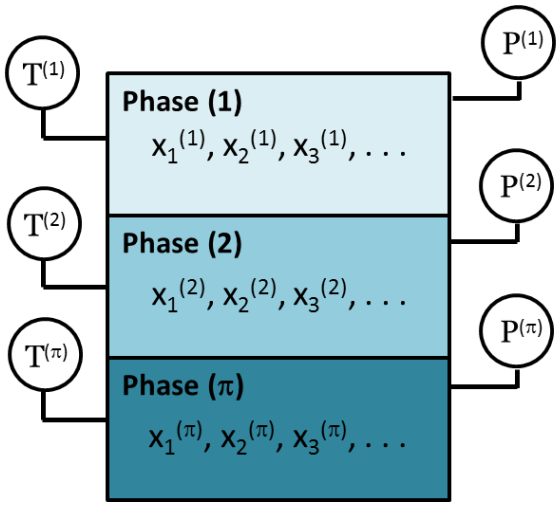

Figure 3.1. A heterogeneous closed system with more than one phase. It is assumed that the heterogeneous system is in a state of internal equilibrium.

For an isolated system which is at stable equilibrium, the entropy must have a maximum value with respect to any allowed variations. Therefore, the equilibrium criterion becomes:

$$dS = \sum_{i} dS^{(i)} = 0 \qquad (3-9)$$

Where i is the phase. The entropy representation of the Fundamental Equation is written as:

$$dS = \frac{1}{T} dU + \frac{P}{T} dV - \sum_{j=1}^{m} \frac{\mu_j}{T} dn_j \qquad (3-10)$$

Thus, for a multi-phase system:

$$dS = \sum_{i=1}^{\pi} \frac{1}{T^{(i)}} dU^{(i)} + \sum_{i=1}^{\pi} \frac{P^{(i)}}{T^{(i)}} dV^{(i)} - \sum_{i=1}^{\pi} \sum_{j=1}^{m} \frac{\mu_j{}^{(i)}}{T^{(i)}} dn_j{}^{(i)} \qquad (3-11)$$

Where π is the number of phases. The isolated system with no chemical reaction means:

$$dU = \sum_{i=1} dU^{(i)} = 0 \qquad \rightarrow \qquad \sum_{i=2} dU^{(i)} = -\, dU^{(1)} \tag{3-12}$$

$$dV = \sum_{i=1} dV^{(i)} = 0 \qquad \rightarrow \qquad \sum_{i=2} dV^{(i)} = -\, dV^{(1)} \tag{3-13}$$

$$dn_j = \sum_{i=1} dn_j{}^{(i)} = 0 \qquad \rightarrow \qquad \sum_{i=2} dn_j{}^{(i)} = -\, dn_j{}^{(1)} \tag{3-14}$$

To apply the equilibrium criterion and equation 3-12,13,14 for the multi-phase system results equation 3-15.

$$dS = \sum_{i=2}^{\pi} \left(\frac{1}{T^{(i)}} - \frac{1}{T^{(1)}}\right) dU^{(i)} + \sum_{i=2}^{\pi} \left(\frac{P^{(i)}}{T^{(i)}} - \frac{P^{(1)}}{T^{(1)}}\right) dV^{(i)} - \sum_{i=2}^{\pi} \sum_{j=1}^{m} \left(\frac{\mu_j{}^{(i)}}{T^{(i)}} - \frac{\mu_j{}^{(1)}}{T^{(1)}}\right) dn_j{}^{(i)} \tag{3-15}$$

Since each variation in $dU^{(i)}$, $dV^{(i)}$ and $dn_j{}^{(i)}$ is independent, it is obvious at equilibrium:

$$T^{(1)} = T^{(2)} = T^{(3)} = \cdots = T^{(\pi)} \tag{3-16}$$

$$P^{(1)} = P^{(2)} = P^{(3)} = \cdots = P^{(\pi)} \tag{3-17}$$

$$\mu_i{}^{(1)} = \mu_i{}^{(2)} = \mu_i{}^{(3)} = \cdots = \mu_i{}^{(\pi)} \tag{3-18}$$

The chemical potential does not have an immediate equivalent in the physical world and it is therefore desirable to express the chemical potential in terms of some auxiliary function that might be more easily identified with physical reality.

3.3. Gibbs-Duhem equation

The Fundamental Equation may be written after integration at constant temperature, pressure and compositions as the following equation:

$$U = TS - PV + \sum_i \mu_i n_i \qquad (3-19)$$

Differentiation of equation 3-19 to obtain a general expression for dU gives:

$$dU = TdS + SdT - PdV - VdP + \sum_i \mu_i dn_i + \sum_i n_i d\,\mu_i \qquad (3-20)$$

Comparing equations 3-1 and 3-20, it results:

$$SdT - VdP + \sum_i n_i d\,\mu_i = 0 \qquad (3-21)$$

Equation 3-21 is called the Gibbs-Duhem equation, a fundamental equation.

3.4. Chemical potential for a pure, ideal gas

The Gibbs-Duhem equation may be written for a pure component as the following equation:

$$sdT - vdP + d\mu_i = 0 \qquad (3-22)$$

Where $s=S/n$ and $v=V/n$ are the molar entropy and the molar volume, respectively. At constant temperature, equation 3-22 gives:

$$d\mu_i = vdP \qquad (3-23)$$

or

$$\left(\frac{\partial \mu_i}{\partial P}\right)_T = v \qquad (3-24)$$

Substituting the ideal-gas equation, $v=RT/P$, gives:

$$\left(\frac{\partial \mu_i}{\partial P}\right)_T = \frac{RT}{P} \qquad (3-25)$$

or

$$d\mu_i = RT\frac{dP}{P} \qquad at\ constant\ T \qquad (3-26)$$

Integrating at constant temperature results:

$$\mu_i - {\mu_i}^0 = RTln\frac{P}{P^0} \qquad (3-27)$$

Where superscript 0 refers to standard state. Equation 3-27 is valid only for pure, ideal gases.

3.5. Fugacity and fugacity coefficient

Lewis defined a function, called fugacity, by writing for an isothermal change for any component in any system, solid, liquid, or gas, pure or mixed, ideal or not.

$$\mu_i - {\mu_i}^0 = RTln\frac{f_i}{{f_i}^0} \qquad (3-28)$$

or

$$d\mu_i = RTdlnf_i \qquad at\ constant\ T \qquad (3-29)$$

While either μ_i^o or f_i^o is arbitrary, both may not be chosen independently; when one is chosen, the other is fixed. For a pure, ideal gas, the fugacity is equal to the pressure, and for a component *i* in a mixture of ideal gases, it is equal to its partial pressure, y_iP.

If equation 3-28 is applied for both real mixture and ideal-gas mixture, we will have:

$$(\mu_i - {\mu_i}^0) - \left({\mu_i}^{ig} - {\mu_i}^0\right) = RTln\frac{f_i}{{f_i}^0} - RTln\frac{y_i P}{{f_i}^0} \qquad (3-30)$$

$$\rightarrow \quad \mu_i - {\mu_i}^{ig} = RTln\frac{f_i}{y_i P} = RTln\phi_i \qquad (3-31)$$

Where ϕ_i is called the fugacity coefficient.

$$\phi_i = \frac{f_i}{y_i P} \rightarrow 1 \quad as \quad P \rightarrow 0 \qquad (3-32)$$

Using the definition of fugacity, we can derive *the fundamental equation of phase equilibrium*.

$${f_i}^{(1)} = {f_i}^{(2)} = {f_i}^{(3)} = \cdots = {f_i}^{(\pi)} \qquad (3-33)$$

3.6. Activity and activity coefficient

The activity of component i at some temperature, pressure, and composition is defined as the ratio of the fugacity of i at these conditions to the fugacity of i in the standard state.

$$a_i = \frac{f_i}{{f_i}^0} \qquad (3-34)$$

The activity coefficient, γ_i, is the ratio of the activity of i to some convenient measure of the concentration of i, usually the mole fraction.

$$\gamma_i = \frac{a_i}{x_i} \qquad (3-35)$$

or

$$\gamma_i = \frac{f_i}{x_i {f_i}^0} \qquad (3-36)$$

When the activity coefficient is equal to one, the liquid mixture is called ideal solution. In other words, the fugacity, at constant temperature and pressure, is proportional to the mole fraction in the ideal solution.

$$f_i^L = x_i {f_{i,pure}}^L \quad for\ ideal\ solution \qquad (3-37)$$

3.7. Raoult's law

When vapor and liquid mixtures are assumed ideal solutions at vapor-liquid equilibrium, we have:

$$f_i^V(P,T,y_i) = f_i^L(P,T,x_i) \qquad (3-38)$$

thus

$$y_i P = x_i {f_i}^0 \qquad (3-39)$$

Also, we can assume that the effect of pressure on the fugacity of a condensed phase is negligible at moderate pressures. It means that

$${f_i}^0 = P_i^{sat} \qquad (3-40)$$

So, we can obtain:

$$y_i P = x_i P_i^{sat} \qquad (3-41)$$

Equation 3-41 is known as the Raoult's law. It is a limited utility because it is based on severe simplifying assumptions.

3.8. γ-ϕ approach

A useful method for calculation of VLE is the γ-ϕ approach. The fugacities of vapor phase and liquid phase are respectively calculated by the fugacity and activity coefficients.

$$y_i \phi_i P = x_i \gamma_i {f_i}^0 \qquad (3-42)$$

Where ${f_i}^o$ is the fugacity of pure liquid component i at pressure and temperature of the system.

$${f_i}^0 = {\phi_i}^{sat} {P_i}^{sat} exp \frac{{v_i}^L \left(P - {P_i}^{sat}\right)}{RT} \qquad (3-43)$$

Where $exp \frac{{v_i}^L \left(P - {P_i}^{sat}\right)}{RT}$ is called the Poynting factor. Equations of 3-42 and 3-43 can be simplified for low and moderate pressure.

- Low pressure

At low pressure, the Poynting factor and $\phi_i / {\phi_i}^{sat}$ are approaching to one. It gives that:

$$y_i P = x_i \gamma_i {P_i}^{sat} \qquad (3-44)$$

- Moderate pressure

At moderate pressure, the Poynting factor is almost one. Thus

$$y_i \phi_i P = x_i \gamma_i {\phi_i}^{sat} {P_i}^{sat} \qquad (3-45)$$

However, at high pressure, all terms should be considered.

$$y_i \phi_i P = x_i \gamma_i {\phi_i}^{sat} {P_i}^{sat} exp \frac{{v_i}^L \left(P - {P_i}^{sat}\right)}{RT} \qquad (3\text{-}46)$$

3.9. Excess Gibbs free energy models

According to the previous section, we should calculate the activity coefficient for γ-ϕ approach. Equation 3-47 gives the relation between activity coefficient and excess Gibbs energy

$$RTln\gamma_i = \left(\frac{\partial n_t g^{ex}}{\partial n_i}\right)_{T,n_j} \qquad (3-47)$$

Therefore, we need an excess Gibbs energy model to obtain the activity coefficient. There are several models to represent non-ideal behavior. The most important models include:

- **Extended polynomial expansion models**
- Two-suffix Margules
- Three-suffix Margules
- Four-suffix Margules
- Van Laar
- General Redlich-Kister

- **Volume-fraction based models**
- Hildebrand-Scatchard
- Flory-Huggins
- General Wohl expansion
- **Local-composition based models**
- Wilson
- TK-Wilson
- NRTL

- NRTL-NRF
- UNIQUAC

3.10. ϕ-ϕ approach

Another method to calculate VLE of mixtures is the ϕ-ϕ approach. In this technique, fugacities of both vapor and liquid phases are computed by the fugacity coefficient. The required equations are:

Pure component mixture

Independent Variables P and T:

$$RTln\phi_{pure} = RTln\left(\frac{f}{P}\right)_{pure} = \int_0^P \left(v - \frac{RT}{P}\right) dP = RT\int_0^P \frac{Z-1}{P} dP \qquad (3-48)$$

Independent Variables V and T:

$$RTln\phi_{pure} = RTln\left(\frac{f}{P}\right)_{pure} = \int_V^\infty \left(\frac{P}{n} - \frac{RT}{V}\right) dV - RTln\, Z + RT(Z-1) \qquad (3-49)$$

Multi-component mixture

Independent Variables P and T:

$$RTln\phi_i = \int_0^P \left(\overline{v_i} - \frac{RT}{P}\right) dP \qquad (3-50)$$

and

$$\overline{v_i} = \left(\frac{\partial V}{\partial n_i}\right)_{T,P,n_j} \qquad (3-51)$$

Independent Variables V and T:

$$RTln\phi_i = \int_V^\infty \left[\left(\frac{\partial P}{\partial n_i}\right)_{T,V,n_j} - \frac{RT}{V}\right] dV - RTlnZ_{mix} \qquad (3-52)$$

Since cubic equations of state (CEOS) such as the Peng-Robinson (PR) EOS are pressure explicit, equation 3-52 will be useable for VLE calculation. Substitution the PR EOS and the Van der Waals (VdW) mixing rule in equation 3-52, the fugacity coefficient may be calculated by the following equation.

$$ln\phi_i = \frac{b_i}{b_m}(Z_m - 1) - \ln(Z_m - B) + \frac{A}{2\sqrt{2}B}\left(\frac{2\sum_k y_k a_{ik}}{a_m} - \frac{b_i}{b_m}\right) ln\frac{Z_m + c_2 B}{Z_m + c_1 B} \qquad (3-53)$$

and

$$A = \frac{a_m P}{(RT)^2} \quad , \quad B = \frac{b_m P}{RT} \qquad (3-54)$$

The VdW Mixing Rules are defined as:

$$a_m = \sum_i \sum_j x_i x_j a_{ij} \qquad (3-55)$$

$$b_m = \sum_i x_i b_i \qquad (3-56)$$

$$a_{ij} = \sqrt{a_i a_j}\left(1 - k_{ij}\right) \quad , k_{ii} = 0 \qquad (3-57)$$

Where k_{ij} is the interaction parameter. For a binary mixture, we have:

$$a_m = {x_1}^2 a_1 + {x_2}^2 a_2 + 2x_1 x_2 a_{12} \qquad (3-58)$$

$$b_m = x_1 b_1 + x_2 b_2 \qquad (3-59)$$

$$a_{12} = \sqrt{a_1 a_2}(1 - k_{12}) \qquad (3-60)$$

The PR EOS will be explained in detail in chapter 4.

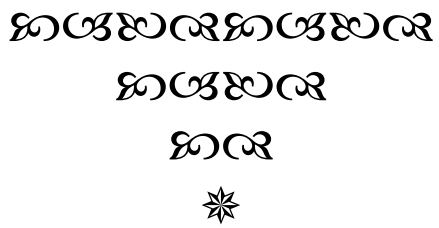

CHAPTER FOUR

4

Vapor-liquid Equilibria of Low Boiling Point Gaseous Mixture[2]

4.1. Thermodynamic model

Since one of the components in a low boiling point gas mixture is above its critical temperature and pressure, there is no equation to calculate the vapor pressure. Thus, γ-ϕ approach cannot provide VLE calculation of the mixtures. Consequently, we need ϕ-ϕ approach for thermodynamic modeling.

4.1.1. VLE calculation by the ϕ-ϕ approach

Equation 4-1 is the fundamental relation to describe phase equilibrium of mixtures.

$$f_i^{\alpha} = f_i^{\beta} = f_i^{\gamma} = \cdots \qquad (4-1)$$

Where f_i is the fugacity of component i in the mixture and α, β, ... are the different phases.

Equation 4-1 can be developed as the following equation for VLE calculation by the $\phi - \phi$ approach.

$$y_i \phi_i^{V} P = x_i \phi_i^{L} P \qquad (4-2)$$

[2] This chapter has been presented in the 11th International Symposium on Supercritical Fluids (ISSF), Seoul, S. Korea, October 11-14, 2015 (invited lecturer).

P is the pressure, y_i is the mole fraction of species i, and ϕ_i is the fugacity coefficient of species i.

4.1.2. Peng Robinson equation of state

Equation 4-3 is the Peng Robinson equation of state (PR EOS), which is used in this research [4.1].

$$P = \frac{RT}{v-b} - \frac{a}{(v+c_1 b)(v+c_2 b)} \qquad (4-3)$$

and

$$c_1 = 1+\sqrt{2} \quad , \quad c_2 = 1-\sqrt{2}$$

T is the temperature, v is the molar volume, and R is the gas constant. The parameter a is the molecular attraction parameter, and b is the volume parameter. They are defined in equations 4-4, 4-5, and 4-6.

$$a = a_c \alpha(\omega, T_r) \quad , \quad a_c = \frac{0.45724 R^2 {T_c}^2}{P_c} \qquad (4-4)$$

$$\alpha(\omega, T_r) = \left[1 + (0.37464 + 1.5422\omega - 0.26992\omega^2)(1-\sqrt{T_r})\right]^2 \quad , \quad T_r = T/T_c \qquad (4-5)$$

$$b = \frac{0.0778 R T_c}{P_c} \qquad (4-6)$$

Where ω is the acentric factor, P_C is the critical pressure, and T_C is the critical temperature of the fluid.

4.1.3. Wong-Sadler mixing rule

The PR EOS can be written for any fluid that is a pure species. For mixtures, a and b must be modified. Equations 4-7 through 4-10 describe the Wong-Sadler mixing rule for a and b [4.2].

$$\frac{a_{mix}}{RT} = Q\frac{D}{1-D} \qquad (4-7)$$

$$b_{mix} = \frac{Q}{1-D} \qquad (4-8)$$

$$Q = \sum_i \sum_j x_i x_j \left(b_{ij} - \frac{a_{ij}}{RT}\right) \qquad (4-9)$$

$$D = \sum_i x_i \frac{a_i}{b_i RT} + \frac{G^{ex}}{c^* RT} \qquad (4-10)$$

Where c^* is a constant with a value of -0.623225 for the PR EOS and G^{ex} is the excess molar Gibbs free energy.

Using the cross second virial coefficient, Orbey and Sandler [4.2 , 4.3] proposed equation 4-11 as the combination rule.

$$b_{ij} - \frac{a_{ij}}{RT} = \frac{b_i + b_j}{2} - \frac{\sqrt{a_i a_j}}{RT}\left(1 - k_{ij}\right) \qquad (4-11)$$

4.1.4. Calculation of fugacity coefficient

The fugacity coefficients for both vapor and liquid phases are obtained by the equation 4-12.

$$RTln\phi_i = \int_V^{\infty} \left[\left(\frac{\partial P}{\partial n_i} \right)_{T,v,n_j} - \frac{RT}{V} \right] dV - RTlnZ_{mix} \qquad (4-12)$$

Where V and n_i are total volume and the moles of component i, respectively.

The compressibility factors, Z_{mix}, for vapor and liquid phases can be computed by solving the equations 4-13 and 4-14. The largest and the smallest roots are Z_{mix} for vapor and liquid phases, respectively.

$$Z_{mix}{}^3 - (1 - B_{mix})Z_{mix}{}^2 + \left(A_{mix} - 3B_{mix}{}^2 - 2B_{mix}\right)Z_{mix} - \left(A_{mix}B_{mix} - B_{mix}{}^2 - B_{mix}{}^3\right) = 0 \qquad (4-13)$$

and

$$A_{mix} = \frac{a_{mix}P}{(RT)^2} \quad , \quad B_{mix} = \frac{b_{mix}P}{RT} \qquad (4-14)$$

Developing the equation 4-12 using the PR EOS and WS mixing rules as described above results in the required equations to compute the fugacity coefficients as:

$$ln\phi_i = \frac{1}{b_{mix}} \left(\frac{\partial n_t b_{mix}}{\partial n_i} \right)_{T,n_j} (Z_{mix} - 1) - \ln(Z_{mix} - B_{mix}) + \frac{A_{mix}}{2\sqrt{2}B_{mix}} \times \left[\frac{1}{a_{mix}n_t} \left(\frac{\partial n_t{}^2 a_{mix}}{\partial n_i} \right)_{T,n_j} - \frac{1}{b_{mix}} \left(\frac{\partial n_t b_{mix}}{\partial n_i} \right)_{T,n_j} \right] ln \frac{Z_{mix} + c_2 B_{mix}}{Z_{mix} + c_1 B_{mix}} \qquad (4-15)$$

$$\frac{1}{n_t} \left(\frac{\partial n_t{}^2 a_{mix}}{\partial n_i} \right)_{T,n_j} = RTD \left(\frac{\partial n_t b_{mix}}{\partial n_i} \right)_{T,n_j} + RTb_{mix} \left(\frac{\partial n_t D}{\partial n_i} \right)_{T,n_j} \qquad (4-16)$$

$$\left(\frac{\partial n_t b_{mix}}{\partial n_i} \right)_{T,n_j} = \frac{1}{1-D} \frac{1}{n_t} \left(\frac{\partial n_t{}^2 Q}{\partial n_i} \right)_{T,n_j} - \frac{Q}{(1-D)^2} \left[1 - \left(\frac{\partial n_t D}{\partial n_i} \right)_{T,n_j} \right] \qquad (4-17)$$

$$\frac{1}{n_t}\left(\frac{\partial {n_t}^2 Q}{\partial n_i}\right)_{T,n_j} = 2\sum_j x_j \left(b - \frac{a}{RT}\right)_{ij} \qquad (4-18)$$

$$\left(\frac{\partial n_t D}{\partial n_i}\right)_{T,n_j} = \frac{a_i}{b_i RT} + \frac{1}{c^* RT}\left(\frac{\partial n_t G^{ex}}{\partial n_i}\right)_{T,n_j} = \frac{a_i}{b_i RT} + \frac{ln\gamma_i}{c^*} \qquad (4-19)$$

Where n_t and γ_i are the total mole and the activity coefficient of component i, respectively.

4.1.5. Non-Random Two-Liquid (NRTL) model

In this work, the NRTL model is used to estimate G^{ex}, as shown in the equation 4-10 [4.4]. The NRTL model is defined for a binary mixture by equations 4-20 and 4-21.

$$G^{ex} = x_1 x_2 \left(\frac{\tau_{21} G_{21}}{x_1 + x_2 G_{21}} + \frac{\tau_{12} G_{12}}{x_2 + x_1 G_{12}}\right) \qquad (4-20)$$

and

$$G_{12} = \exp(-\alpha_{12}\tau_{12}), G_{21} = \exp(-\alpha_{21}\tau_{21}), \tau_{12} = \frac{g_{12} - g_{22}}{RT}, \tau_{21} = \frac{g_{21} - g_{11}}{RT} \qquad (4-21)$$

Where g_{11}, g_{22}, g_{12} and g_{21} are related to the interaction energy between molecules 1 and 2. In equation 4-21, α_{12} and α_{21} are the non-randomness factors and assumed to be symmetric (α_{12}= α_{21}=α).

Using NRTL model, the activity coefficient will be obtained for a binary mixture by the following equations:

$$ln\gamma_1 = {x_2}^2 \left[\tau_{21}\left(\frac{G_{21}}{x_1 + x_2 G_{21}}\right)^2 + \frac{\tau_{12} G_{12}}{(x_2 + x_1 G_{12})^2}\right] \qquad (4-22)$$

$$ln\gamma_2 = {x_1}^2\left[\tau_{12}\left(\frac{G_{12}}{x_2 + x_1 G_{12}}\right)^2 + \frac{\tau_{21}G_{21}}{(x_1 + x_2 G_{21})^2}\right] \quad (4-23)$$

Where γ_1 and γ_2 are the activity coefficients of components 1 and 2.

4.1.6. Adjustable parameters as functions of temperature

In this research, the parameters τ_{12} and τ_{21} for NRTL model are defined as a function of reduced temperature in equation 4-24.

$$\tau_{ij} = f(T_{ri}) + \frac{constatnt}{T_{ri}} \quad (4-24)$$

Function f is a quadratic function and can be written for a binary mixture as equations 4-25 and 4-26.

$$\tau_{12} = A_{12} + B_{12}T_{r1} + C_{12}{T_{r1}}^2 + \frac{D_{12}}{T_{r1}} \quad (4-25)$$

$$\tau_{21} = A_{21} + B_{21}T_{r2} + C_{21}{T_{r2}}^2 + \frac{D_{21}}{T_{r2}} \quad (4-26)$$

Where A_{ij}, B_{ij}, C_{ij} and D_{ij} are the constant coefficients.

In equation 4-11, k_{ij} is a binary interaction parameter. It is assumed to be a quadratic function of the temperature as shown in equation 4-27.

$$k_{ij} = k_0 + k_1 T + k_2 T^2 \quad (4-27)$$

Where k_0, k_1 and k_2 are constant coefficients.

4.2. Calculation method

Using an algorithm of bubble point and P [4.3] presented in figure 4.1, the coefficients of equations 4-25, 4-26, and 4-27 are computed by optimizing the following objective function (OF):

$$OF = \sum_{i=1}^{M} \sum_{j=1}^{N} \left(\frac{P_j^{exp} - P_j^{cal}}{P_j^{exp}} \right)_i^2 \qquad (4-28)$$

Where M and N are related to the number of experimental temperatures of system and the number of experimental points at each temperature, respectively. Also, P_i^{exp} and P_i^{cal} are experimental and calculated pressure of component i in the mixture, respectively.

The parameters of WS mixing rule and G^{ex} are computed by the functions of temperature in this work and highlighted in the algorithm of the bubble point and P (figure 4.1).

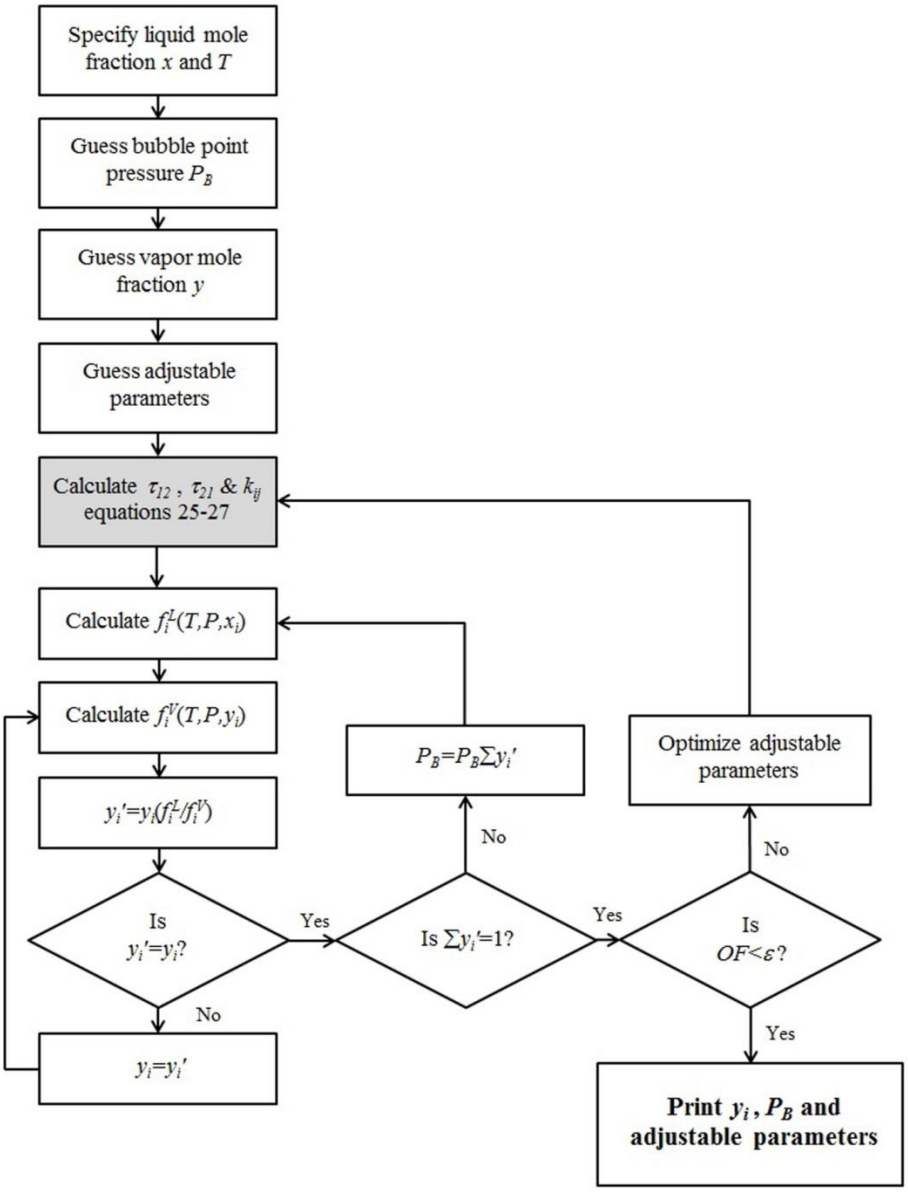

Figure 4.1. Algorithm of the bubble point and P for VLE calculation.

The steps of VLE calculation are:

1) Specify liquid mole fraction and temperature (x and T).
2) Guess bubble point pressure (P_B).
3) Guess vapor mole fraction (y).
4) Guess adjustable parameters (A_{ij}, B_{ij}, C_{ij}, D_{ij}, k_o, k_1, k_2, α).

5) Calculate a_i (equation 4-4 and 4-5).

6) Calculate b_i (equation 4-6).

7) Calculate b_{ij}-a_{ij}/RT (equation 4-11).

8) Calculate τ_{12} and τ_{21} (equations 4-25 and 4-26).

9) Calculate k_{ij} (equations 4-27).

10) Calculate G_{ij} (equation 4-21).

11) Calculate G^{ex} for liquid phase using liquid mole fraction (equation 4-20).

12) Calculate Q for the liquid phase using liquid mole fraction (equation 4-9).

13) Calculate D for the liquid phase using liquid mole fraction (equation 4-10).

14) Calculate a_{mix} for the liquid phase (equation 4-7).

15) Calculate b_{mix} for the liquid phase (equation 4-8).

16) Calculate A_{mix} and B_{mix} for the liquid phase (equation 4-14).

17) Solve equation 4-13 and find Z_{mix} for the liquid phase (the smallest root of equation 4-13).

18) Calculate $ln\gamma_i$ (equations 4-22 and 4-23).

19) Calculate $\partial n_t D/\partial n_i$ (equations 4-19).

20) Calculate $\partial n_t^2 Q/\partial n_i$ (equations 4-18).

21) Calculate $\partial n_t b_{mix}/\partial n_i$ (equations 4-17).

22) Calculate $\partial n_t^2 a_{mix}/\partial n_i$ (equations 4-16).

23) Calculate $ln\phi_i$ and fugacity coefficient for liquid phase (equations 4-15).

24) Calculate f_i^L for liquid phase (equations 4-2).

25) Calculate G^{ex} for vapor phase using vapor mole fraction (equation 4-20).

26) Calculate Q for the vapor phase using vapor mole fraction (equation 4-9).

27) Calculate D for the vapor phase using vapor mole fraction (equation 4-10).

28) Calculate a_{mix} for the vapor phase (equation 4-7).

29) Calculate b_{mix} for the vapor phase (equation 4-8).

30) Calculate A_{mix} and B_{mix} for the vapor phase (equation 4-14).

31) Solve equation 3-13 and find Z_{mix} for the vapor phase (the largest root of equation 4-13).

32) Calculate $ln\gamma_i$ (equations 4-22 and 4-23).

33) Calculate $\partial n_t D/\partial n_i$ (equations 4-19).

34) Calculate $\partial n_t^2 Q/\partial n_i$ (equations 4-18).

35) Calculate $\partial n_t b_{mix}/\partial n_i$ (equations 4-17).

36) Calculate $\partial n_t^2 a_{mix}/\partial n_i$ (equations 4-16).

37) Calculate $ln\phi_i$ and fugacity coefficient for vapor phase (equations 4-15).

38) Calculate f_i^V for vapor phase (equations 4-2).

39) Calculate $y_i'=y_i(f_i^L/f_i^V)$.

40) If $y_i'\neq y_i$, go to step 25.

41) If $y_i'=y_i$, calculate $\Sigma y_i'$.

42) If $\Sigma y_i'\neq 1$, calculate $P_B=P_B\Sigma y_i'$, then go to step 11.

43) If $\Sigma y_i'=1$, calculate OF (equation 4-28).

44) If $OF>\varepsilon$, go to optimization steps , optimize adjustable parameters , then go to step 8.

45) If $OF<\varepsilon$, print y_i and P , end.

4.3. Optimization method

The conjugate gradient method [4.5] has been applied for minimizing the *OF*. In this method, we need to define some parameters.

4.3.1. Gradient vector

Consider a general function, *f*, as the following:

$$f(x_1, x_2, x_3, \dots, x_n) = f(\boldsymbol{X}) \tag{4-29}$$

Where $\boldsymbol{X}$ is a vector.

$$\boldsymbol{X} = [x_1, x_2, x_3, \dots, x_n] \tag{4-30}$$

The gradient vector, ∇f, is defined as equation 4-31.

$$\nabla f(\boldsymbol{X}) = \begin{bmatrix} \frac{\partial f}{\partial x_1} \\ \frac{\partial f}{\partial x_2} \\ \frac{\partial f}{\partial x_3} \\ \vdots \\ \frac{\partial f}{\partial x_n} \end{bmatrix} \tag{4-31}$$

4.3.2. Hessian Matrix

For the function *f*, the Hessian matrix is the matrix of second partial derivative of $f(\mathbf{X})$ with respect to each x_i:

$$H(\boldsymbol{X}) = \nabla^2 f(\boldsymbol{X}) = \begin{bmatrix} \frac{\partial^2 f}{\partial {x_1}^2} & \frac{\partial^2 f}{\partial x_1 x_2} & \frac{\partial^2 f}{\partial x_1 x_3} & \cdots & \frac{\partial^2 f}{\partial x_1 x_n} \\ \frac{\partial^2 f}{\partial x_2 x_1} & \frac{\partial^2 f}{\partial {x_2}^2} & \frac{\partial^2 f}{\partial x_2 x_3} & \cdots & \frac{\partial^2 f}{\partial x_2 x_n} \\ \frac{\partial^2 f}{\partial x_3 x_1} & \frac{\partial^2 f}{\partial x_3 x_2} & \frac{\partial^2 f}{\partial {x_3}^2} & \cdots & \frac{\partial^2 f}{\partial x_3 x_n} \\ \vdots & & & & \vdots \\ \frac{\partial^2 f}{\partial x_n x_1} & \frac{\partial^2 f}{\partial x_n x_2} & \frac{\partial^2 f}{\partial x_n x_3} & \cdots & \frac{\partial^2 f}{\partial {x_n}^2} \end{bmatrix} \tag{4-32}$$

4.3.3. Conjugate gradient method

The required equation for minimizing the function f using the conjugate gradient method is:

$$\boldsymbol{X}^{k+1} - \boldsymbol{X}^{k} = -\alpha^{k}[H(\boldsymbol{X}^{k})]^{-1}\nabla f(\boldsymbol{X}^{k}) \qquad (4-33)$$

Where k is the iteration number, $[H(\boldsymbol{X}^{k})]^{-1}$ is the inverse of the Hessian matrix, and α^{k} is the step length that can be evaluated numerically. Here, we used the Newton's method to find α^{k} using equation 4-34.

$$\alpha^{k} = \alpha^{k-1} - \frac{f'(\alpha^{k-1})}{f''(\alpha^{k-1})} \qquad (4-34)$$

Figure 4.2 shows the algorithm of optimization.

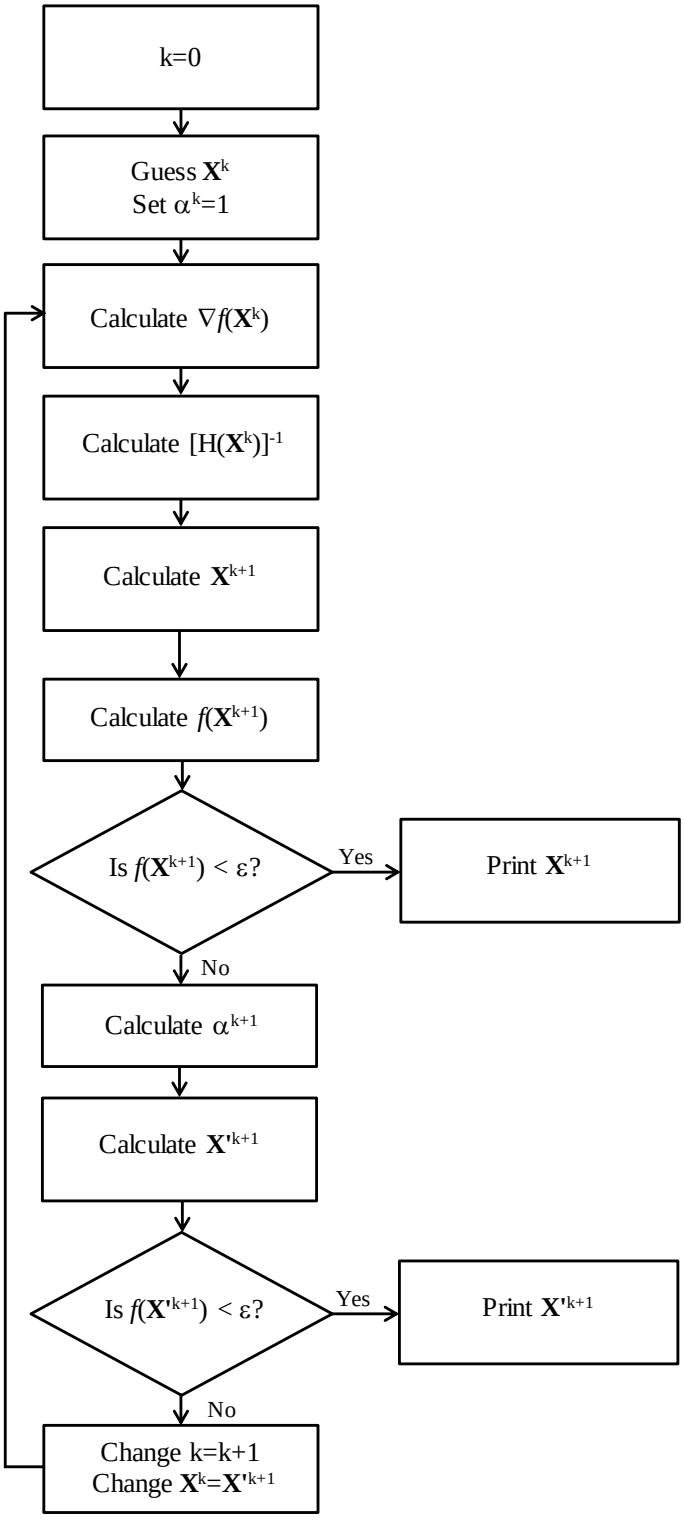

Figure 4.2. The algorithm of optimization using the conjugate gradient method.

In this study, partial derivatives have been numerically computed using the following equations:

$$\frac{\partial f}{\partial x_i} = \frac{f(x_i + h, x_j) - f(x_i - h, x_j)}{2h} \quad (4-35)$$

$$\frac{\partial^2 f}{\partial {x_i}^2} = \frac{f(x_i + h, x_j) - 2f(x_i, x_j) + f(x_i - h, x_j)}{h^2} \quad (4-36)$$

$$\frac{\partial^2 f}{\partial x_i x_j} = \frac{f(x_i + h, x_j + h) - f(x_i + h, x_j - h) - f(x_i - h, x_j + h) + f(x_i - h, x_j - h)}{4h^2} \quad (4-37)$$

4.4. Thermodynamic properties of components

Table 4.1 shows the required parameters of materials studied in this research for VLE calculation.

Table 4.1. The thermodynamic properties of components used in the modeling [4.6].

component	Molecular weight	T_C (K)	P_C (bar)	ω
H_2	2.016	33.25	12.97	-0.216
N_2	28.014	126.20	33.98	0.37
CH_4	16.043	190.56	45.99	0.011
CO_2	44.010	304.12	73.74	0.225
C_2H_4 (ethylene)	28.054	282.34	50.41	0.087
C_3H_6 (propylene)	42.081	364.90	46.00	0.142
C_3H_8 (propane)	44.097	369.83	42.48	0.152
C_4H_{10} (isobutane)	58.123	407.85	36.40	0.186

4.5. Results and discussion

The PR-WS-NRTL model has been used for prediction of VLE of the systems (N_2 + CO_2), (CH_4 + CO_2), (CH_4 + C_2H_4), (N_2 + C_3H_6), (N_2 + C_3H_8), (N_2 + C_4H_{10}) and (H_2 + N_2) at different temperatures. The coefficients of the adjustable parameter functions are reported in tables 4.2 and 4.3.

Table 4.2. The required coefficients of equations 4-25 and 4-26 for different systems at temperature range.

System	Temperature range (K)	A_{12}	B_{12}	C_{12}	D_{12}	A_{21}	B_{21}	C_{21}	D_{21}
(N_2 + CO_2)	218.15-273.15	-34.3459	37.2378	-9.7970	-0.9455	-12.6181	-13.6932	17.2659	10.6068
	273.15-298.15	-288.8781	61.0433	0.0036	339.0718	-146.5827	-125.4997	162.5459	115.8152
(CH_4 + CO_2)	193.15-270.00	133.8970	-208.4229	81.1392	0.00061	-59.4810	154.1687	-97.3065	-0.3488
(CH_4 + C_2H_4)	148.09-198.15	36.0239	-38.3656	12.8076	-10.7679	-67.9643	107.5703	-54.4760	14.1283
	198.15-248.15	7.1912	10.7852	-8.1028	-10.4242	-21.8481	-10.9756	21.5187	13.8875
(N_2 + C_4H_{10})	255.37-394.26	-129.9264	38.6389	-3.2096	134.4718	62.6835	-78.9206	32.6512	-16.1321
(N_2 + C_3H_8)	230.00-290.00	25.1592	-6.3420	0.0000	-23.0216	-16.1048	12.0448	0.0000	5.6473
(N_2 + C_3H_6)	260.00-290.00	0.1186	0.0000	0.0000	1.3068	1.2778	0.0000	0.0000	-0.5137
(H_2 + N_2)	77.35-113.00	-0.4060	1.4826	-0.2381	-0.8081	-7.5394	-3.2641	6.6284	5.0756

Also, the results of the present model have been compared with the VdW mixing rule. The VdW mixing rule is defined as:

$$a_{mix} = \sum_i \sum_j x_i x_j \sqrt{a_i a_j}\left(1 - k_{ij}\right) \qquad (4-38)$$

$$b_{mix} = \sum_i x_i b_i \qquad (4-39)$$

Using reference [4.7], the parameter k_{ij} for the VdW mixing rule is also reported in table 4.3.

Table 4.3. The parameter k_{ij} from reference [4.7] and the parameter α and the coefficients of equation 4-27 calculated by the PR-WS-NRTL model.

		VdW mixing rule	WS mixing rule			
System	T (K)	k_{ij}	α	k_o	k_1	k_2
(N_2 + CO_2)	218.15	-0.0193	0.55	7.7555	-0.0636	0.00013
	223.15	-0.0222				
	232.85	-0.0193				
	253.15	-0.0122				
	273.15	-0.0193				
	288.15	-0.0122				
	298.15	-0.0122				
(CH_4 + CO_2)	193.15	0.0885	0.55	0.0575	0.00025	0.0000
	230.00	0.0889				
	250.00	0.0889				
	270.00	0.0889				
(CH_4 + C_2H_4)	148.09	0.0204	0.75	0.3695	-0.00363	0.0000
	150.00	0.0244				
	159.21	0.0204				
	160.00	0.0244				
	170.00	0.0244				
	180.00	0.0244				
	190.00	0.0244				
	198.15	0.0378				
	223.15	0.0378				
	248.15	0.0378				
(N_2 + C_4H_{10})	255.37	0.1033	0.84	-3.6454	0.0242	-0.00004
	283.21	0.1033				
	310.87	0.1033				
	338.71	0.1033				
	366.32	0.1033				
(N_2 + C_3H_8)	230.00	0.0678	0.89	0.0000	0.0000	0.0000
	260.00	0.0678				
	290.00	0.0678				
(N_2 + C_3H_6)	260.00	0.0900	0.95	0.0000	0.0000	0.0000
	290.00	0.0900				
(H_2 + N_2)	77.35	0.1200	0.75	0.5467	-0.0099	0.000051
	90.00	0.0711				
	107.65	0.0711				
	113.00	0.0711				

Average Absolute Deviation of pressure (AAD_P) and Average Absolute Deviation of vapor phase mole fraction (AAD_y) are defined as:

$$AAD_P = \frac{1}{NP}\sum_i \frac{\left|{P_i}^{exp} - {P_i}^{cal}\right|}{{P_i}^{exp}} \times 100 \qquad (4-40)$$

$$AADy = \frac{1}{NP}\sum_i \frac{\left|{y_i}^{exp} - {y_i}^{cal}\right|}{{y_i}^{exp}} \times 100 \qquad (4-41)$$

Where *NP* is related to the number of experimental points. AAD_y and AAD_P have been reported in table 4.4 for both the VdW mixing rule and the present model. Also, the references of experimental data have been presented in table 4.4.

The results obtained from thermodynamic modeling have been shown in figures 4.3 through 4.27. Three general types of diagrams are provided. The first is a P-x-y diagram (for example, figure 4.3), in which equilibrium pressure is plotted versus equilibrium compositions of vapor and liquid phases. Multiple temperatures are represented by multiple curves. The P-x-y diagrams also show quality of agreement between models (continuous lines) and experimental data (discrete points). This attribute is further demonstrated in a subset of the P-x-y diagrams that compare the predictions of the WS mixing rule (this work) and the VdW mixing rule with experimental data at one temperature (for example, figure 4.5).

The second type of figure is the y-x diagram (for example figure 4.4). It demonstrates the corresponding mole fraction of a component in vapor and liquid phases. Since the more volatile component is plotted, the 45° line is a relevant baseline. The curves are isothermal, and the pressure varies continually along each curve.

The third type of diagram is the locus of critical points (for example, figure 4.6). The maxima of each curve in the P-x-y diagrams is the critical point. The locus of critical points is shown as a P vs T curve for all systems. The dash lines show vapor-pressure curves for the pure components.

Table 4.4. Average Absolute Deviation for different systems calculated by the VdW and WS mixing rules.

System	T (K)	NP	VdW mixing rule		WS mixing rule		Ref.
			AAD_y (%)	AAD_P (%)	AAD_y (%)	AAD_P (%)	
(N_2 + CO_2)	218.15	7	4.25	8.15	0.90	2.27	[4.8]
	223.15	8	1.33	5.58	0.98	1.08	[4.9]
	232.85	11	4.22	5.54	1.72	2.90	[4.8]
	253.15	4	2.36	3.08	1.91	1.13	[4.10]
	273.15	6	3.48	1.02	2.71	0.71	[4.9]
	288.15	2	5.66	2.56	4.51	0.89	[4.10]
	298.15	2	2.24	1.52	3.17	0.29	[4.10]
overall		**40**	**3.36**	**3.92**	**2.24**	**1.29**	
(CH_4 + CO_2)	193.15	7	0.17	1.35	0.12	0.19	[4.11]
	230.00	12	2.72	1.64	1.80	0.65	[4.12]
	250.00	10	3.81	1.33	3.83	0.46	[4.12]
	270.00	9	6.38	1.75	4.01	1.79	[4.12]
overall		**38**	**3.40**	**1.53**	**2.55**	**0.79**	
(CH_4 + C_2H_4)	148.09	19	0.16	2.21	0.16	1.11	[4.13]
	150.00	9	0.91	2.10	0.66	0.80	[4.14]
	159.21	16	0.33	1.61	0.28	1.68	[4.13]
	160.00	9	1.06	1.97	0.67	0.89	[4.14]
	170.00	11	1.03	1.31	0.49	0.57	[4.14]
	180.00	9	0.57	0.96	0.64	1.10	[4.14]
	190.00	9	1.17	1.36	0.38	0.37	[4.14]
	198.15	3	3.85	2.61	4.48	6.04	[4.15]
	223.15	3	1.70	0.42	0.77	0.10	[4.15]
	248.15	5	3.56	1.61	2.01	1.07	[4.15]
overall		**93**	**0.94**	**1.69**	**0.64**	**1.14**	
(N_2 + C_4H_{10})	255.37	11	0.69	3.77	0.58	2.43	[4.16]
	283.21	10	2.05	7.02	0.72	2.25	[4.16]
	310.87	9	1.74	6.05	0.97	2.09	[4.16]
	338.71	8	4.47	4.11	2.81	5.32	[4.16]
	366.32	4	1.66	1.82	1.62	0.29	[4.16]
overall		**42**	**2.05**	**4.91**	**1.22**	**2.66**	
(N_2 + C_3H_8)	230.00	9	0.75	5.69	0.49	2.82	[4.17]
	260.00	10	1.87	7.28	0.88	3.77	[4.17]
	290.00	13	2.32	6.09	1.77	0.50	[4.17]
overall		**32**	**1.74**	**6.35**	**1.13**	**2.17**	
(N_2 + C_3H_6)	260.00	9	1.61	11.31	1.26	0.78	[4.17]
	290.00	11	3.53	6.12	0.97	1.07	[4.17]
overall		**20**	**2.67**	**8.46**	**1.10**	**0.94**	
(H_2 + N_2)	77.35	10	1.38	19.09	1.10	7.79	[4.18]
	90.00	10	3.00	3.69	1.40	3.78	[4.19]
	107.65	8	8.52	5.43	2.30	5.70	[4.19]
	113.00	3	12.85	4.15	3.70	6.53	[4.19]
overall		**31**	**4.86**	**9.15**	**1.76**	**5.84**	

4.5.1. (N_2 + CO_2) mixture

Figures 4.3 and 4.4 show the diagrams of VLE (P-x-y) and y-x for the (N_2 + CO_2) system at different temperatures. The coefficients of equations 4-28 and 4-29 have been presented in table 4.2 at two ranges of temperature for more accurate calculation. These two functions are continuous at 273.15 K. However, parameters α and k are the same for all temperatures.

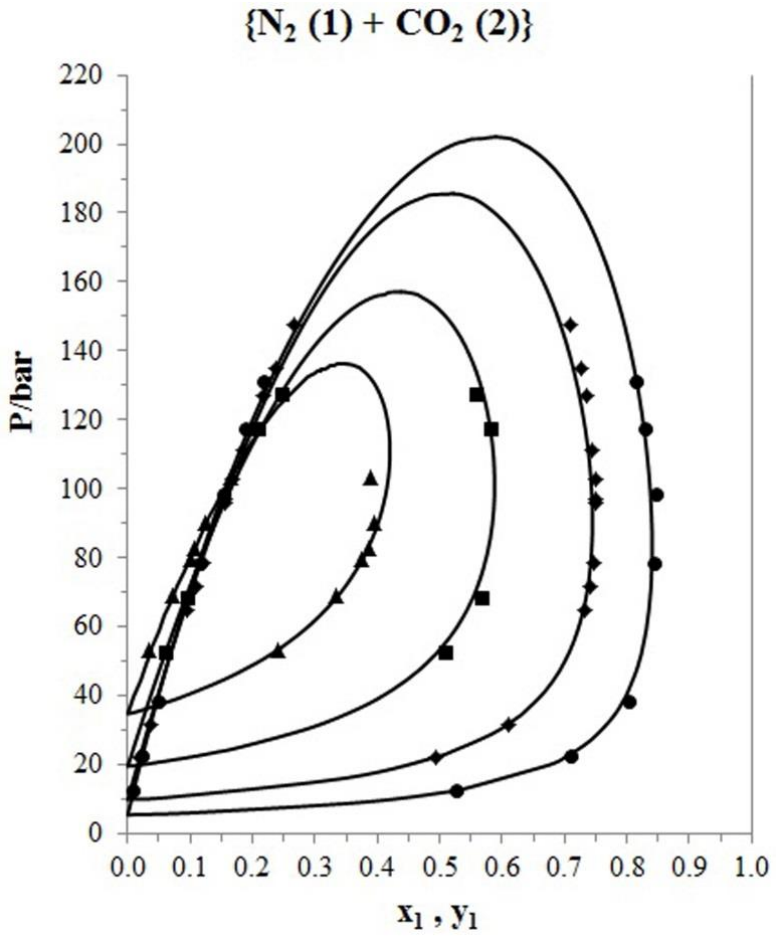

Figure 4.3. The diagram of P-x-y for the (N_2 + CO_2) mixture at different temperatures. The solid lines show the calculated results. Experimental data: • 218.15 K [4.8], ◆ 232.85 K [4.8], ■ 253.15 K [4.10], and ▲ 273.15 K [4.9].

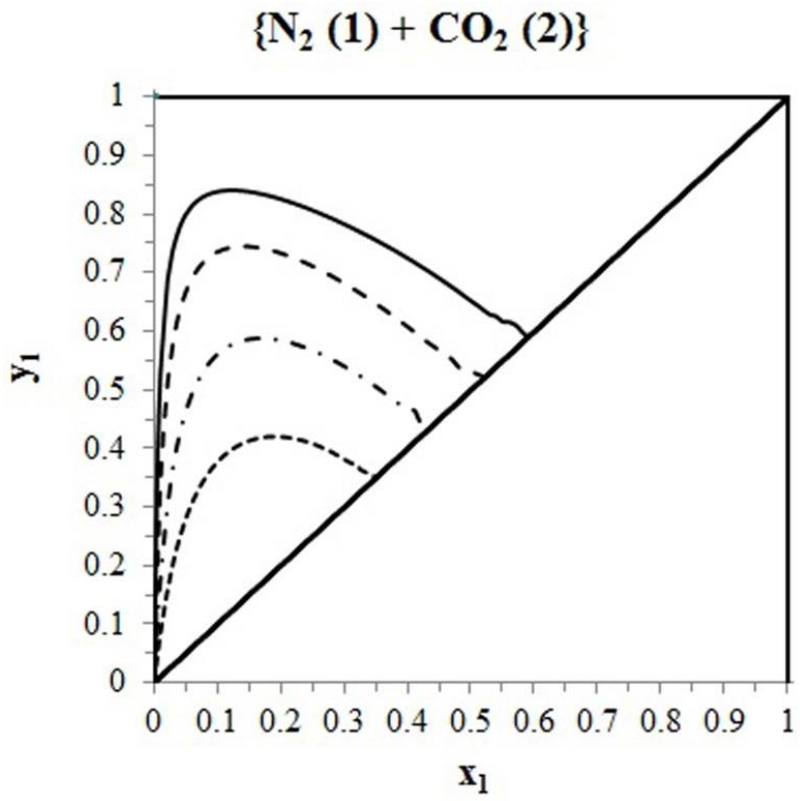

Figure 4.4. The diagram of y-x for N_2 mole fraction in the (N_2 + CO_2) mixture at different temperatures using the PR-WS-NRTL model; —— 218.15 K, ---- 232.85 K, -·-·- 253.15 K, ------- 273.15 K.

VLE at 218.15 K calculated by the WS mixing rule is compared with the VdW mixing rule in figure 4.5. AAD_y and AAD_P of this system at 218.15 K are 4.25% and 8.15% for the VdW mixing rule and 0.9% and 2.27% for this work, respectively. Overall AAD presented in table 4.4 also shows that the results of the WS mixing rule are more accurate than calculated data by the VdW mixing rule. The locus of the critical points for (N_2 + CO_2) system has been shown in figure 4.6 at the temperature range of 218.15 K to 304.12 K.

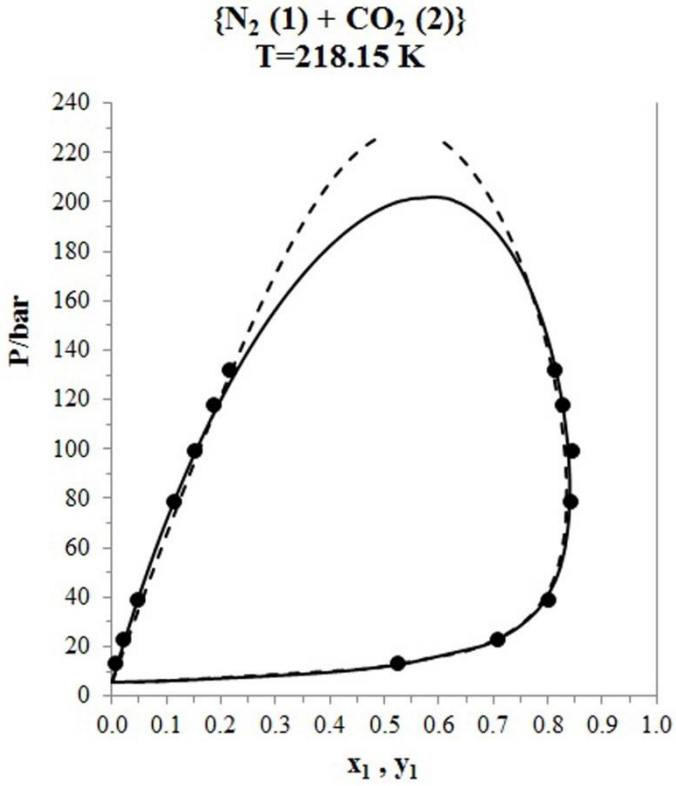

Figure 4.5. The diagram of P-x-y for the (N_2 + CO_2) mixture at 218.15 K calculated by the WS mixing rule (solid line) and VdW mixing rule (dash line). For the WS mixing rule: AAD_y=0.9%, AAD_P =2.27%; for the VdW mixing rule: AAD_y=4.25%, AAD_P =8.15%.

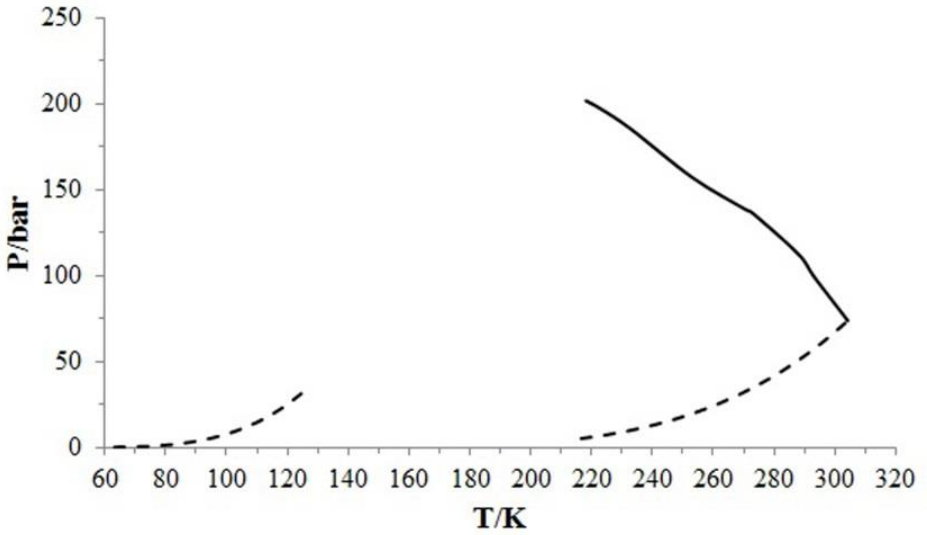

Figure 4.6. The locus of critical points of the (N_2 + CO_2) system using the PR-WS-NRTL model. The dash lines show vapor-pressure curves for pure nitrogen and carbon dioxide.

4.5.2. (CH_4 + CO_2) mixture

For the mixture of (CH_4 + CO_2), the best fitting results a linear function for computing the binary interaction parameter (k_{ij}). Figures 4.7 and 4.8 illustrate the diagrams of P-x-y and y-x for (CH_4 + CO_2) system, respectively. The locus of critical points of this mixture calculated by the present model has been represented by figure 4.9. Overall AAD_y and AAD_P for this system are 2.55% and 0.79% using the PR-WS-NRTL model; however, they are obtained 3.40% and 1.53% by the VdW mixing rule.

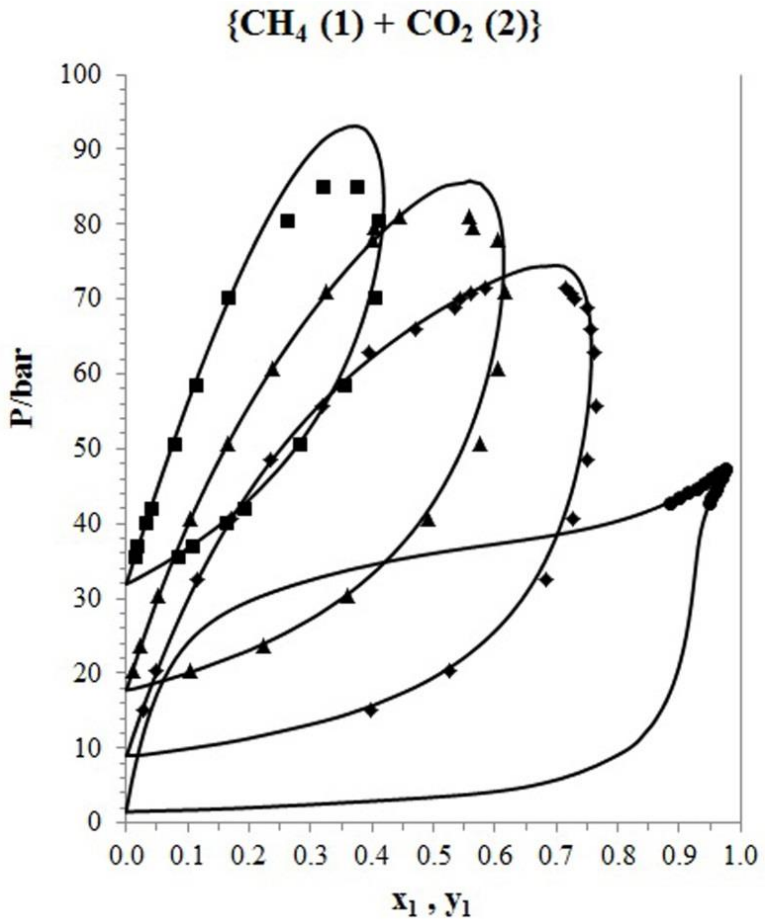

Figure 4.7. The diagram of P-x-y for the (CH_4 + CO_2) mixture at different temperatures. The solid lines show the calculated results. Experimental data: • 193.15 K [4.11], ◆ 230K [4.12], ▲ 250 K [4.12], and ■ 270 K [4.12].

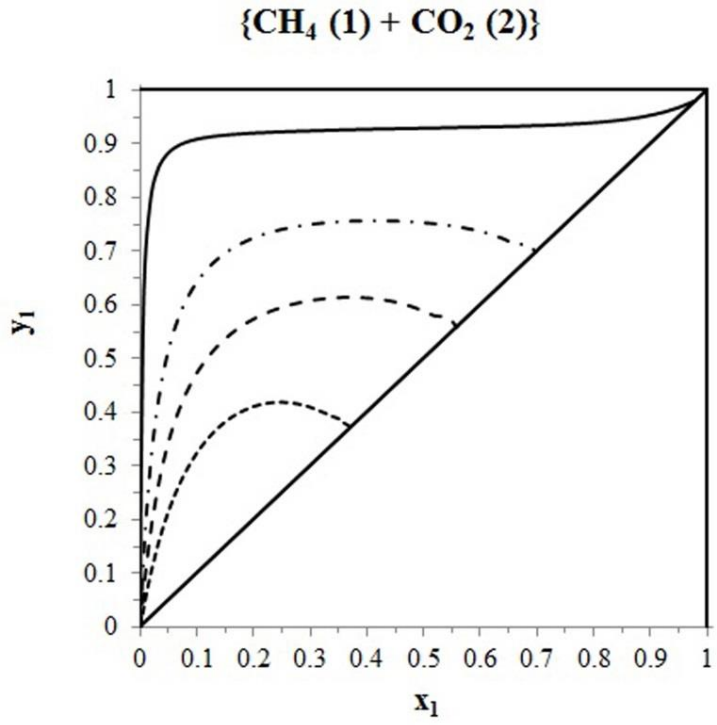

Figure 4.8. The diagram of y-x for CH_4 mole fraction in the (CH_4 + CO_2) mixture at different temperatures using the PR-WS-NRTL model; ——193.15 K, – · –230 K, - - - -250 K, ------- 270 K.

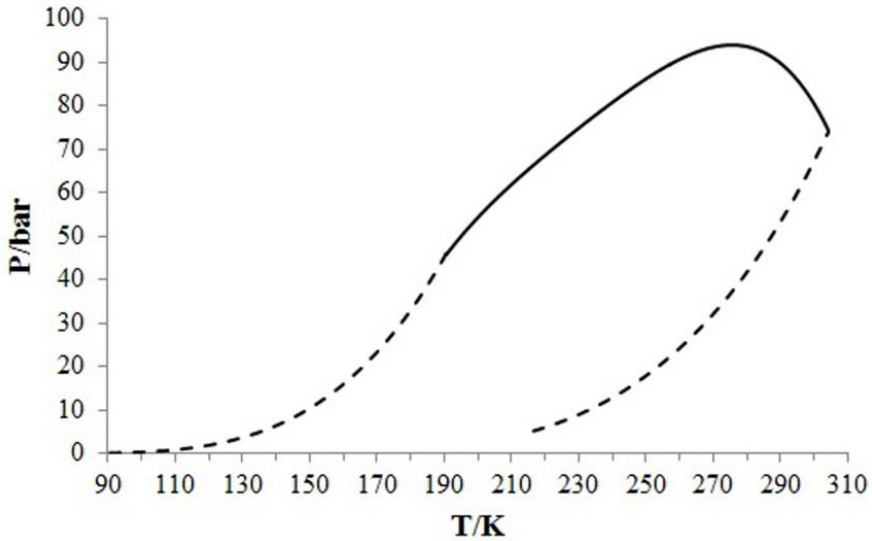

Figure 4.9. The locus of critical points of the (CH_4 + CO_2) system using the PR-WS-NRTL model. The dash lines show vapor-pressure curves for pure methane and carbon dioxide.

4.5.3. (CH_4 + C_2H_4) mixture

Figures 4.10 and 4.11 demonstrate the phase diagrams of (CH_4 + C_2H_4) at different temperatures. Considering two temperature ranges results better fitting for calculation of τ_{ij} for the (CH_4 + C_2H_4) system. But the parameter k_{ij} of the WS mixing rule can be satisfied by one linear function for all temperatures. Using the PR-WS-NRTL model, average AAD_y and AAD_P for this system are calculated 0.64% and 1.14%; however, they are obtained 0.94% and 1.69% by the VdW mixing rule. The locus of critical points of (CH_4 + C_2H_4) mixture calculated by the PR-WS-NRTL model has been shown by figure 4.12.

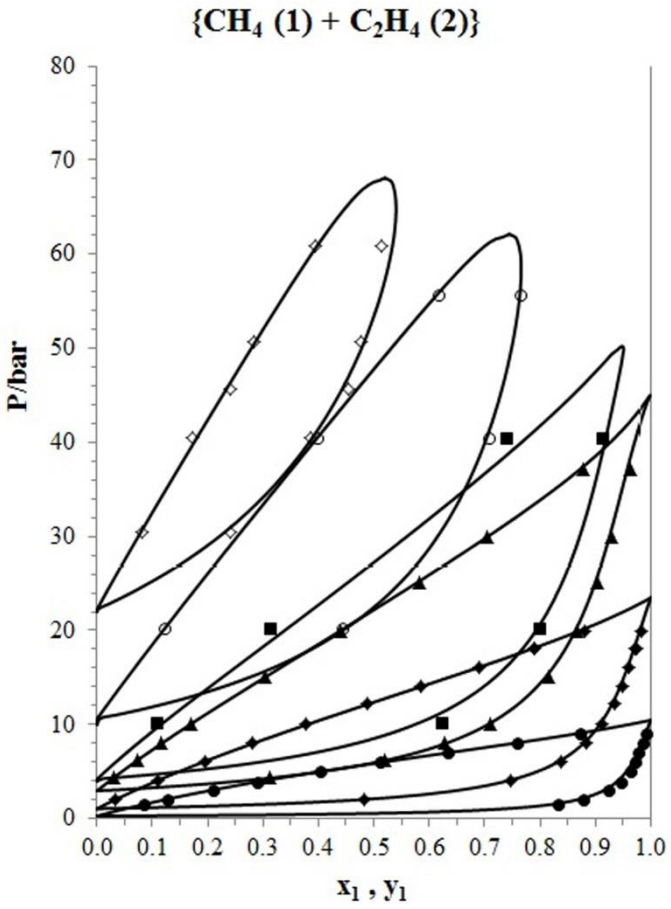

Figure 4.10. The diagram of P-x-y for the (CH_4 + C_2H_4) mixture at different temperatures. The solid lines show the calculated results. Experimental data: • 150 K [4.14], ◆ 170 K [4.14], ▲ 190 K [4.14], ■ 198.15 K [4.15], ○ 223.15 K [4.15], ◇ 248.15 K [4.15].

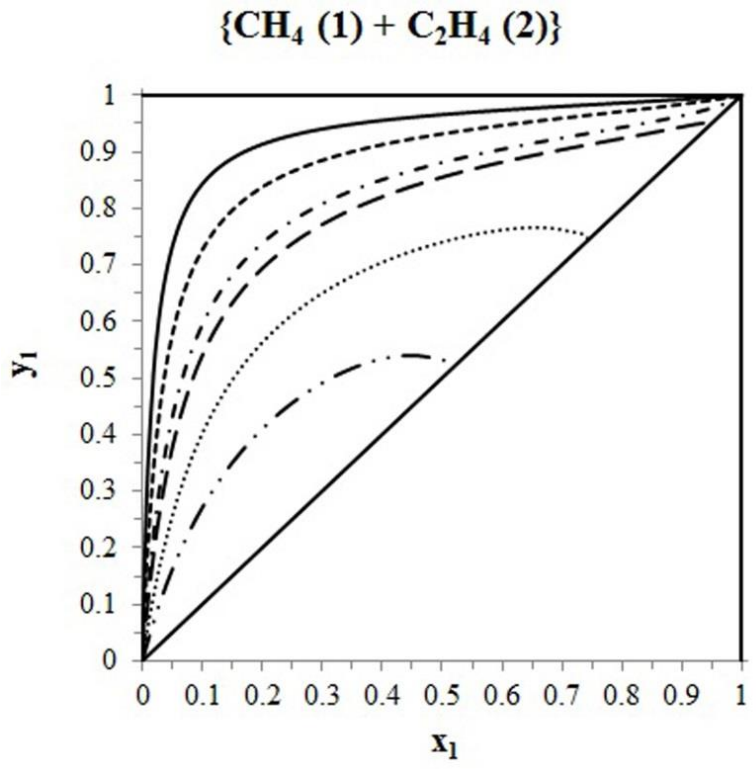

Figure 4.11. The diagram of y-x for CH_4 mole fraction in the (CH_4 + C_2H_4) mixture at different temperatures using the PR-WS-NRTL model; —— 150 K, ------- 170 K, —·— 190 K, - - - - 198.15 K, ... 223.15 K, —··— 248.15 K.

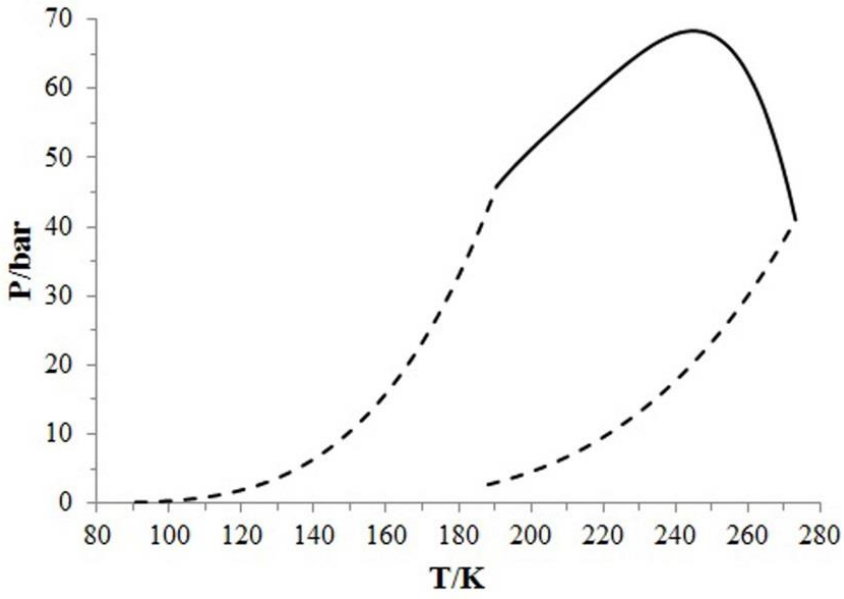

Figure 4.12. The locus of critical points of the (CH_4 + C_2H_4) system using the PR-WS-NRTL model. The dash lines show vapor-pressure curves for pure methane and ethylene.

4.5.4. (N_2 + C_3H_6) mixture

VLE and y-x diagrams of (N_2 + C_3H_6) system has been shown in figure 4.13 and 4.14, respectively. For this mixture, optimization of OF results that the binary interaction parameter can be neglected (k_{ij}=0).

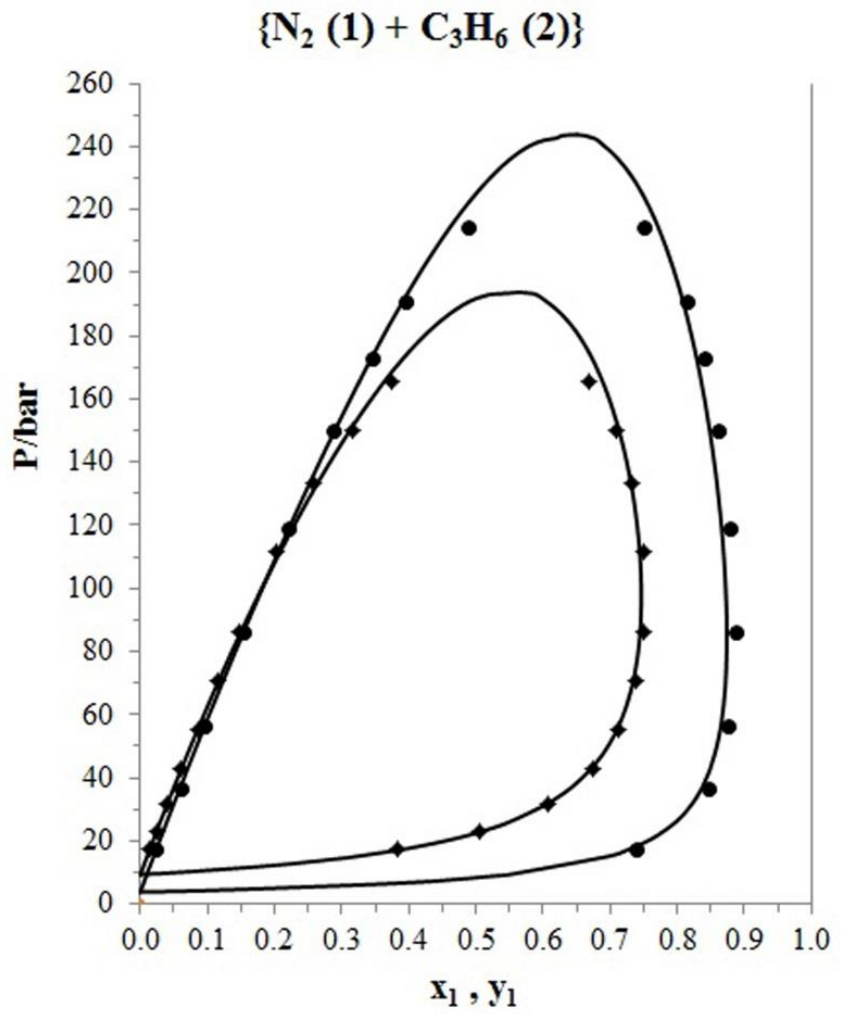

Figure 4.13. The diagram of P-x-y for the (N_2 + C_3H_6) mixture at different temperatures. The solid lines show the calculated results. Experimental data: • 260 K [4.17], ◆ 290 K [4.17].

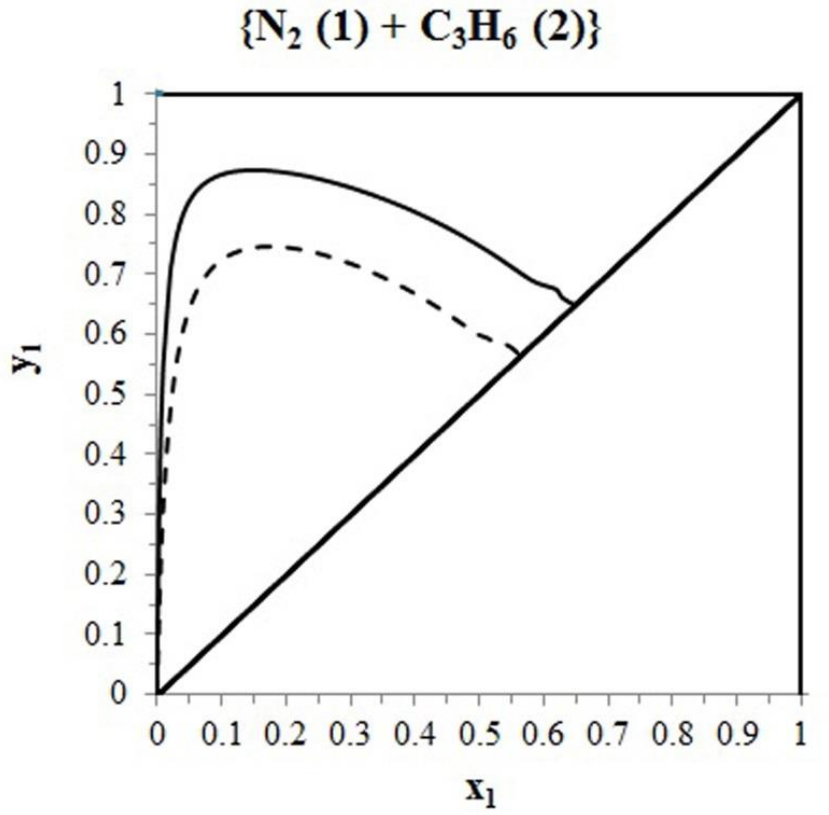

Figure 4.14. The diagram of y-x for N_2 mole fraction in the (N_2 + C_3H_6) mixture at different temperatures using the PR-WS-NRTL model; —— 260 K, ---- 290 K.

Overall AAD_P of (N_2 + C_3H_6) system using the VdW mixing rule is 8.46%; however, the result obtained from the PR-WS-NRTL model is 0.94% for this mixture and show better agreement compared to the VdW mixing rule. For example, figure 4.15 shows the difference between calculated data using the VdW mixing rule and this study for (N_2 + C_3H_6) system at 260 K. For this mixture, AAD_P is 0.78% using the PR-WS-NRTL model and shows better fitting compared to the VdW mixing rule with AAD_P =11.31%. Figure 4.16 demonstrates the locus of critical points of (N_2 + C_3H_6) system using the present model.

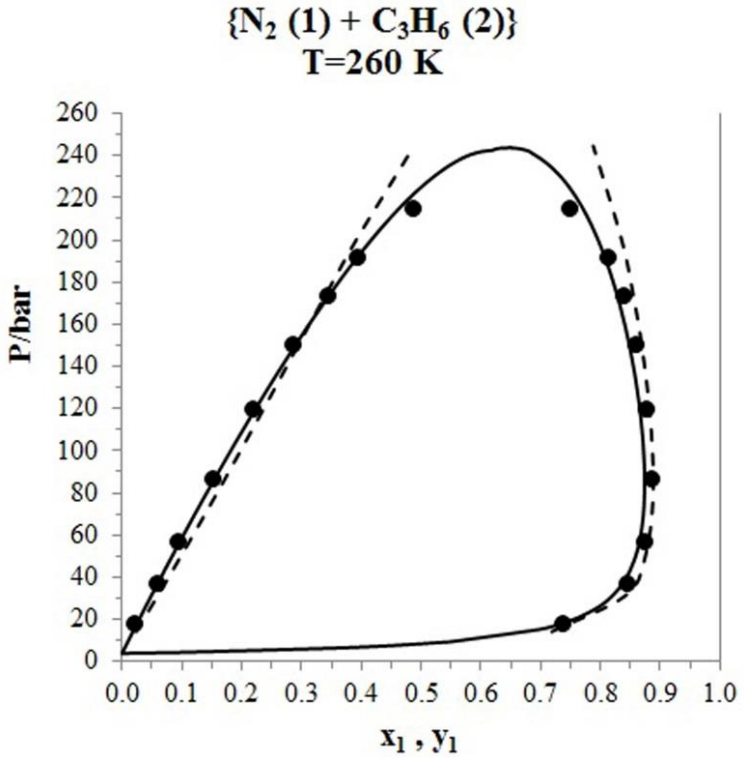

Figure 4.15. The diagram of P-x-y for the (N_2 + C_3H_6) mixture at 260 K calculated by the WS mixing rule (solid line) and VdW mixing rule (dash line). For the WS mixing rule: AAD_y=1.26%, AAD_P =0.78%; for the VdW mixing rule: AAD_y=1.61%, AAD_P =11.31%.

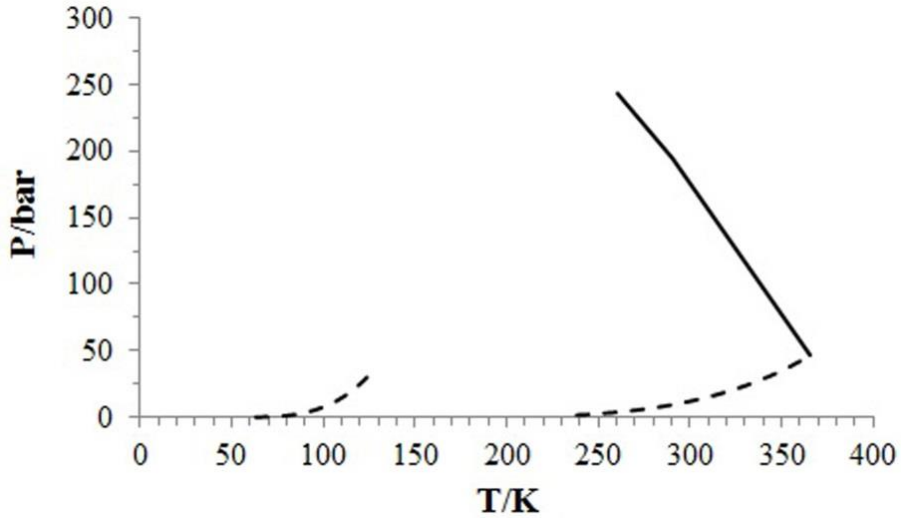

Figure 4.16. The locus of critical points of the (N_2 + C_3H_6) system using the PR-WS-NRTL model. The dash lines show vapor-pressure curves for pure nitrogen and propylene.

3.5.5. (N_2 + C_3H_8) mixture

Figures 4.17 and 4.18 show the figures of P-x-y and y-x for (N_2 + C_3H_8) mixture at various temperatures. Average AAD_P of (N_2 + C_3H_8) system using the PR-WS-NRTL model is 2.17% compared to the result obtained from the VdW mixing rule with AAD_P=6.35%. Figure 4.19 illustrates the locus of critical points of (N_2 + C_3H_8) mixture using the PR-WS-NRTL model.

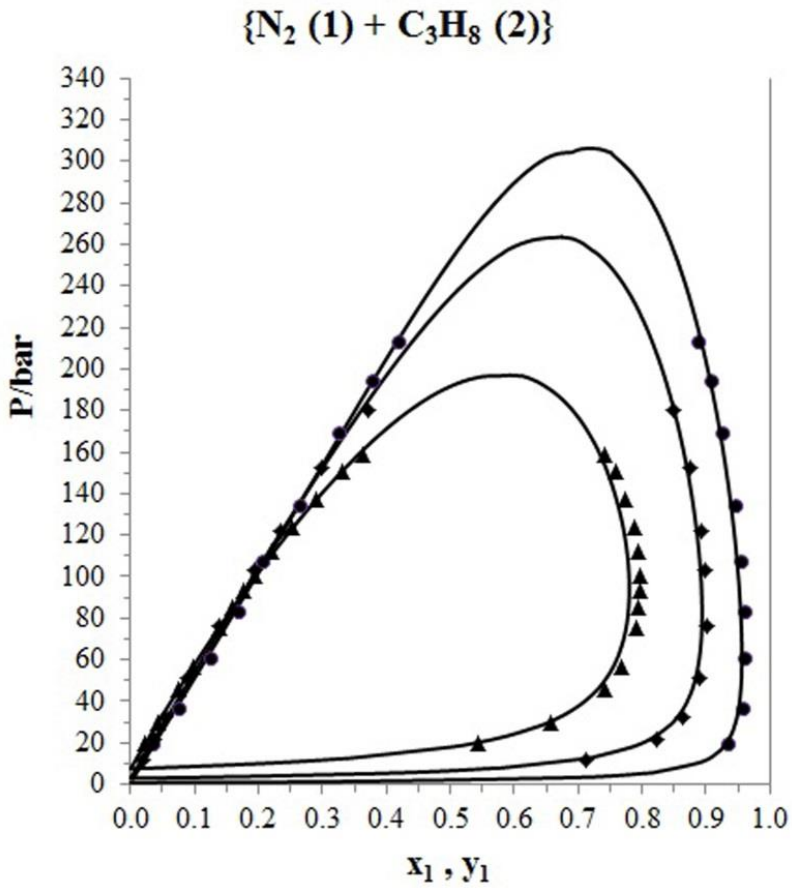

Figure 4.17. The diagram of P-x-y for the (N_2 + C_3H_8) mixture at different temperatures. The solid lines show the calculated results. Experimental data: • 230 K [4.17], ◆ 260 K [4.17], ▲ 290 K [4.17].

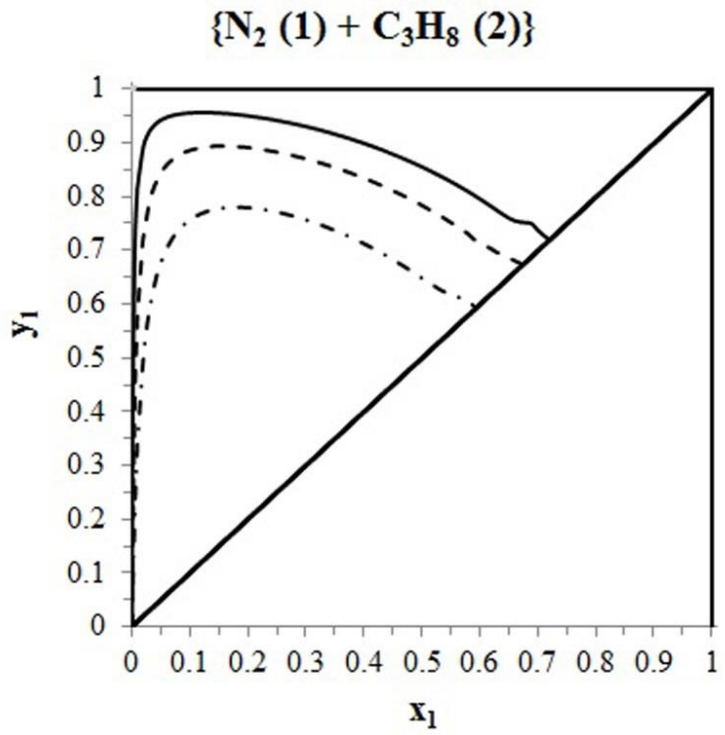

Figure 4.18. The diagram of y-x for N_2 mole fraction in the (N_2 + C_3H_8) mixture at different temperatures using the PR-WS-NRTL model; —— 230 K, - - - - 260 K,- - - - 290 K.

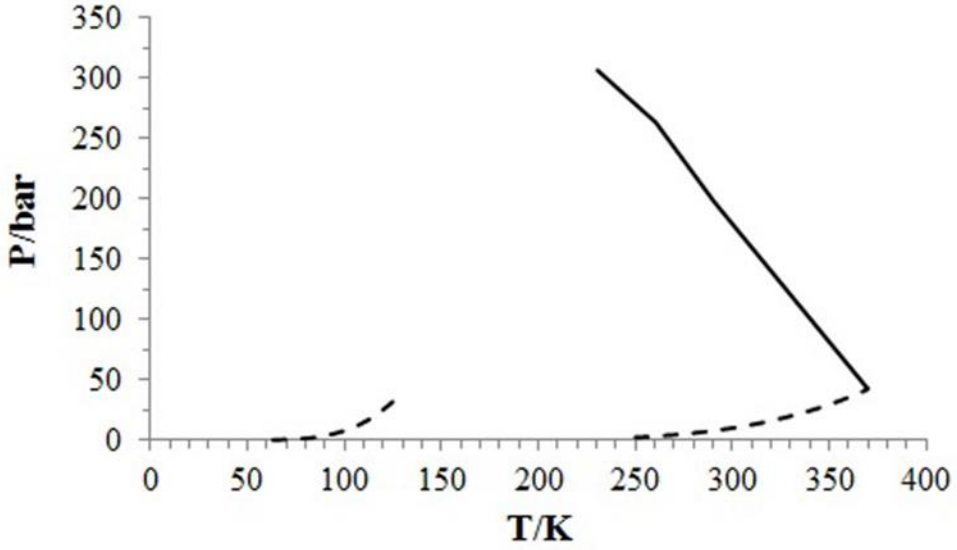

Figure 4.19. The locus of critical points of the (N_2 + C_3H_8) system using the PR-WS-NRTL model. The dash lines show vapor-pressure curves for pure nitrogen and propane.

4.5.6. (N_2 + C_4H_{10}) mixture

Figures 4.20 and 4.21 illustrate the diagrams of VLE and y-x for (N_2 + C_4H_{10}) at the range of 255.37 K-366.32 K. Overall AAD_y and AAD_P have been calculated 1.22% and 2.66%, respectively using the WS mixing rule and shows the PR-WS-NRTL model is more accurate than the VdW mixing rule with overall AAD_y=2.05% and AAD_P=4.91%. For instance, figure 4.22 shows that experimental data can be fitted by the WS and VdW mixing rules at 310.87 K. AAD_y and AAD_P of this system calculated by the present model are 0.97% and 2.09% compared to 1.74% and 6.05% for the VdW mixing rule. The locus of critical points of (N_2 + C_4H_{10}) system is shown in figure 4.23 using the present model at T=(283-408) K.

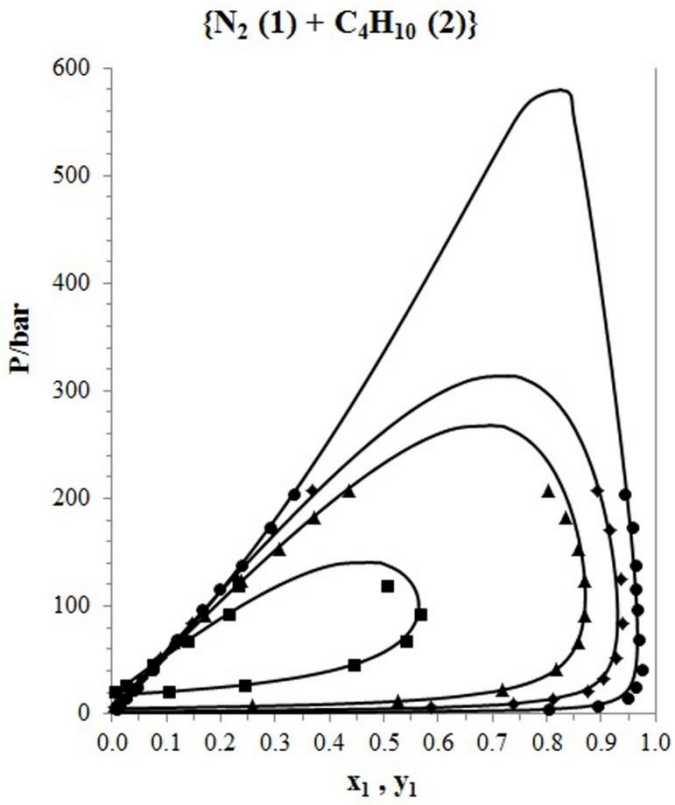

Figure 4.20. The diagram of P-x-y for (N_2 + C_4H_{10}) mixture at different temperatures. The solid lines show the calculated results. Experimental data: • 255.37 K [4.16], ◆ 283.21 [4.16], ▲ 310.87 K [4.16], ■ 366.32 K [4.16].

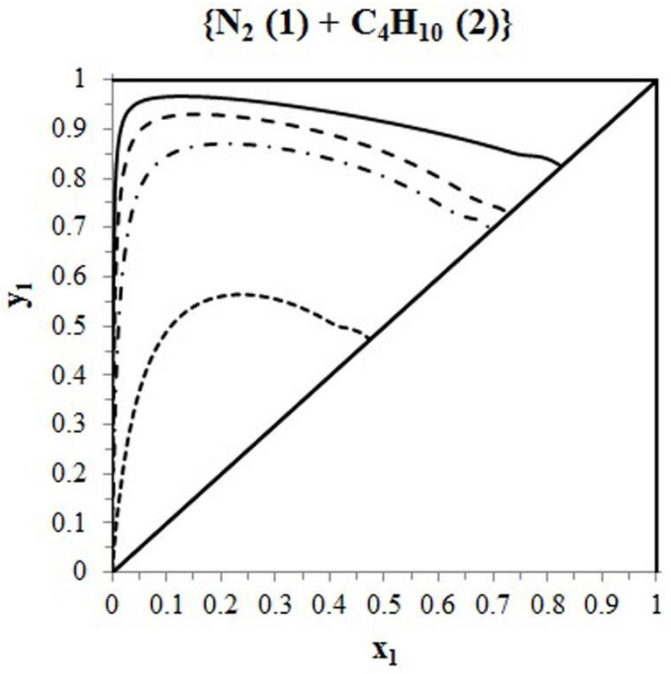

Figure 4.21. The diagram of y-x for N_2 mole fraction in the (N_2 + C_4H_{10}) mixture at different temperatures using the PR-WS-NRTL model; —— 255.37 K, - - - - - 283.21 K, - · - · - 310.87 K, -------366.32 K.

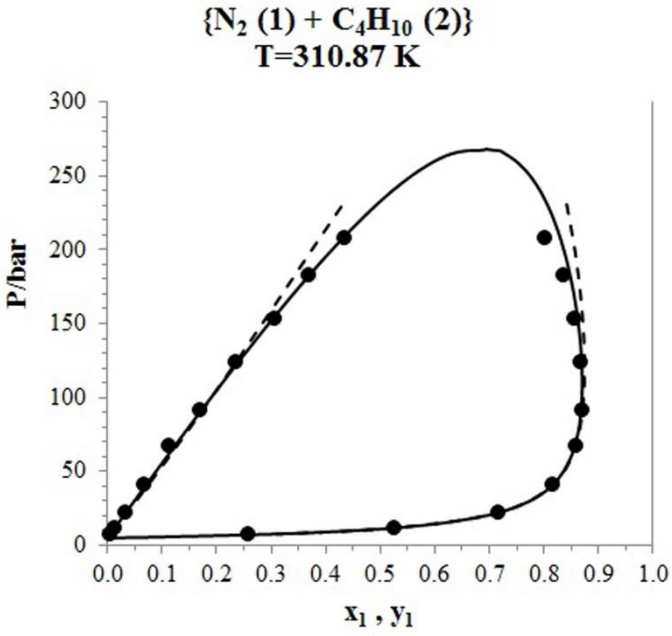

Figure 4.22. The diagram of P-x-y for (N_2 + C_4H_{10}) mixture at 310.87 K calculated by the WS mixing rule (solid line) and VdW mixing rule (dash line). For the WS mixing rule: AAD_y=0.97%, AAD_P =2.09%; for the VdW mixing rule: AAD_y=1.74%, AAD_P =6.05%.

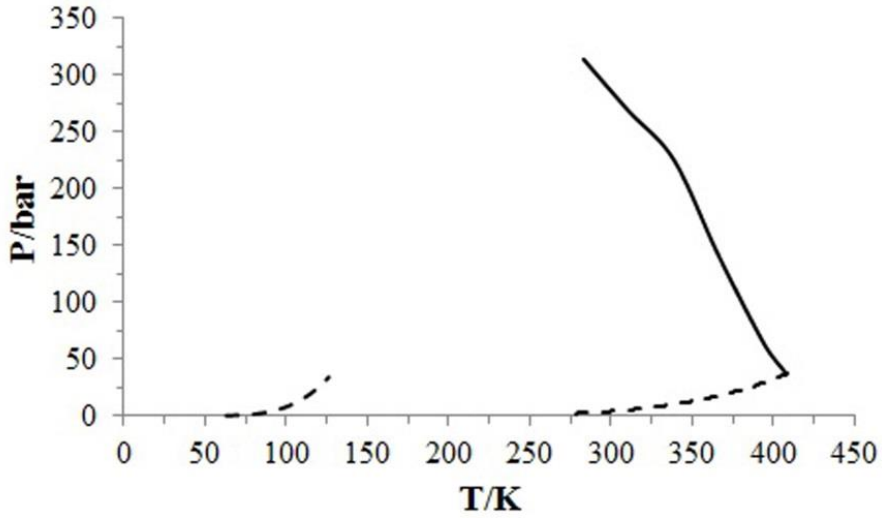

Figure 4.23. The locus of critical points of the (N_2 + C_4H_{10}) system using the PR-WS-NRTL model. The dash lines show vapor-pressure curves for pure nitrogen and isobutane.

4.5.7. (H_2 + N_2) mixture

VLE diagram of (H_2 + N_2) mixture at 77.35 K has been presented in figure 4.24 for both models. AAD_P is obtained 19.09% using the VdW mixing rule. However, the PR-WS-NRTL shows better agreement with experimental data and AAD_P is computed 7.79% using the WS mixing rule. Figures 4.25 and 4.26 demonstrate the diagrams of VLE and y-x for (H_2 + N_2) system using the present model at various temperatures. For this mixture, the present model has overall AAD_y=1.76% and AAD_P =5.84%; while overall AAD_y and AAD_P are calculated 4.86 and 9.15 using the VdW mixing rule. At T=(77-126) K, figure 4.27 shows the locus of critical points of (H_2 + N_2) system using the PR-WS-NRTL model.

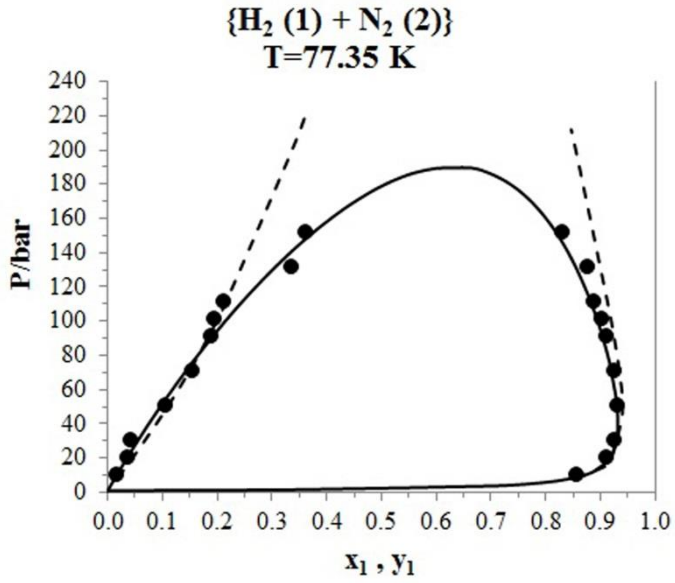

Figure 4.24. The diagram of P-x-y for (H_2 + N_2) mixture at 77.35 K calculated by the WS mixing rule (solid line) and VdW mixing rule (dash line). For the WS mixing rule: AAD_y=1.10%, AAD_P =7.79%; for the VdW mixing rule: AAD_y=1.38%, AAD_P =19.09%.

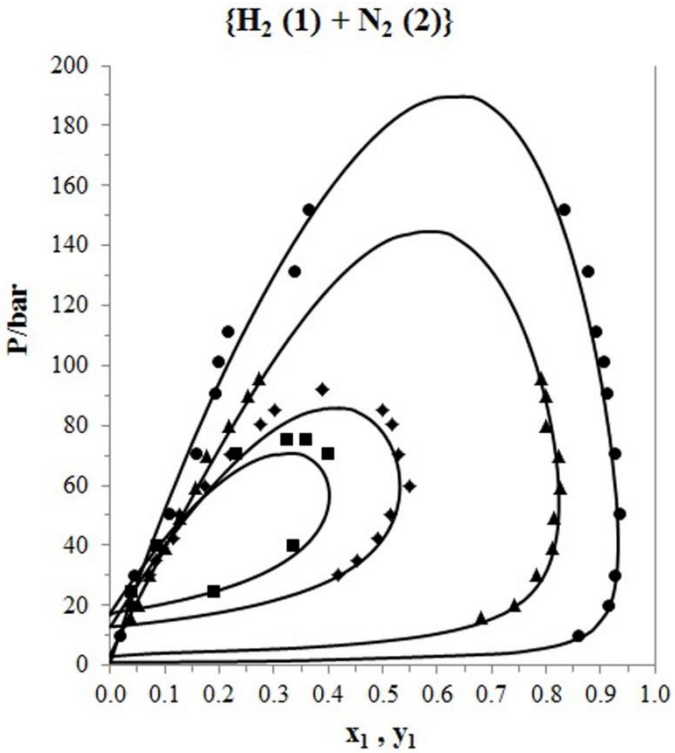

Figure 4.25. The diagram of P-x-y for (H_2 + N_2) mixture at different temperatures. The solid lines show the calculated results. Experimental data: • 77.35 K [4.18], ▲ 90 K [4.19], ◆ 107.65 [4.19], ■ 113 K [4.19].

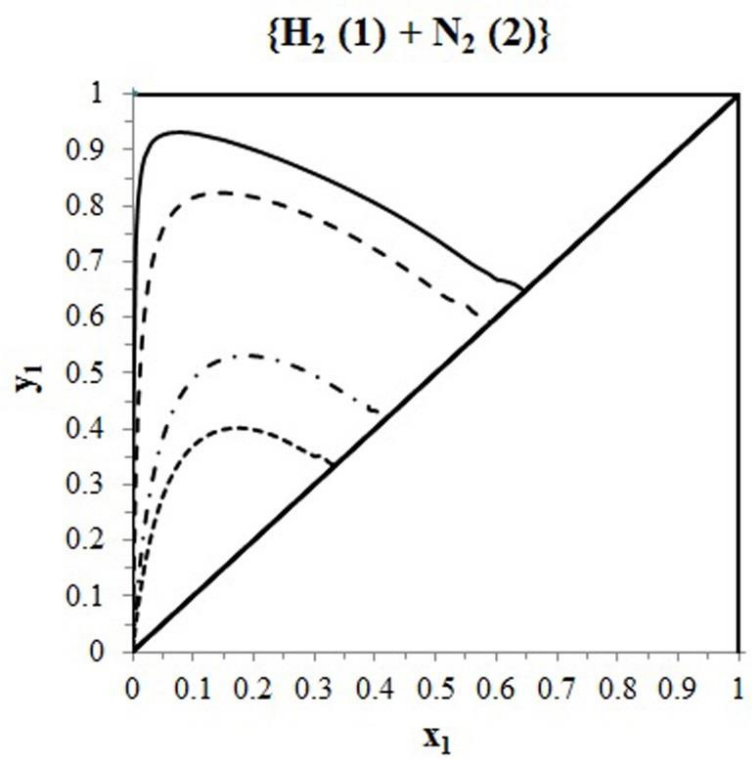

Figure 4.26. The diagram of y-x for N_2 mole fraction in the (H_2 + N_2) mixture at different temperatures using the PR-WS-NRTL model; ——77.35 K, - - -90 K, - · - · -107.65 K, ------- 113 K.

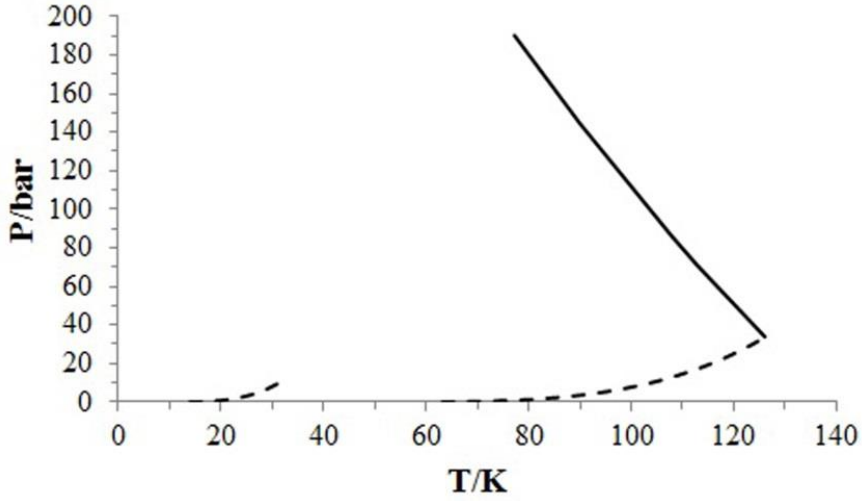

Figure 4.27. The locus of critical points of the (H_2 + N_2) system using the PR-WS-NRTL model. The dash lines show vapor-pressure curves for pure hydrogen and nitrogen.

ꦲꦔꦶꦪꦺꦴꦲꦔꦶꦪꦺꦴꦫ꧀
ꦲꦔꦶꦪꦺꦴꦫ꧀
ꦲꦫ꧀
✵

CHAPTER FIVE

5

Separation of N_2/CO_2 Mixture Using A Continuous High-pressure Density-driven Separator[3]

5.1. Experimental

Combustion of fuel using air as an oxidant creates a mixture of (primarily) N_2 and CO_2. This is true for conventional combustion, as well as for SCWO. However, in the latter case, the N_2/CO_2 mixture is produced at high pressure (> 22 MPa). We had investigated N_2/CO_2 separation at high-pressure on a batch basis in previous work [5.1].

Figure 5.1 shows the densities of pure N_2 and CO_2 at various pressure and 25 °C. At high pressure (> 80 bar), there is a large difference between the densities of pure N_2 and CO_2. Therefore, we note that the density difference at high pressure can be a driving force for separation of the N_2/CO_2 mixture.

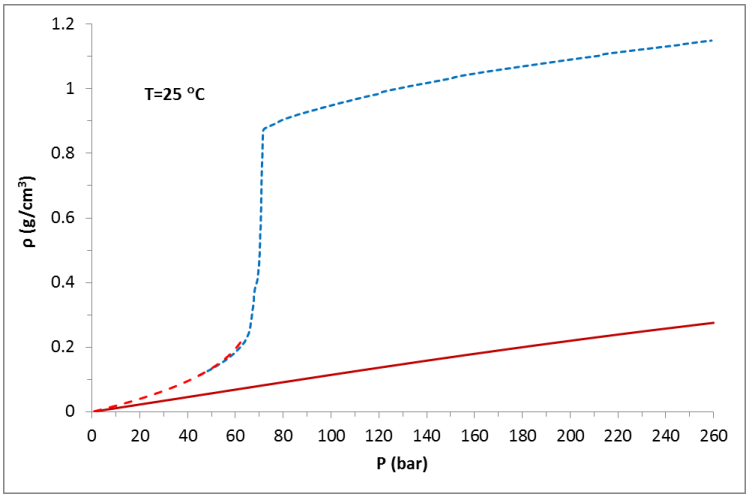

Figure 5.1. Densities of pure N_2 and pure CO_2 against pressure at 25 °C. —— Density of N_2 at 1-260 bar calculated by the PR EOS; - - - - - density of pure CO_2 at 1-63 bar calculated by the PR EOS; ..... density of pure CO_2 at 45-260 bar measured at our lab.

[3] This chapter has been published under the following citation:
R. Espanani, A. Miller, A. Busick, D. Hendry, W. Jacoby; "Separation of N2/CO2 Mixture Using A Continuous High-pressure Density-driven Separator"; *Journal of CO2 Utilization* 14 (2016) 67-75.

Here, we describe separation of the mixture on a continuous basis using a high-pressure, density-driven separator (HDS). We explore the effects of process parameters such as pressure, flow rate and separator geometry. We also define a new dimensionless parameter that accurately defines separator performance thereby informing process and equipment design.

5.1.1. Chemicals

High pressure cylinders of nitrogen and carbon dioxide were used for experiments. The high-quality of N_2 (minimum purity=99.9993%) and CO_2 (minimum purity=99.999%) were purchased from Airgas® (USA) and mixed to prepare the mixture of N_2/CO_2 containing 15 mol% of CO_2.

5.1.2. Experimental apparatus

Figure 5.2 shows the schematic diagram of the experimental apparatus used for this work. A continuous High-pressure Density-driven Separator (HDS) made from stainless steel 316 (extra-thick wall pipe, schedule 160) is the main part of the apparatus. The inner diameter and length of the cylindrical separator are 4.3 cm and 86.4 cm with volume of 1245 cm^3 (figures 5.3, 5.4). Two identical systems are used to pressurize and meter N_2 and CO_2 into the system. Each system uses two syringe pumps (figure 5.5) from Teledyne Isco (model 260D, USA). Each pump has capacity of 266 cm^3 and is designed for flow rate of 0.001-107 cm^3/min with flow accuracy of 0.5% of set point and pressure capacity of 0-7500 psi (0-517 bar). A digital controller (figure 5.6) allows the dual-pump systems to deliver non-stop continuous flow of both species at the prescribed volumetric

rate and pressure (and ambient temperature). Pure species mass flow rates are calculated using the Peng Robinson equation of state (PR EOS).

Pure N_2 and CO_2 are mixed together in the mixing tee. Two observations indicate good mixing. First, the mixing tee temperature decreases as a result of the evaporation of liquid CO_2. Second, certain data points reported below show no separation. Although the Reynolds number in the mixing tee is less than 2600, the vapor also passes through a check valve and a needle valve where the flow is turbulent. Since the vapor species are fully miscible and possess high kinetic energy, a homogeneous solution is formed.

The mixture flows into the HDS through the inlet tube (figure 5.7). The length of the inlet tube (L) determines the inlet point of N_2/CO_2 mixture. The longer the inlet tube, the greater the distance between the entrance port and the exit port. This is an important variable in this study.

On the outlet streams, there are two back-pressure regulators (BPRs). Function of the BPRs is to provide an obstruction to flow and regulate pressure in the HDS. The BPRs were purchased from Tescom Corporation and work at 0-6000 psi (0-408 bar). Pressure and temperature of the HDS are specified by the pressure indicator (figure 5.4) from Ashcroft (designed up 10000 psi) and the temperature detector (figure 5.8) from Extech Instruments (SD200).

Concentration of CO_2 is monitored by the CO_2 detector (figure 5.9) from Vaisala CARBOCAP® (model: GMM221). It is designed to operate in the range between 0-20%. The accuracy of the calibration was determined empirically, and is discussed in section 2.4. Finally, the downstream flow rate from both ports (lines B and C) can be measured by the dry test meter (figure 5.10) from Elster American Meter (DTM-200A). The combined volumetric flow rate of these ambient pressure vapor streams is converted to

molar and mass flow rates using the ideal gas law. This calculation confirms the estimates of inlet flow rates from the Peng-Robinson EOS, which is the basis for our calibration.

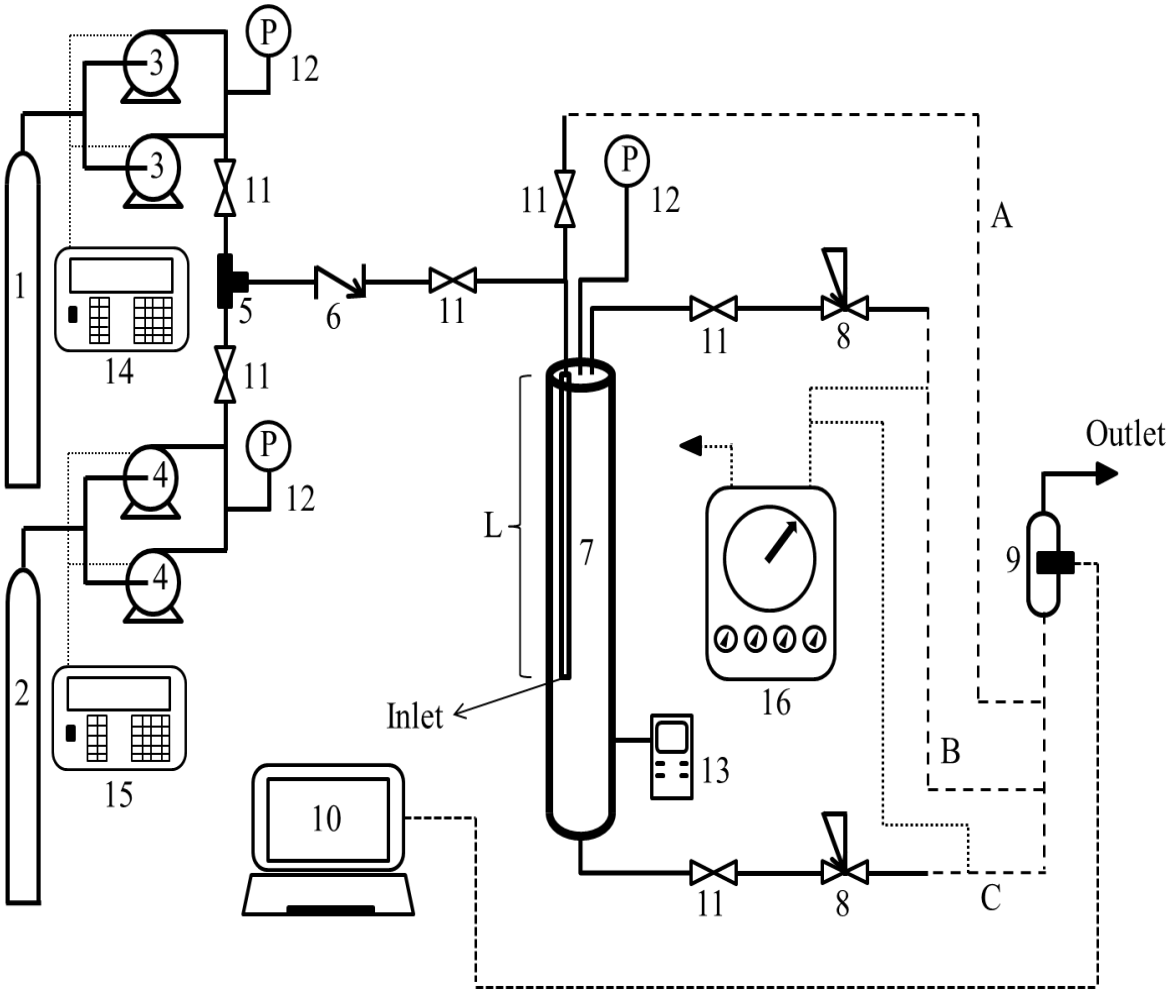

Figure 5.2. Schematic diagram of the experimental apparatus: (1) N_2 tank, (2) CO_2 tank, (3) High pressure syringe pumps of N_2, (4) High pressure syringe pumps of CO_2, (5) Mixing tee, (6) Check valve, (7) HDS, (8) Back-pressure regulators, (9) CO_2 detector, (10) Computer, (11) Valves, (12) Pressure indicators, (13) Temperature indicator, (14) Controller of N_2 pumps, (15) Controller of CO_2 pumps, (16) Flowmeter.

(a) (b)

Figure 5.3. High-pressure, Density-driven Separator (HDS). (a) Before insulation; (b) After insulation.

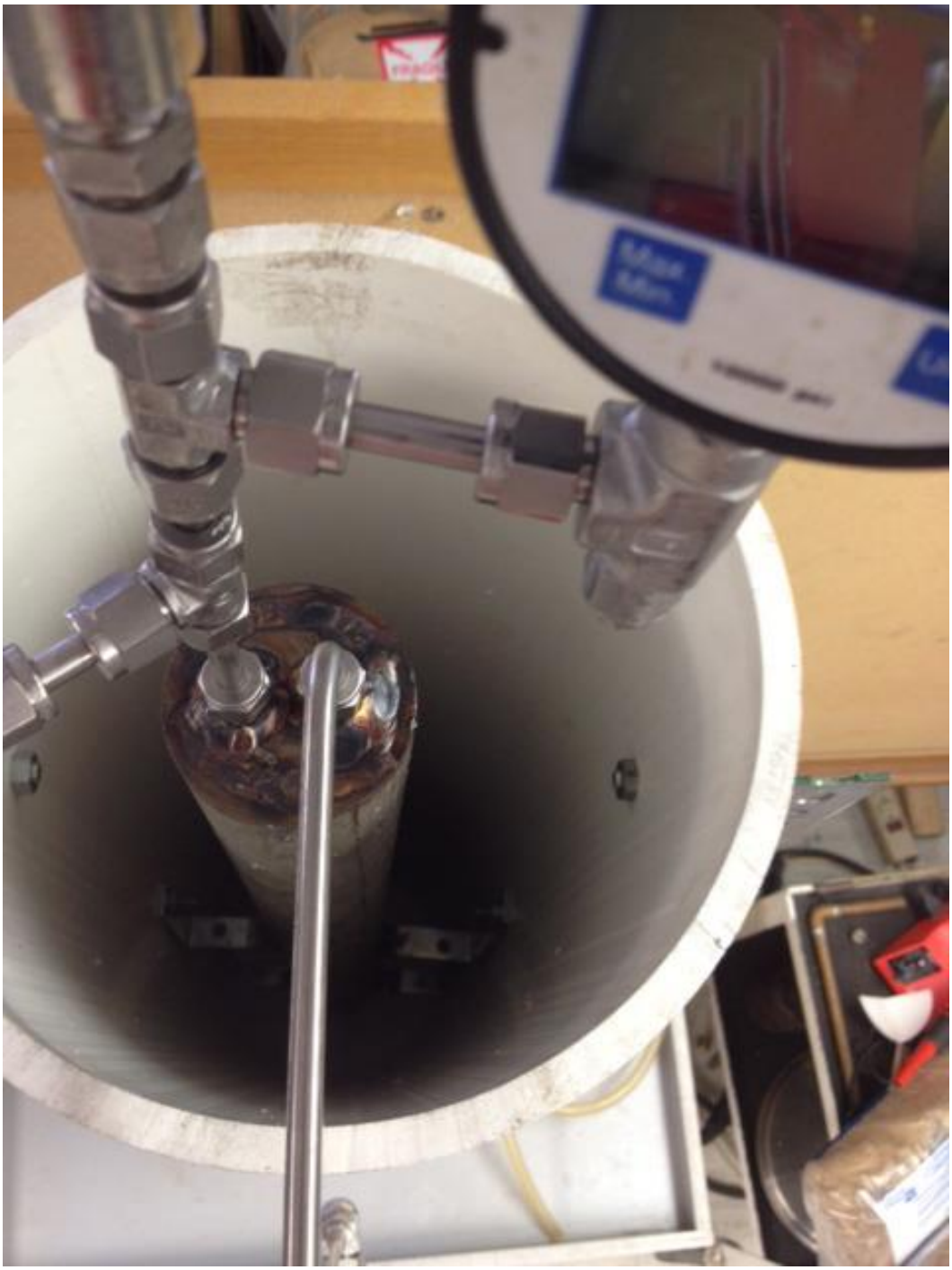

Figure 5.4. High-pressure, Density-driven Separator (HDS) from top. Inlet and outlet streams as well as the pressure indicator are seen in the figure.

(a)

(b)

Figure 5.5. (a) High-pressure syringe pumps; (b) Controller.

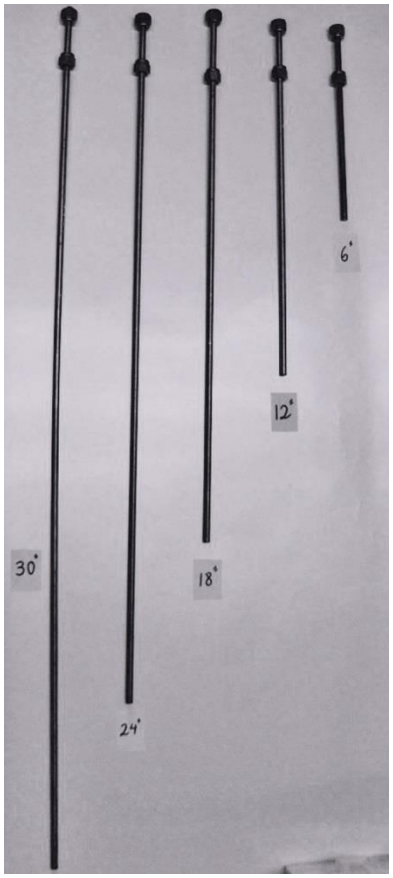

Figure 5.6. L, the inlet position, at different sizes: 15.24, 30.48, 45.72, 60.96, and 76.2 cm.

Figure 5.7. The mixing tee. There is an one-way valve after the mixing tee.

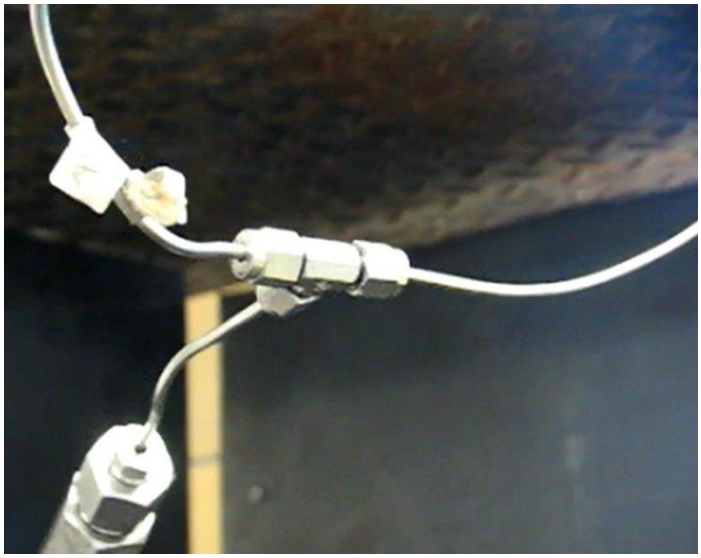

Figure 5.8. The digital temperature indicator.

Figure 5.9. The CO_2 detactor.

Figure 5.10. The dry test meter.

5.1.3. Experimental procedure

Experiments to investigate the separation of N_2/CO_2 solutions at various inlet tube lengths (L), pressures and flow rates were performed by the following procedures. First, the HDS is evacuated. Next, N_2 and CO_2 are metered into the HDS to create an 85%/15% mixture at the desired pressure of system. When the HDS reaches the desired pressure, outlet valves are opened and adjusted to operate the process at constant pressure. In this condition, the temperature of the HDS stabilizes at ambient (25 °C). CO_2 molar concentration downstream of the HDS is monitored at the top or bottom ports by directing streams B or C in figure 5.2 through the CO_2 monitor. The data are compiled on the computer and the results reported below were achieved under steady-state conditions (1-3 hours of operation depending on flow rate).

5.2. Accuracy of the CO_2 detector

The mass flow rates of inlet streams for pure N_2 and CO_2 are controlled independently. They are also accurately estimated using the PR EOS. This provides a basis for calibration of the CO_2 detector. Figure 5.11 shows calibration data taken under continuous flow conditions at 48 bar and ambient temperature. The solid curves are output signals from the CO_2 monitor, and the dashed horizontal lines represent the calculated compositions. Their comparison allows a qualitative assessment of accuracy and precision.

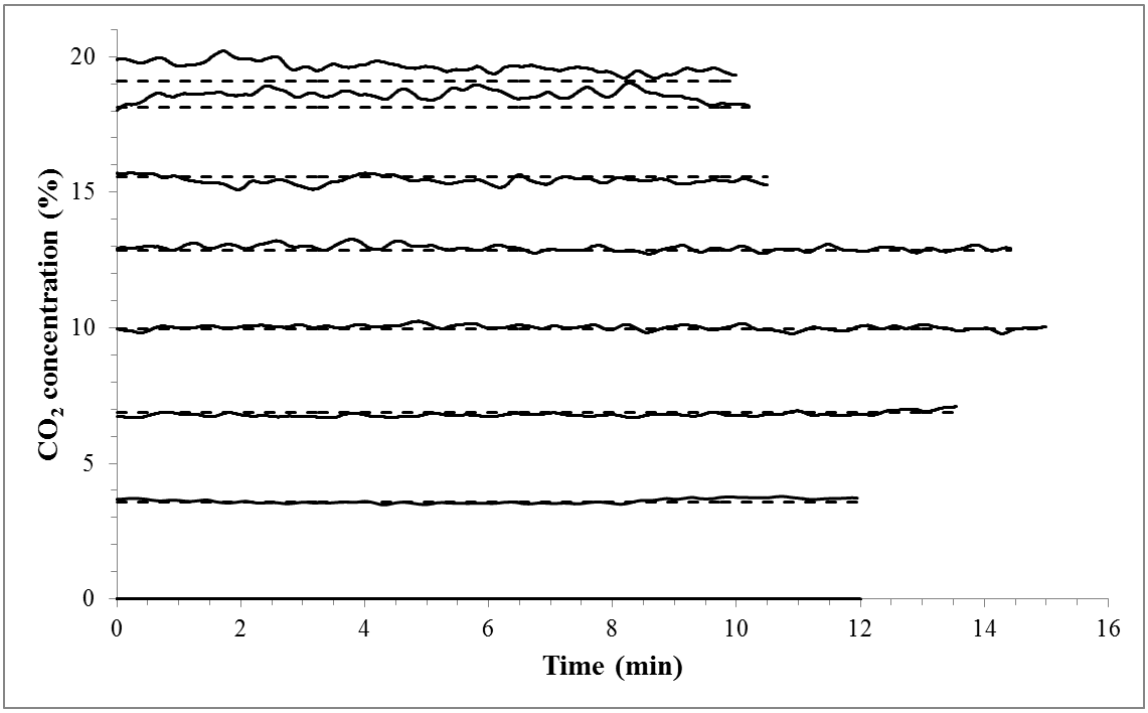

Figure 5.11. Graphs of CO_2 molar concentration detected by CO_2 sensor at steady state condition. The solid curves are output signals from the CO_2 monitor and the dashed lines are the calculated compositions using the PR EOS.

Table 5.1 contains calibration data. It allows calculation of a percentage error at each concentration, which are also tabulated. A more holistic quantitative estimate of accuracy is achieved through linear regression and shown in figure 5.12. The fit is excellent ($R^2 > 0.999$). Also included in figure 4.3 are upper and lower 95% confidence lines generated by the regression analysis. These indicate good precision. However, examination of both figure 5.11 and figure 5.12 shows that the noise increases with the concentration, and this observation is confirmed by the standard deviation estimates for each steady state measurement, also included in table 5.1.

Table 5.1. Measured and calculated parameters from the CO_2 probe.

y_{CO2} (PR EOS)	$y_{CO2, ave}$ (CO_2 probe)	σ (Standard deviation)	Error (%)
0.00000	0.00000	0.000000	0.00
0.03557	0.03607	0.000831	1.41
0.06870	0.06795	0.000772	1.09
0.09962	0.10010	0.000835	0.48
0.12856	0.12939	0.001056	0.64
0.15570	0.15431	0.001378	0.89
0.18119	0.18588	0.001883	2.59
0.19096	0.19629	0.002020	2.79
			Average error=1.24%

The correlation between noise and signal magnitude is mitigated by the fact that the maximum CO_2 concentration in this study is 15%. Further, critical data are taken at high separation efficiency (and correspondingly low CO_2 concentration in stream B) where the monitor is most precise and accurate.

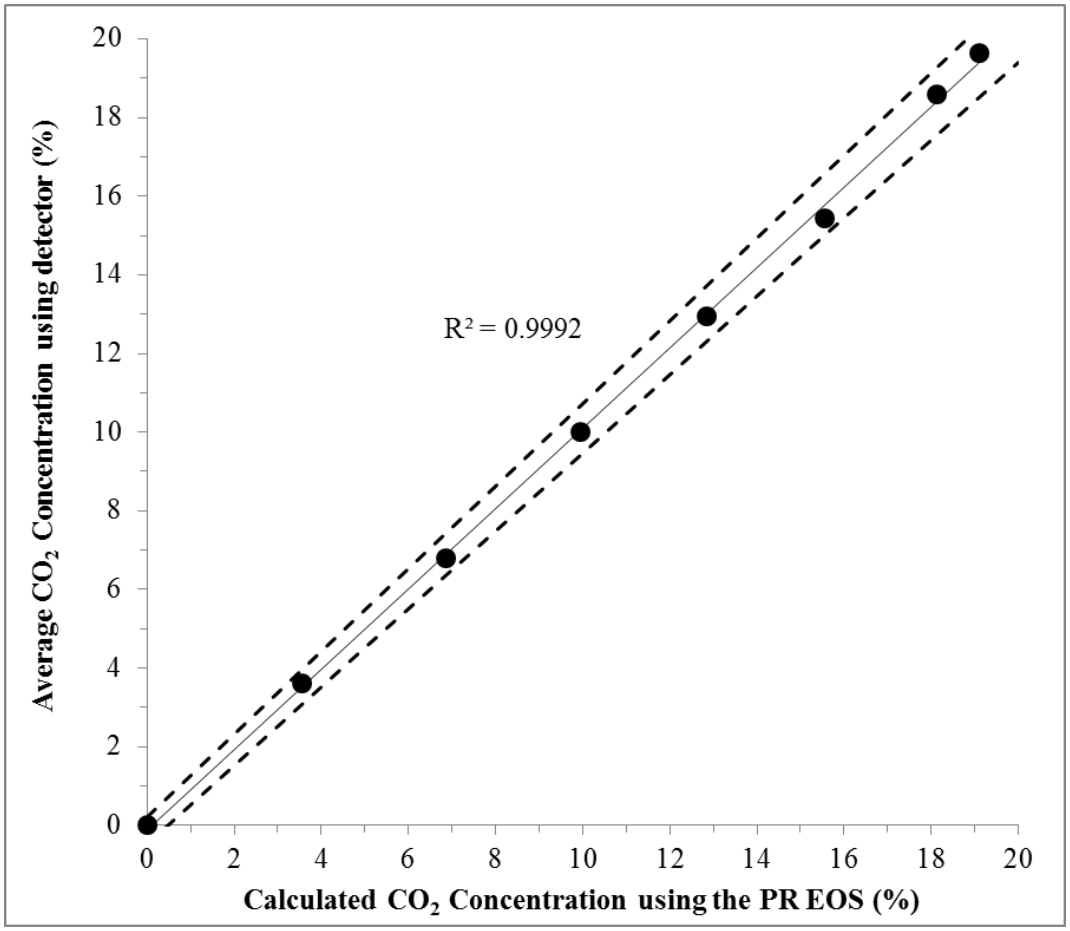

Figure 5.12. The diagram of average CO_2 concentration using the probe vs calculated CO_2 concentration using the PR EOS in the N_2/CO_2 mixture at steady state. The dashed lines are the upper and lower 95% confidence limits.

5.3. Results and Discussion

5.3.1. Effect of Archimedes number

In this study, the steady state separation of the N_2/CO_2 mixture was evaluated using an HDS featuring a variable inlet tube position (L, refer to figures 5.2, 5.5). In all experiments, the molar concentration of CO_2 in the inlet flow is 15% and the continuous separations are carried out at constant temperature of 25 ± 0.3 °C. Pressure and inlet

flow rate are included (along with L) as experimental variables. We studied the effect of these variables on separation efficiency (S).

$$S = \left(\frac{y_{N_2,out} - y_{N_2,in}}{1 - y_{N_2,in}} \right)_{top} \qquad (5-1)$$

In this equation, $y_{N2,in}$ is the N_2 mole fraction in inlet flow and $y_{N2,out}$ is the N_2 mole fraction in outlet flow from the top of the HDS. For this binary solution, $y_{N2,out}$ is calculated from $y_{CO2,out}$, which is measured by the CO_2 monitor using line B in figure 5.2 (the top port).

Table 5.2 provides details about the 34 steady state separations performed for this study. The levels of the three experimental variables are shown. L, the inlet position (refer to figures 5.2 and 5.5), is placed at five values between 15 and 76 cm. There are three pressure levels (P) between 170 and 238 bar. The inlet volumetric flow rate varies between 7 and 21 cm^3/min. It is a function of pressure, and the flow rates of the pure species are set to provide 85% N_2 and 15% CO_2. The density of the inlet solution, ρ_{mix}, is calculated using the PR EOS. It provides the link between volumetric data and mass (or mole) data.

Table 5.2. Parameters of experiments, average mole fraction of CO_2 from detector and *S*.

#	L (cm)	P (bar)	$Q_{in,\ N2}$ (cm^3/min)	$Q_{in,\ CO2}$ (cm^3/min)	ρ_{mix}* (g/cm^3)	$y_{CO2,\ top}$	S
1	76.2	238.1	7	0.49	0.312	0.0000	1.0000
2		238.1	10	0.70	0.312	0.0000	1.0000
3		238.1	15	1.05	0.312	0.0000	1.0000
4		238.1	20	1.40	0.312	0.0000	1.0000
5		204.1	7	0.44	0.272	0.0000	1.0000
6		204.1	10	0.63	0.272	0.0000	1.0000
7		204.1	15	0.94	0.272	0.0000	1.0000
8		204.1	20	1.26	0.272	0.0000	1.0000
9		170.1	7	0.39	0.230	0.0000	1.0000
10		170.1	10	0.56	0.230	0.0000	1.0000
11		170.1	15	0.83	0.230	0.0000	1.0000
12		170.1	20	1.11	0.230	0.1370	0.0957
13	61.0	238.1	7	0.49	0.312	0.0000	1.0000
14		238.1	10	0.70	0.312	0.0000	1.0000
15		238.1	15	1.05	0.312	0.1388	0.0814
16		238.1	20	1.40	0.312	0.1500	0.0337
17		204.1	7	0.44	0.272	0.0009	0.9937
18		204.1	10	0.63	0.272	0.1394	0.0816
19		204.1	15	0.94	0.272	0.1454	0.0422
20		204.1	20	1.26	0.272	0.1500	0.0000
21		170.1	7	0.39	0.230	0.0011	0.9927
22		170.1	10	0.56	0.230	0.1431	0.0561
23		170.1	15	0.83	0.230	0.1500	0.0000
24	45.7	238.1	7	0.49	0.312	0.0000	0.0000
25		238.1	10	0.70	0.312	0.1500	0.0000
26		204.1	7	0.44	0.272	0.0011	0.0000
27		204.1	10	0.63	0.272	0.1500	0.0000
28		170.1	7	0.39	0.230	0.1500	0.0000
29	30.5	238.1	7	0.49	0.312	0.1500	0.0000
30		204.1	7	0.44	0.272	0.1500	0.0000
31		170.1	7	0.39	0.230	0.1500	0.0000
32	15.2	238.1	7	0.49	0.312	0.1500	0.0000
33		204.1	7	0.44	0.272	0.1500	0.0000
34		170.1	7	0.39	0.230	0.1500	0.0000

* density of mixture is calculated by the PR EOS.

The results obtained in this research are also shown in table 5.2. Interpretation of these results is facilitated by figure 5.13 in which S is plotted against L at three pressures. The trend towards perfect separation involves long L (separator design variable), as well

as high-pressure and low flow rate (fluid variables). However, there is interaction among the variables that requires further elucidation.

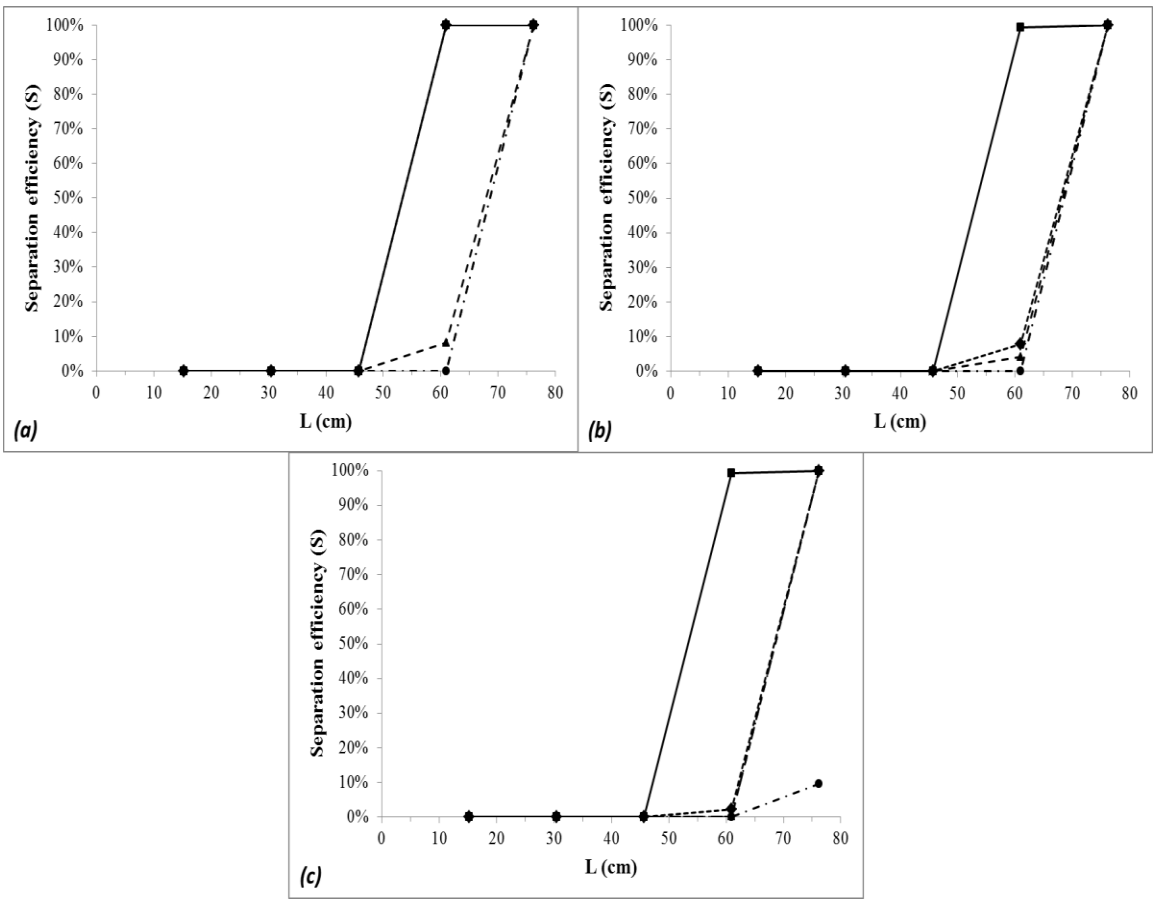

Figure 5.13. Diagrams of S vs L at various pressures and inlet flow rates of nitrogen. (a) P=238.1 bar, (b) P=204.1 bar, and (c) P=170.1 bar. —■— 7 cm³/min, --◆-- 10 cm³/min, - -▲- - 15 cm³/min, - -●- - 20 cm³/min.

Hendry et al. [5.1] reasoned that the main driving force for separation at a batch HEPS is natural convection between two components of different densities within a single phase. In heat transfer, the Grashof number (Gr) is the dimensionless number that governs natural convection of fluid flow. In fluid mechanics, Archimedes number

(Ar) is equivalent to Gr where there is a different density between two components. Therefore, Ar is defined for the N_2/CO_2 mixture.

$$Ar = \frac{buoyant\ force}{viscous\ force} = \frac{gL^3\rho_{mix}\left(\rho_{CO_2} - \rho_{N_2}\right)}{{\mu_{N_2}}^2} \qquad (5-2)$$

Where g is the acceleration of gravity; L is the distance between the inlet point and the outlet point in the HDS (refer to figure 5.2); ρ is the density and is a function of pressure; μ is the viscosity.

Figure 5.14 shows S vs Ar at various flow rates of N_2. As expected, the trend toward perfect separation is with increasing Ar, as buoyant forces dominate viscous forces. The trend with respect to flow rate is similar to figure 5.13. Also as in figure 5.13, the behavior is complex and requires further elucidation.

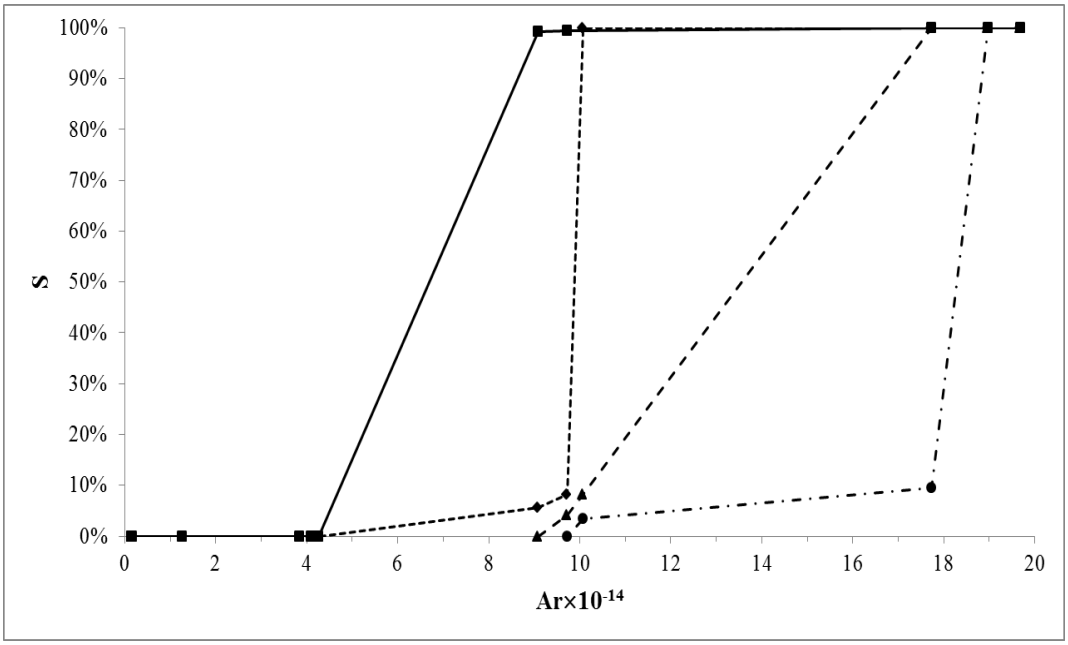

Figure 5.14. Diagram of S vs Ar at different flow rates of N_2. —■— 7 cm³/min, ---◆--- 10 cm³/min, - -▲- - 15 cm³/min, - -●- - 20 cm³/min.

5.3.2. Definition of Espanani number using Buckingham Pi Theorem

We note that Ar does not include the effect of flow rate (or velocity of fluid in the HDS) that is an important characteristic of a continuous process. Further, although density indirectly provides the effect of pressure on Ar, this effect is small compared to the effect of L^3. We seek to define another parameter to show the effects of velocity and pressure on the separation efficiency.

The effective parameters for separation of N_2/CO_2 mixture are pressure, linear velocity of fluid in the HDS, and L. In addition, for a viscous flow, the viscosity is an important factor which should be considered. Dimensions of these variables are listed in table 5.3.

Table 5.3. Dimensions of effective parameters used in the Buckingham Pi method.

Variable	Symbol	Dimensions
Pressure	P	$ML^{-1}T^{-2}$
Velocity	U	LT^{-1}
Significant length	L	L
Viscosity	μ	$ML^{-1}T^{-1}$

So, we are able to write 4-3=1 dimensionless group as the following:

$$\pi = P^a U^b L^c \mu^d \qquad (5-3)$$

The dimensional matrix can be obtained as:

$$\begin{array}{c} \\ M \\ L \\ T \end{array} \begin{array}{c} \begin{array}{cccc} \text{P} & \text{U} & \text{L} & \mu \end{array} \\ \begin{bmatrix} 1 & 0 & 0 & 1 \\ -1 & 1 & 1 & -1 \\ -2 & -1 & 0 & -1 \end{bmatrix} \end{array}$$

So, the variables of a, b, c, and d will be calculated by solving equation 5-4:

$$\begin{bmatrix} 1 & 0 & 0 & 1 \\ -1 & 1 & 1 & -1 \\ -2 & -1 & 0 & -1 \end{bmatrix} \begin{bmatrix} a \\ b \\ c \\ d \end{bmatrix} = \begin{bmatrix} 0 \\ 0 \\ 0 \\ 0 \end{bmatrix} \qquad (5-4)$$

$$\therefore \quad a = 1 \;\; ; \;\; b = -1 \;\; ; \;\; c = 1 \;\; ; \;\; d = -1$$

Therefore, Π group can be written as:

$$\pi = \frac{P.L}{U.\mu} = \frac{P.\tau'}{\mu} \qquad (5-5)$$

In equation 5-5, $\tau'=L/U$ is the time that the average molecule of fluid travels from inlet point to outlet point on the top of the HDS (this differs from the average residence time of a molecule in the HDS). Thus, the Espanani number (Es) is defined as the ratio of pressure force to vicious force acting on a fluid.

$$Es = \frac{pressure\ force}{viscous\ force} = \frac{P.L}{U.\mu} = \frac{P.\tau'}{\mu} \qquad (5-6)$$

Figure 5.15 shows S vs Es at various flow rates. As in figures 5.13 and 5.14, increasing the independent variable (in this case Es) trends toward perfect separation. Once again, the behavior is complex and correlation with intermediate separations is apparent.

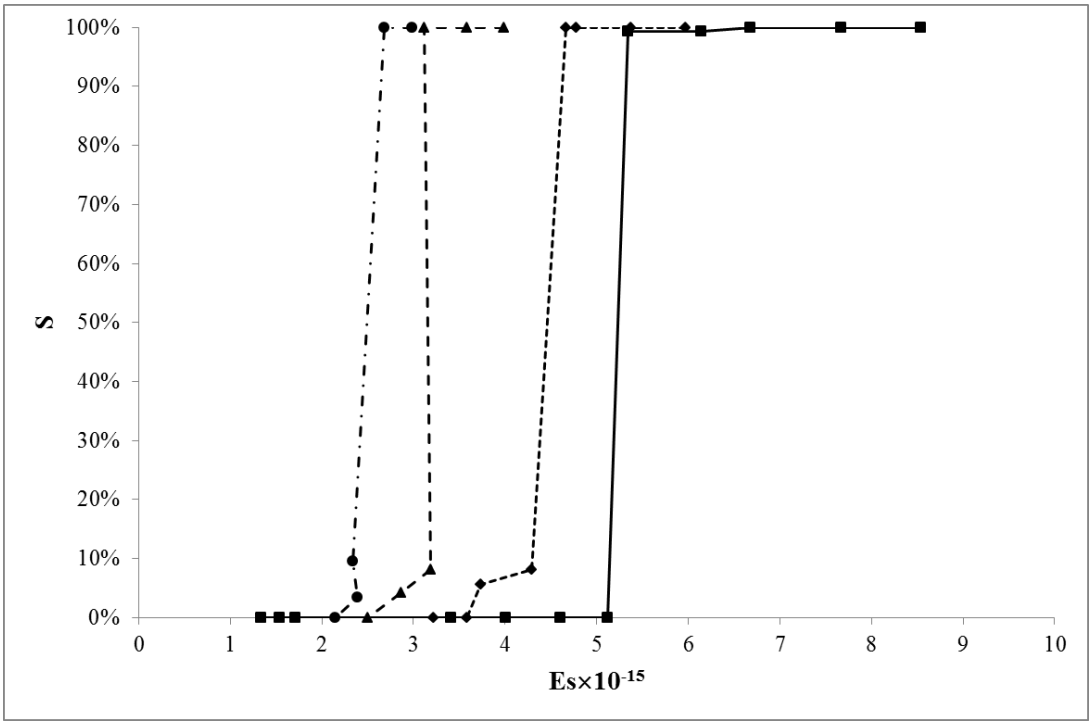

Figure 5.15. Diagram of S vs Es at different flow rates for N_2/CO_2 mixture. —■— 7 cm³/min, --◆-- 10 cm³/min, - -▲- - 15 cm³/min, - -●- - 20 cm³/min.

Separation in a continuous process depends on both Ar and Es. Ar provides the effect of buoyancy and Es indicates the roles of pressure and velocity (or flow rate).

$$S = f(Ar, Es) \qquad (5-7)$$

We suggest a simple product function, Ar×Es. This is illustrated in figure 5.16, which shows S vs Ar×Es for all 34 steady state data points. Three regimes are identified for separation of N_2/CO_2 mixture using the HDS and continuous process:

2.3×10^{30} > Ar×Es : no separation

2.3×10^{30} < Ar×Es < 4.5×10^{30} : partial separation

4.5×10^{30} < Ar×Es : perfect separation

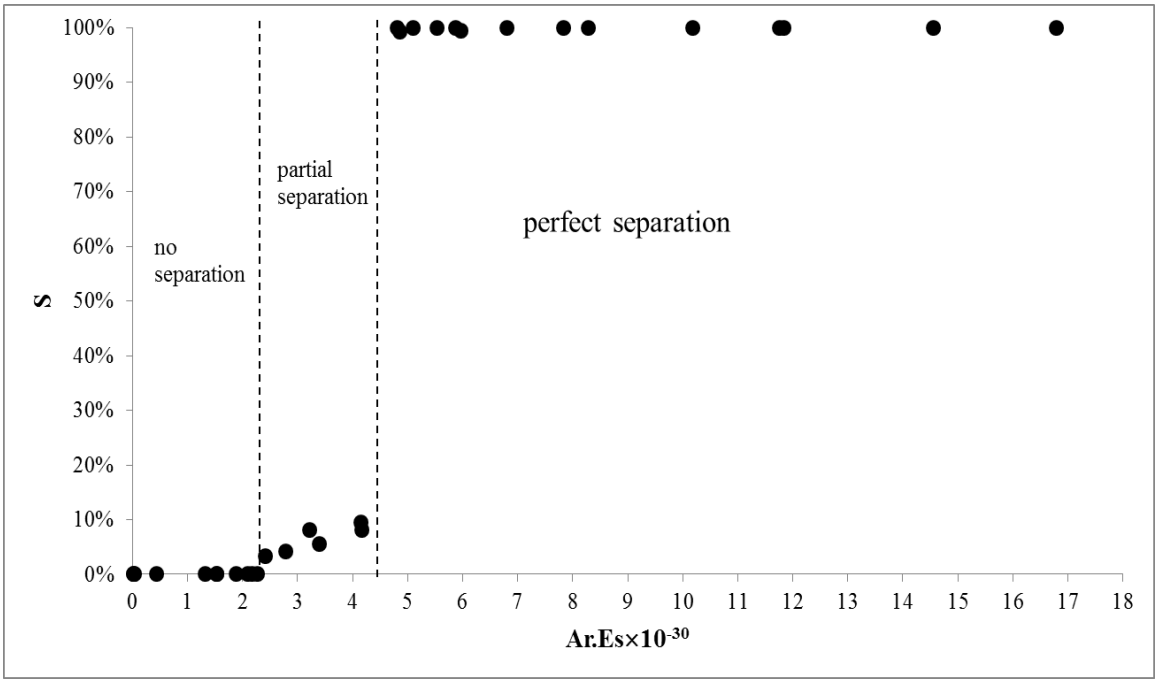

Figure 5.16. Diagram of S vs Ar×Es for the N_2/CO_2 mixture.

The results obtained for various conditions are summarized in table 5.4.

Table 5.4. Ar, Es, and Ar×Es calculated for different conditions.

#	L (cm)	P (bar)	$Q_{in, N2}$ (cm^3/min)	Ar $\times10^{-14}$	Es $\times10^{-15}$	Ar×Es $\times10^{-30}$	S
1	76.2	238.1	7	19.68	8.53	16.80	1.0000
2		238.1	10	19.68	5.97	11.76	1.0000
3		238.1	15	19.68	3.98	7.84	1.0000
4		238.1	20	19.68	2.99	5.88	1.0000
5		204.1	7	18.98	7.67	14.56	1.0000
6		204.1	10	18.98	5.37	10.19	1.0000
7		204.1	15	18.98	3.58	6.80	1.0000
8		204.1	20	18.98	2.68	5.09	1.0000
9		170.1	7	17.74	6.68	11.84	1.0000
10		170.1	10	17.74	4.67	8.28	1.0000
11		170.1	15	17.74	3.12	5.54	1.0000
12		170.1	20	17.74	2.34	4.15	0.0957
13	61.0	238.1	7	10.08	6.11	6.16	1.0000
14		238.1	10	10.08	4.78	4.82	1.0000
15		238.1	15	10.08	3.19	3.21	0.0814
16		238.1	20	10.08	2.39	2.41	0.0337
17		204.1	7	9.72	6.14	5.96	0.9937
18		204.1	10	9.72	4.29	4.17	0.0816
19		204.1	15	9.72	2.87	2.79	0.0422
20		204.1	20	9.72	2.15	2.09	0.0000
21		170.1	7	9.08	5.34	4.85	0.9927
22		170.1	10	9.08	3.73	3.39	0.0561
23		170.1	15	9.08	2.50	2.27	0.0000
24	45.7	238.1	7	4.25	5.12	2.18	0.0000
25		238.1	10	4.25	3.58	1.52	0.0000
26		204.1	7	4.10	4.60	1.89	0.0000
27		204.1	10	4.10	3.22	1.32	0.0000
28		170.1	7	3.83	4.01	1.53	0.0000
29	30.5	238.1	7	1.26	3.41	0.430	0.0000
30		204.1	7	1.26	3.07	0.386	0.0000
31		170.1	7	1.26	2.67	0.337	0.0000
32	15.2	238.1	7	0.158	1.71	0.027	0.0000
33		204.1	7	0.152	1.53	0.023	0.0000
34		170.1	7	0.142	1.34	0.019	0.0000

The analysis above allows design calculations. The maximum capacity of our existing HDS, which has a diameter of 4.3 cm and a maximum L of 76.2 cm is 28 cm^3/min. It is estimated based on two criteria; 1) perfect separation (Ar×Es > 4.5×10^{30}), and 2) laminar flow in the HDS (Re < 2000). Figure 5.17 illustrates the L required for

perfect separation as a function of inlet flow rate and 238.1 bar. Figure 11 also shows that the computed Re for all inlet flow rates are less than 200 which confirms flow in the HDS is laminar.

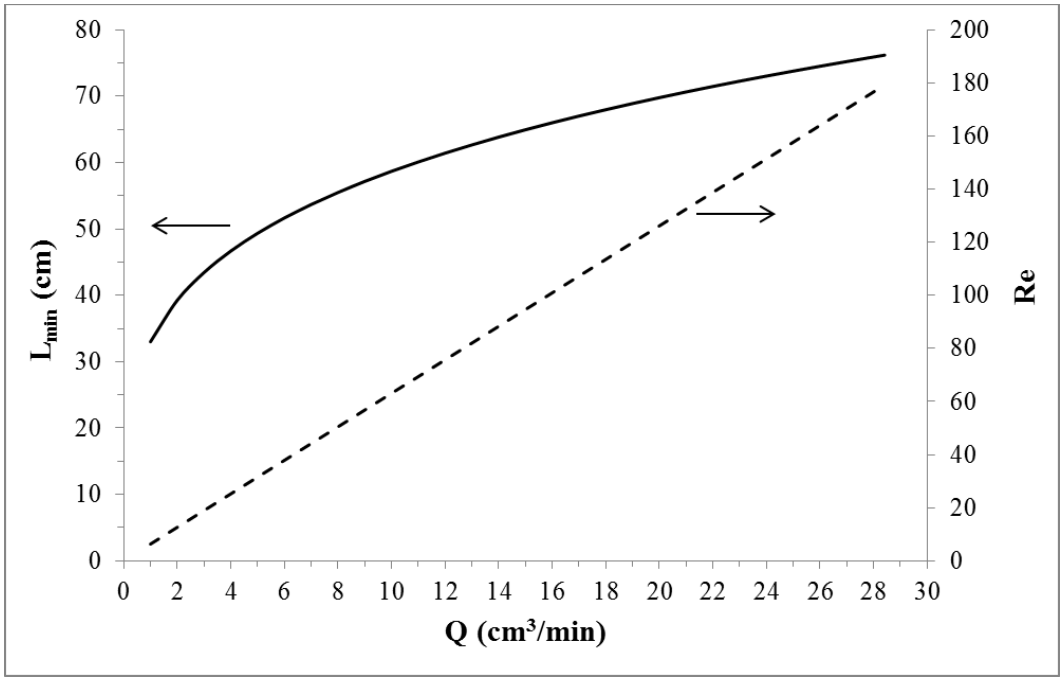

Figure 5.17. Minimum L and Re vs inlet flow rate for the HDS at 238.1 bar and 25 °C. The diameter of the HDS is 4.3 cm and maximum flow rate of the N_2/CO_2 mixture has been calculated 28.4 cm^3/min.

The effect of the diameter of the HDS on maximum inlet flow rate and required L can also be calculated according to the criteria discussed above. The results, at ambient temperature and 238.1 bar, are shown in figure 5.18. The maximum inlet flow rate is increases linearly with larger diameter; while the required L decreases to an asymptotic value of about 35 cm. The utility of the chart is demonstrated by considering an HDS with a diameter of 100 cm. The maximum flow rate is 444 lit/hr, and the required L is 63 cm. If the diameter of the HDS is increased to 800 cm, the maximum flow rate is 3551 lit/hr, while the required L is 38 cm.

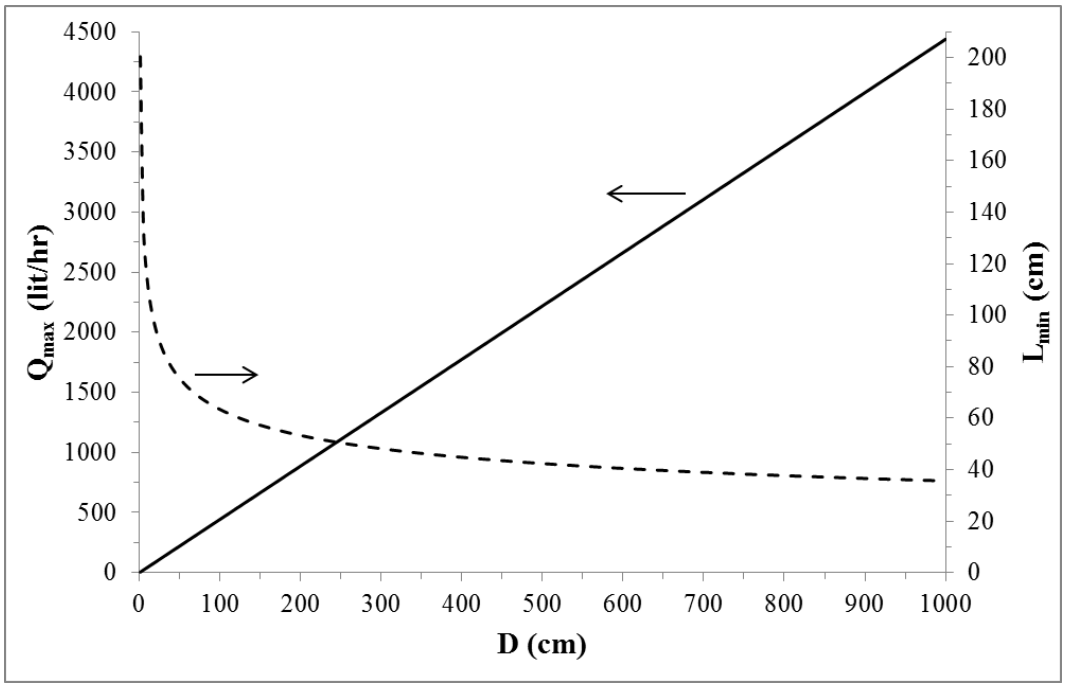

Figure 5.18. Maximum flow rate of the N_2/CO_2 mixture and minimum L vs diameter of the HDS at 238.1 bar, 25 °C, and Re=2000.

Therefore, our analysis informs HDS design and predicts HDS performance.

CHAPTER SIX

6

Conclusions and Recommendations

6.1. Conclusions

Based on the experiments and results detailed in the chapters 4 and 5 and supplemented with literature sources, the following conclusions can be drawn.

6.1.1. VLE of low boiling point mixtures

In this research, (vapor + liquid) equilibria for different systems at high pressure and low temperature were studied by the PR EOS and the Wong-Sandler mixing rule. We chose the NRTL model and applied adjustable parameters that are functions of temperature. The coefficients of the temperature functions can be computed by fitting experimental data. The results show that the present model is an appropriate thermodynamic model to predict VLE of mixtures containing the low boiling point substances for wide ranges of temperature. Thermodynamic modeling of N_2/CO_2 mixture also indicates that it is impossible to separate CO_2 from flue gas using distillation method.

6.1.2. Separation of N_2/CO_2 mixture

In this study, perfect separation of 85/15-N_2/CO_2 mixture is carried out using a high-pressure, density-driven separator under steady-state conditions. The effects of pressure, inlet mixture flow rate, and distance between inlet and outlet of the HDS (L) were evaluated. The monitored response was a separation metric (S). Experimental results showed that the separation efficiency depends on two dimensionless groups: the Archimedes number (Ar) and the Espanani number (Es). Their product incorporates the effects of buoyant forces, pressure forces, and viscous forces and is highly correlated with separation efficiency. For the N_2/CO_2 mixture, perfect separation takes place while Ar×Es is more than 4.5×10^{30}. The use of this analysis to inform HDS design and predict HDS performance is also illustrated.

6.2. Future recommendations

In the SCWO process (figure 1.6), the pressure of gaseous products is very high. So, there is a potential energy after reactor which can be converted to useful energy. One possibility is to apply a turbo-expander instead of the back-pressure regulator in downstream. In this situation, temperature of gas mixture goes down. As a result, cold gas mixture can be utilized to cool intercoolers of the compressor. Therefore, the total efficiency of the process will be increased and cooling water consumption will be decreased. Here, the modified process, mass and energy balance is presented.

6.2.1. Work of compressor

A compressor is a mechanical device that increases the pressure of a gas by reducing its volume. Equation 6-1 is used to calculate the required work of a compressor at an isentropic process. During the isentropic process, Pv^{κ} is constant for an ideal gas and κ is C_P/C_V.

$$W_{comp} = \frac{\kappa \dot{m} R T_1}{\kappa - 1}\left[\left(\frac{P_2}{P_1}\right)^{\frac{\kappa-1}{\kappa}} - 1\right] \qquad (6-1)$$

and outlet temperature becomes:

$$\frac{T_2}{T_1} = \left(\frac{P_2}{P_1}\right)^{\frac{\kappa-1}{\kappa}} \qquad (6-2)$$

To reach a high pressure, the isentropic pressurizing requires more work and produces a very hot outlet stream. Thus, compressors are usually designed multi-stages and the compression ratio is considered about 2. There is an intercooler between two stages to cool the outlet stream of each stage.

For example, consider a multi-stage air compressor with $m^{\bullet}$=1 kg/s of inlet stream and the compression ratio, P_{out}/P_{in} =2 for each stage. κ is about 1.4 for air and inlet temperature of each stage is assumed 25 °C (298.15 K). The rate of required work for compression from 1 bar to 250 bar is calculated:

P1=1 → P2=2 → P3=4 → P4=8 → P5=16 → P6=32 → P7=64 → P8=128 → P9=250 bar

$$W_{comp,\ stage\ 1-7} = \frac{1.4\times\left(\frac{1000}{28.8}\right)\times 8.314\times 298.15}{1.4-1}\left[(2)^{\frac{1.4-1}{1.4}} - 1\right] = 65.98\ kW$$

$$W_{comp,\ stage\ 8} = \frac{1.4 \times (\frac{1000}{28.8})\times 8.314\times 298.15}{1.4-1}\left[\left(\frac{250}{128}\right)^{\frac{1.4-1}{1.4}} - 1\right] = 63.5\ kW$$

$$W_{comp,\ total} = 7 \times 65.98 + 63.5 = 525.4\ kW$$

and outlet temperatures become:

$$T_{out,\ stage\ 1-7} = 298.15(2)^{\frac{1.4-1}{1.4}} = 363.45\ K = 90.3\ °C$$

$$T_{out,\ stage\ 8} = 298.15\left(\frac{250}{128}\right)^{\frac{1.4-1}{1.4}} = 361\ K = 87.9\ °C$$

However, required work for compression by only one-stage compressor and outlet temperature are computed:

$$W_{comp,\ 1-250\ bar} = \frac{1.4 \times (\frac{1000}{28.8}) \times 8.314 \times 298.15}{1.4-1}\left[\left(\frac{250}{1}\right)^{\frac{1.4-1}{1.4}} - 1\right] = 1157.7\ kW$$

$$T_{out} = 298.15\left(\frac{250}{1}\right)^{\frac{1.4-1}{1.4}} = 1444\ K = 1170.9\ °C$$

6.2.2. Work of turbo-expander

A turbo-expander is a turbine which a high pressure gas is expanded to produce work. Work of turbo-expander is obtained from the enthalpy difference between inlet and outlet streams at an isentropic process. In addition, temperature is decreased through the expansion process.

6.2.3. Mass and energy balance

Figure 6.1 shows the modified process for SCWO of biomass and energy recovery using the turbo-expander and CO_2 capture. This process needs an 8-stage compressor to pressurize air from ambient to 250 bar (only 2 stages has been shown) and depressurizing is carried out by 4-stage turbo-expander (figure 6.1 illustrates only one).

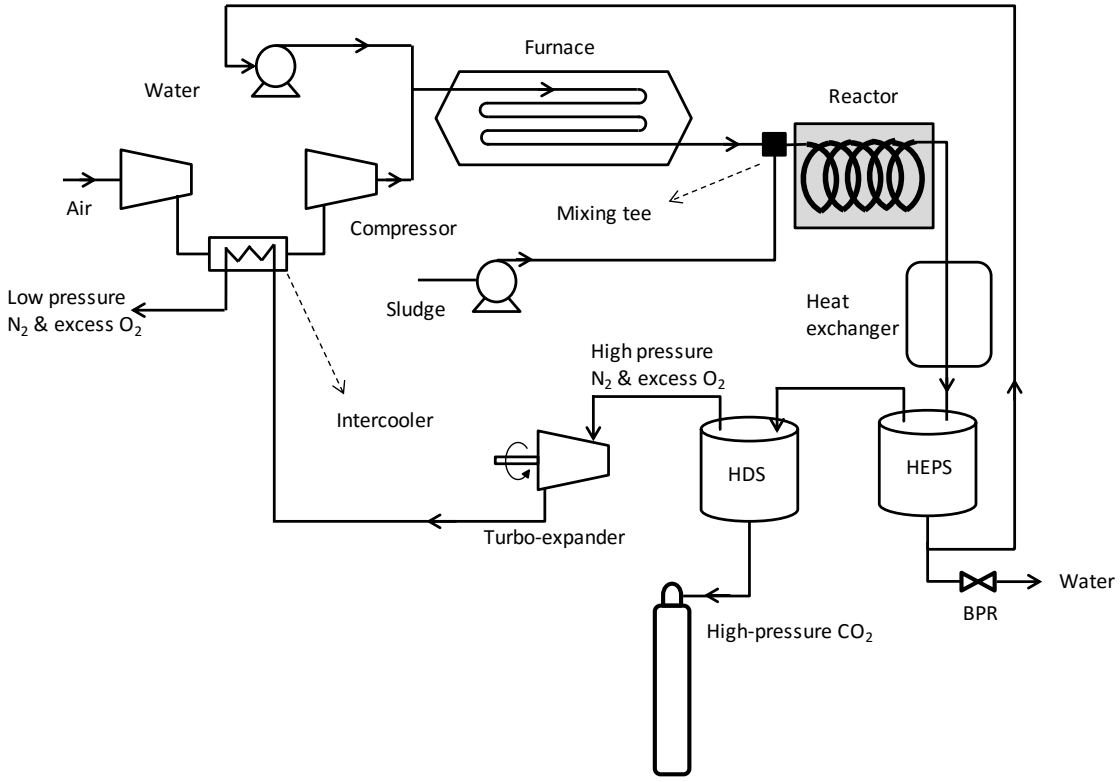

Figure 6.1. SCWO process with energy recovery and CO_2 capture.

The sludge mixture included 20% of solid content is pumped to the mixing tee and its concentration is decreased to 5% of solid content after adding hot water to the sludge. Sludge formula is $CH_{1.89}O_{0.77}$ where biomass is represented on a one-carbon basis and its LHV is 19.88 MJ/kg of dry solid.

6.2.4. Stoichiometry of oxidation reaction

Molecular weight of biomass ($CH_{1.89}O_{0.77}$) is 26.21 g/gmol. Mole balance for the oxidation reaction may be written as the following:

$$CH_{1.89}O_{0.77} + 1.0875\ O_2 \rightarrow CO_2 + 0.9450\ H_2O$$

Basis of 1 kg/s of dry sludge, required stoichiometric air is calculated as:

$$O_2: \quad \left(\frac{1000}{26.21}\right)_{\text{g of dry sludge}} \times \left(\frac{1.0875_{\text{mol of O2}}}{1_{\text{mol of sludge}}}\right) \times \left(\frac{32_{\text{g}}}{1_{\text{mol of O2}}}\right) = 1.3277\ kg/s$$

and

$$N_2: \quad 13277_{\text{g of O2}} \times \left(\frac{1_{\text{mol of O2}}}{32_{\text{g of O2}}}\right) \times \left(\frac{79_{\text{mol of O2}}}{21_{\text{mol of O2}}}\right) \times \left(\frac{28_{\text{g of N2}}}{1_{\text{mol of N2}}}\right) = 4.3705\ kg/s$$

Amount of water in sludge mixture before and after the mixing tee are 4 kg/s and 19 kg/s of water

6.2.5. Required work of compressor and heat transfer

We calculated the required work of the compressor in section 6.2.1. Also, it may be computed by enthalpy difference of inlet and outlet streams through an isentropic process. It gives:

For stage 1: P_{in}=1 bar, T_{in}=25 °C → P_{out}=2 bar, T_{out}=90.3 °C

$H_{O2,\,in}$=463.7 kJ/kg , $S_{O2,\,in}$=4.31 kJ/kg.K , $H_{O2,\,out}$ =523.73 kJ/kg

$H_{N2,\,in}$=459.6 kJ/kg , $S_{N2,\,in}$=4.38 kJ/kg.K , $H_{N2,\,out}$ =527.17 kJ/kg

$$\rightarrow W_{comp,\ stage\,1} = 1.3277(523.73 - 463.7) + 4.3705(527.17 - 459.6) = 375.0\ kW$$

and the isentropic process: $S_{O2,\,out}$=4.31 kJ/kg.K , $S_{N2,\,out}$=4.38 kJ/kg.K

Outlet stream of each stage should be cooled to 25 °C. So, amount of heat transfer can be calculated as below:

For intercooler 1: P_{in}=2 bar, T_{in}=90.3 °C → P_{out}=2 bar, T_{out}=25 °C

$H_{O2,\,in}$=523 kJ/kg , $S_{O2,\,in}$=4.31 kJ/kg.K , $H_{O2,\,out}$ =462.49 kJ/kg

$H_{N2,\,in}$=526.1 kJ/kg , $S_{N2,\,in}$=4.38 kJ/kg.K , $H_{N2,\,out}$ =459.33 kJ/kg

$\rightarrow\ Q_{intercooler\,1} = 1.3277(462.49 - 523) + 4.3705(459.33 - 526.1) = -377.8\ kW$

and $S_{O2,\,out}$= 4.1269 kJ/kg.K , $S_{N2,\,out}$= 4.1855 kJ/kg.K

For other stages and intercoolers, we have:

$W_2 = 375.8\ kW\ , W_3 = 373.6\ kW\ , W_4 = 371.4\ kW\ , W_5 = 369.4\ kW\ , W_6 = 364.5\ kW\ ,$

$W_7 = 366.6\ kW\ , W_8 = 378.3\ kW$

$Q_2 = -377.6\ kW, Q_3 = -379.8\ kW\ , Q_4 = -384.5\ kW\ , Q_5 = -392.9\ kW\ ,$

$Q_6 = -409.5\ kW\ , Q_7 = -435.1\ kW$

Thus, total work and heat transfer become:

$W_{comp,\ total} = 2974.6\ kW\ ,\qquad Q_{intercooler,\ total} = -2757.3\ kW$

However, according to section 6.2.1, if $\dot{m}$ is 5.6982 kg/s, the compressor work is obtained 2993.8 kW. It is obvious that difference between calculation methods of the compressor work is very small (19.2 kW or 0.65%). The reason is the calculation methods when air is considered as an ideal gas (section 6.2.1) or a real gas (section 6.2.5).

6.2.6. Energy recovery using turbo-expander

According to figure 6.1, outlet stream from HDS is just included high-pressure nitrogen at ideal state (stoichiometric reaction without excess O_2). Produced work using a multi-stage turbo-expander may be computed as the following:

Stage 1:
Intercooler (temperature increasing at constant pressure):
P_{in}=250 bar, T_{in}=25 °C, H_{in}=418.78 kJ/kg, S_{in}=2.6371 kJ/kg.K
P_{out}=250 bar, T_{out}=65 °C, H_{out}=470.87 kJ/kg, S_{out}=2.8011 kJ/kg.K
$Q_1 = 4.3705(470.87 - 418.78) = 227.7\ kW$

Turbo-expander (temperature decreasing at constant entropy):
P_{in}=250 bar, T_{in}=65 °C, H_{in}=470.87 kJ/kg, S_{in}=2.8011 kJ/kg.K
Isentropic process: $S_{in} = S_{out} \rightarrow$ P_{out}=75 bar, T_{out}=-35 °C, H_{out} =368.69 kJ/kg
$W_1 = 4.3705(368.69 - 470.87) = -446.6\ kW$

Stage 2:
Intercooler (temperature increasing at constant pressure):
P_{in}=75 bar, T_{in}=-35 °C, H_{in}=368.69 kJ/kg, S_{in}=2.8011 kJ/kg.K
P_{out}=75 bar, T_{out}=65 °C, H_{out}=487.98 kJ/kg, S_{out}=3.2188 kJ/kg.K
$Q_1 = 4.3705(487.98 - 368.69) = 521.4\ kW$

Turbo-expander (temperature decreasing at constant entropy):
P_{in}=75 bar, T_{in}=65 °C, H_{in}=487.98 kJ/kg, S_{in}=3.2188 kJ/kg.K
Isentropic process: $S_{in} = S_{out} \rightarrow$ P_{out}=19.6 bar, T_{out}=-45 °C, H_{out} =378.4 kJ/kg
$W_1 = 4.3705(378.4 - 487.98) = -478.9\ kW$

Stage 3:
Intercooler (temperature increasing at constant pressure):
P_{in}=19.6 bar, T_{in}=-45 °C, H_{in}=378.4 kJ/kg, S_{in}=3.2188 kJ/kg.K
P_{out}=19.6 bar, T_{out}=65 °C, H_{out}=497.56 kJ/kg, S_{out}=3.6456 kJ/kg.K
$Q_1 = 4.3705(497.56 - 378.4) = 520.8\ kW$

Turbo-expander (temperature decreasing at constant entropy):
P_{in}=19.6 bar, T_{in}=65 °C, H_{in}=497.56 kJ/kg, S_{in}=3.6456 kJ/kg.K

Isentropic process: $S_{in}= S_{out} \rightarrow P_{out}$=5.1 bar, T_{out}=-45 °C, H_{out} =384.91 kJ/kg

$W_1 = 4.3705(384.91 - 497.56) = -497.6\ kW$

Stage 4:

Intercooler (temperature increasing at constant pressure):

P_{in}=5.1 bar, T_{in}=-45 °C, H_{in}=384.91 kJ/kg, S_{in}=3.6456 kJ/kg.K

P_{out}=5.1 bar, T_{out}=65 °C, H_{out}=500.46 kJ/kg, S_{out}=4.0551 kJ/kg.K

$Q_1 = 4.3705(500.46 - 384.91) = 505.0\ kW$

Turbo-expander (temperature decreasing at constant entropy):

P_{in}=5.1 bar, T_{in}=65 °C, H_{in}=500.46 kJ/kg, S_{in}=4.0551 kJ/kg.K

Isentropic process: $S_{in}= S_{out} \rightarrow P_{out}$=1 bar, T_{out}=-61 °C, H_{out} =370.9 kJ/kg

$W_1 = 4.3705(370.9 - 500.46) = -566.2\ kW$

Stage 5:

Intercooler (temperature increasing at constant pressure):

P_{in}=1 bar, T_{in}=-61 °C, H_{in}=370.9 kJ/kg, S_{in}=4.0551 kJ/kg.K

P_{out}=1 bar, T_{out}=25 °C, H_{out}=459.6 kJ/kg, S_{out}=4.38 kJ/kg.K

$Q_1 = 4.3705(459.6 - 370.9) = 387.7\ kW$

Therefore, total produced work and heat transfer become:

$W_{produced} = -446.6 - 478.9 - 497.6 - 566.2 = 1989.3\ \ kW\ \ ,$

$Q_{total} = 227.7 + 521.4 + 520.8 + 505.0 + 387.7 = 2162.6\ kW$

$$\frac{W_{produced}}{W_{compressor}} = \frac{1989.3}{2974.6} = 66.9\%$$

$$\frac{Q_{turbo-expander}}{Q_{compressor}} = \frac{2162.6}{2757.3} = 78.4\%$$

Consequently, it is possible to save 66.9% of given energy to the process by compressor.

We can also save 78.4% of required cooling water for intercoolers of compressor.

As an alternative process, expanding nitrogen from 250 bar to ambient using one-stage turbo-expander can produce liquid nitrogen at less than -200 °C. Produced heat in the heat exchanger after reactor may be utilized in various ways. Some proposals are:

- Heating recycle water and air of the process instead of using the furnace.
- Using in the air conditioning of buildings.
- Using for pre-heating the feed water in a combined power cycle to generate electricity (figure 6.2).

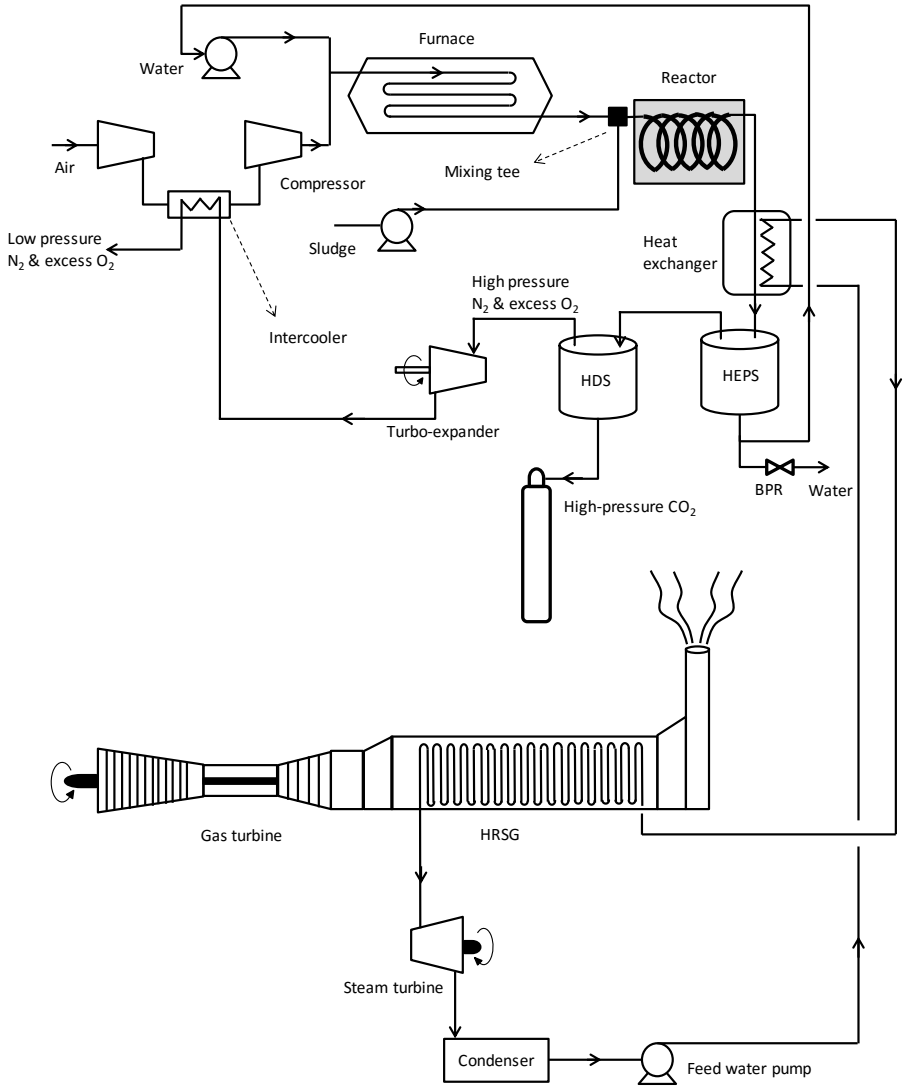

Figure 6.2. Schematic of a combination of SCWO process, gas-turbine and heat recovery steam generation.

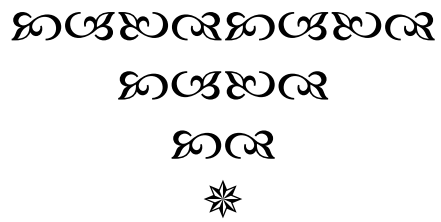

REFERENCES

Chapter 1

[1.1] F. Bilgili, I. Ozturk, "Biomass energy and economic growth nexus in G7 countries: Evidence from dynamic panel data", Renewable and Sustainable Energy Reviews 49 (2015) 132-138.

[1.2] U.S. Energy Information Administration. Website: http://www.eia.gov/beta/MER/index.cfm?tbl=T10.01#/?f=M&start=200001

[1.3] C.B. Field, M.J. Behrenfeld, J.T. Randerson, P. Falkowski, "Primary Production of the Biosphere: Integrating Terrestrial and Oceanic Components", Science 281 (1998) 237-240.

[1.4] R.C. Saxena, Diptendu Seal, Satinder Kumar, H.B. Goyal, "Thermo-chemical routes for hydrogen rich gas from biomass: A review", Renewable and Sustainable Energy Reviews 12 (2008) 1909-1927.

[1.5] C.N. Hamelinck, A.P.C. Faaij, "Future prospects for production of methanol and hydrogen from biomass", J. Power Sources 111 (2002) 1-22.

[1.6] A. Miller, R. Espanani, A. Junker, D. Hendry, N. Wilkinson, D. Bollinger, J.M. Abelleira-Pereira, M.A. Deshusses, E. Inniss, W. Jacoby, "Supercritical water oxidation of a model fecal sludge without the use of a co-fuel", Chemosphere 141 (2015) 189-196.

[1.7] A. Loppinet-Serani, C. Aymonier, F. Cansell, "Current and foreseeable applications of supercritical water for energy and the environment", ChemSusChem 1 (2008) 486- 503.

[1.8] A.A. Peterson, F. Vogel, R.P. Lachance, M. Froling, M.J. Antal, J.W. Tester, "Thermochemical biofuel production in hydrothermal media: A review of sub- and supercritical water technologies", Energy Environ. Sci. 1 (2008) 32-65.

[1.9] I. Okajima, T. Sako, "Energy conversion of biomass with supercritical and subcritical water using large-scale plants", J. of Bioscience and Bioengineering 117 (2014) 1-9.

[1.10] A. Loppinet-Serani, C. Aymonier, F. Cansell, "Supercritical water for environmental technologies", J. Chem. Technol. Biotechnol. 85 (2010) 583-589.

[1.11] M.J. Cocero, E. Alonso, R. Torio, D. Vallelado, F. Fdz-Polanco, "Supercritical water oxidation in a pilot plant of nitrogenous compounds: 2-propanol mixtures in the temperature range 500e750 °C", Ind. Eng. Chem. Res. 39 (2000) 3707-3716.

[1.12] National Oceanic And Atmospheric Administration (NOAA): National centers for environmental information. Website: http://www.ncdc.noaa.gov/cag/time-series/global/globe/land_ocean/ytd/6/1880-2015.

[1.13] A. Daniel, A. Lashof, R. Dilip, R. Ahuja, “Relative contributions of greenhouse gas emissions to global warming”, Nature, 344 (1990) 529-531.

[1.14] M. Halmann, M.Steinberg, “Greenhouse Gas Carbon Dioxide Mitigation: Science and Technology”, Lewis Publishers, Boca Raton, FL, USA (2000).

[1.15] C. Stewart, M. Hessami, “A study of methods of carbon dioxide capture and sequestration-the sustainability of a photosynthetic bioreactor approach Energy”, Conv. Manag. 46 (2005) 403-420.

Chapter 2

[2.1] T.E. Rufford, S. Smart, G.C.Y. Watson, B.F. Graham, J. Boxall, J.C. Diniz da Costa, E.F. May, “The removal of CO_2 and N_2 from natural gas: A review of conventional and emerging process technologies”, J. Petrol. Sci. Eng. 94-95 (2012) 123-154.

[2.2] V. Havran , M.P. Dudukovic , C.S. Lo, “Conversion of Methane and Carbon Dioxide to Higher Value Products”, Ind. Eng. Chem. Res. 50 (2011) 7089-7100.

[2.3] M. Halmann, M.Steinberg, “Greenhouse Gas Carbon Dioxide Mitigation: Science and Technology”, Lewis Publishers, Boca Raton, FL, USA (2000).

[2.4] M.M. Hossain, H.I. de Lasa, “Chemical-looping combustion (CLC) for inherent CO_2 separations-a review”, Chem. Eng. Sci. 63 (2008) 4433-4451.

[2.5] W. Liu, D. King, J. Liu, B. Johnson, Y. Wang, Z. Yang, “Critical Material and Process issues for CO_2 separation from coal-Powered Plants”, JOM 61 (2009) 36-44.

[2.6] B. Hubbard, “New and Emerging Technologies (Petroskills workshop)”, Gas Processors Association Convention (2010), John M. Campbell & Co, Austin, Texas.

[2.7] A. Kohl, R. Nielsen, “Gas Purification”, Gulf Publishing Company, Houston, Texas (1997).

[2.8] J.L.V. Nichols, B.M. Friedman, A.L. Nold, S. McCutcheon, A. Goethe, “Processing technologies for CO_2 rich gas”, 88th Annual Convention of the Gas Processors Association (2009), Gas Processors Association, San Antonio, Texas.

[2.9] J. Wilcox, R. Haghpanah, E.C. Rupp, J. He, K. Lee, “Advancing Adsorption and Membrane Separation Processes for the Gigaton Carbon Capture Challenge”, Annu. Rev. Chem. Biomol. Eng. 5 (2014) 479-505.

[2.10] G. Watson, E.F. May, B.F. Graham, M.A. Trebble, R.D. Trengove, K.I. Chan, “Equilibrium adsorption measurement of pure nitrogen, carbon dioxide, and methane on a carbon molecular sieve at cryogenic temperatures and high pressures” J. Chem. Eng. Data 54 (2009) 2701-2707.

[2.11] B.N. Nair, R.P. Burwood, V.J. Goh, K. Nakagawa, T. Yamaguchi, “Lithium based ceramic materials and membranes for high temperature CO_2 separation”, Prog. Mater. Sci. 54 (2009) 511-541.

[2.12] Y. Wang, X. Lang, S. Fan, “Hydrate capture CO_2 from shifted synthesis gas, flue gas and sour natural gas or biogas”, J. Energy Chemistry 22 (2013) 39-47.

[2.13] P. Englezos, J.D. Lee, “Gas Hydrates: A Cleaner Source of Energy and Opportunity for Innovative Technologies”, Korean J. Chem. Eng. 22 (2005) 671-681.

[2.14] P. Babu, P. Linga, R. Kumar, P. Englezos, “A review of the hydrate based gas separation (HBGS) process for carbon dioxide pre-combustion capture”, Energy 85 (2015) 261-279.

[2.15] M. Walsh, “Molecular dynamics simulations of hydrates”, PhD, Colorado School of Mines (2011).

[2.16] A. Miller, D. Hendry, N. Wilkinson, C. Venkitasamy, W. Jacoby, “Exploration of the gasification of Spirulina algae in supercritical water”, Bioresour. Technol. 119 (2012) 41-47.

[2.17] D. Hendry, A. Miller, and W. Jacoby, “Turbulent operation of a continuous reactor for gasification of alcohols in supercritical water”, Ind. Eng. Chem. Res. 51 (2012) 2578-2585.

[2.18] H. Knapp, R. Döring, L. Oellrich, Plöcker, J.M. Prausnitz, “Vapor-Liquid Equilibria for mixtures of low boiling substances”, Chemistry Data Series, vol. VI, DECHEMA, 1982.

[2.19] J. Vidal, “Mixing rules and excess properties in cubic equations of state”, Chem. Eng. Sci. 33 (1978) 787-791.

[2.20] M.J. Huron, J. Vidal, “New mixing rules in simple equations of state for representing vapour-liquid equilibria of strongly non-ideal mixtures”, Fluid Phase Equilib. 3 (1979) 255-271.

[2.21] M.L. Michelsen, “A method for incorporating excess Gibbs energy models in equations of state”, Fluid Phase Equilib. 60 (1990) 47-58.

[2.22] M.L. Michelsen, “A modified Huron-Vidal mixing rule for cubic equations of state”, Fluid Phase Equilib. 60 (1990) 213-219.

[2.23] S. Dahl, M.L. Michelsen, “High-pressure vapor-liquid equilibrium with a UNIFAC-based equation of state”, AIChE J. 36 (1990) 1829-1836.

[2.24] D.S.H. Wong, S.I. Sandler, “A theoretically correct mixing rule for cubic equations of state”, AIChE J. 38 (1992) 671-680.

[2.25] H. Orbey, S.I. Sandler, “Modeling Vapor–Liquid Equilibria, Cubic Equations of State and their Mixing Rules”, Cambridge University Press, Cambridge, NY, 1998.

[2.26] H. Orbey, C. Balci, G.A. Guruz, “Phase Equilibrium of Asymmetric Systems by Predictive Equations of State Models”, Ind. Eng. Chem. Res. 41 (2002) 963-967.

[2.27] G.N.E. Alvarado, S.I. Sandler, “Prediction of Excess Enthalpies Using a G^{ex}/EOS Model”, Ind. Eng. Chem. Res. 40 (2001) 1261-1270.

[2.28] R.M. Salinas, F.G. Sánchez, G.E. Jiménez, "An equation-of-state-based viscosity model for non-ideal liquid mixtures", Fluid Phase Equilib. 210 (2003) 319-334.

[2.29] A. Haghtalab, R. Espanani, "A new model and extension of Wong-Sandler mixing rule for prediction of (vapour + liquid) equilibrium of polymer solutions using EOS/G^E", J. Chem. Thermodyn. 36 (2004) 901-910.

[2.30] T. Ohta, H. Todoriki, T. Yamada, "Representation of liquid–liquid equilibria at low and high pressures using the EOS-G^E mixing rules", Fluid Phase Equilib. 225 (2004) 23-27.

[2.31] M.C. Wang, D.S.H. Wong, "Calculation of critical lines of hydrocarbon/water systems by extrapolating mixing rules fitted to subcritical equilibrium data", Fluid Phase Equilib. 227 (2005) 183-196.

[2.32] J.O. Valderrama, J. Zavaleta, "Generalized binary interaction parameters in the Wong-Sandler mixing rules for mixtures containing n-alkanols and carbon dioxide", Fluid Phase Equilib. 234 (2005) 136-143.

[2.33] J.A. Lopez, C.A. Cardona, "Phase equilibrium calculations for carbon dioxide + n-alkanes binary mixtures with the Wong–Sandler mixing rules", Fluid Phase Equilib. 239 (2006) 206-212.

[2.34] P. Theveneau, C. Coquelet, D. Richon, "Vapour–liquid equilibrium data for the hydrogen sulphide + n-heptane system at temperatures from 293.25 to 373.22 K and pressures up to about 6.9 MPa", Fluid Phase Equilib. 249 (2006) 179-186.

[2.35] J.S. Lim, G. Seong, H.S. Byun, "Vapor-liquid equilibria for the binary system of 1,1-difluoroethane (HFC-152a) + n-butane (R-600) at various temperatures", Fluid Phase Equilib. 259 (2007) 165-172.

[2.36] G. Seong, K.P. Yoo, J.S. Lim, "Vapor-liquid equilibria for propane (R290) + n-butane (R600) at various temperatures", J. Chem. Eng. Data, 53 (2008) 2783-2786.

[2.37] M.T. Lee, S.T. Lin, "Prediction of mixture vapor-liquid equilibrium from the combined use of Peng-Robinson equation of state and COSMO-SAC activity coefficient model through the Wong-Sandler mixing rule", Fluid Phase Equilib. 254 (2007) 28-34.

[2.38] J.A. Lazzús, "Estimation of solid vapor pressures from supercritical CO_2 + biomolecule systems using a PSO algorithm", J. Supercrit. Fluids, 51 (2010) 312-318.

[2.39] K. Ye, H. Freund, K. Sundmacher, "Modelling (vapour + liquid) and (vapour + liquid + liquid) equilibria of {water (H2O) + methanol (MeOH) + dimethyl ether (DME) + carbon dioxide (CO2)} quaternary system using the Peng-Robinson EoS with Wong-Sandler mixing rule", J. Chem. Thermodyn. 43 (2011) 2002-2014.

[2.40] R.M. Salinas, J.A.C. Velasco, M.A. A. Olivos, J.L.M. de la Cruz, J.C.S. Ochoa, "Accurate Modeling of CO_2 Solubility in Ionic Liquids Using a Cubic EoS", Ind. Eng. Chem. Res. 52 (2013) 7593-7601.

[2.41] A. Wyczesany, “Calculation of vapor-liquid-liquid Equilibria at atmospheric and high pressures”, Ind. Eng. Chem. Res. 53 (2014) 2509-2519.

[2.42] H. Cho, J.H. Yim, J.S. Lim, “Measurement of VLE data of carbon dioxide (CO_2) + methyl iodide (CH_3I) system for the direct synthesis of dimethyl carbonate using supercritical CO_2 and methanol”, J. Supercrit. Fluids, 81 (2013) 7-14.

[2.43] M.G.A. Quevedo, L.A.G. Luna, O.E. Solis., J.A.P. Pimientac, “Vapor-liquid equilibrium for the ternary carbon dioxide-ethanol-nonane and decane systems”, Fluid Phase Equilib. 338 (2013) 30-36.

[2.44] L. Pereira, P.G. dos Santos, A.P. Scheer, P.M. Ndiaye, M.L. Corazza, “High pressure phase equilibrium measurements for binary systems CO_2 + 1-pentanol and CO_2 + 1-hexanol”, J. Supercrit. Fluids, 88 (2014) 38-45.

[2.45] M.V. Brandalize, P.S. Gaschi, M.R. Mafra, L.P. Ramos, M.L. Corazz, “High-pressure phase equilibrium measurements and thermodynamic modeling for the systems involving CO_2, ethyl esters (oleate, stearate, palmitate) and acetone”, Chem. Eng. Res. Des. 92 (2014) 1814-1825.

[2.46] P.F. Arce, P.A. Robles, T.A. Graber, M. Aznar, Modeling of high-pressure vapor-liquid equilibrium in ionic liquids + gas systems using the PRSV equation of state, Fluid Phase Equilib. 295 (2010) 9-16.

[2.47] S.A. Kim, J.S. Lim, J.W. Kang, Isothermal Vapor-liquid equilibria for the binary system of carbon dioxide (CO_2) + 1,1,1,2,3,3,3-heptafluoropropane (R-227ea), J. Chem. Eng. Data, 55 (2010) 4999-5003.

[2.48] M.K. Hsieh, S.T. Lin, Effect of mixing rule boundary conditions on high pressure (liquid + liquid) equilibrium prediction, J. Chem. Thermodyn. 47 (2012) 33-41.

Chapter 3

[3.1] J.M. Prausnitz, R.N. Lichtenthaler, E.G. de Azevedo, “Molecular thermodynamics of fluid-phase equilibria”, Prentice Hall PTR, 3rd ed, 1999.

[3.2] J.W. Tester, M. Modell, :Thermodynamics and its applications”, Prentice Hall PTR, 3rd ed, 1997.

[3.3] J.M. Smith, H.C. Van Ness, M.M. Abbott, “Introduction to chemical engineering thermodynamics”, McGraw-Hill, 2005.

Chapter 4

[4.1] D.Y. Peng, D.B. Robinson, “A new two-constant equation of state”, Ind. Eng. Chem. Fundam. 15 (1976) 59-64.

[4.2] H. Orbey, S.I. Sandler, “Modeling Vapor–Liquid Equilibria, Cubic Equations of State and their Mixing Rules”, Cambridge University Press, Cambridge, NY, 1998.

[4.3] S. Sandler, Chemical, "biochemical and engineering thermodynamics", John Wiley & Sons, 4th ed, 2006.

[4.4] H. Renon, J.M. Prausnitz, "Local compositions in thermodynamic excess functions for liquid mixtures", AIChE J. 14 (1968) 135-144.

[4.5] T.F. Edgar, D.M. Mimmelblau, L.S. Lasdon, "Optimization of chemical processes", McGraw-Hill, 2nd ed, 2001.

[4.6] B.E. Poling, J.M. Prausnitz, J.P. O'Connell, "The properties of Gases and liquids", McGraw Hill, 5th ed, 2007.

[4.7] H. Knapp, R. Döring, L. Oellrich, Plöcker, J.M. Prausnitz, "Vapor-Liquid Equilibria for mixtures of low boiling substances, Chemistry Data Series", vol. VI, DECHEMA, 1982.

[4.8] G.H. Zenn, L.I. Dana, "Liquid-vapor equilibrium compositions of carbon dioxide-oxygen-nitrogen mixtures", Chem. Eng. Prog. Symp. Ser. 59 (1963) 36-41.

[4.9] I.M. Al-Wakeel, "Experimentelle und analytische Bestimm ung von binaren und ternaren Dampf-Flussig-Gleichgewichtsdaten der Stoffe Difluordichlormethan-Kohlendioxyd-Stickstoff im Bereich hoher Drucke und tiefer Temperaturen", PhD Thesis, Technische Universitat Berlin, 1976.

[4.10] G.I. Kaminishi, T. Toriumi, "Gas-liquid equilibrium under high pressures. VI. Vapor-liquid phase equilibrium in the CO_2-H_2, CO_2-N_2, and CO_2-O_2 systems", Kogyo Kagaku Zasshi, 69 (1966) 175-178.

[4.11] S.C. Mraw, S.-C. Hwang, R. Kobayashi, "Vapor-liquid equilibrium of the methane-carbon dioxide system at low temperatures", J. Chem. Eng. Data, 23 (1978) 135-139.

[4.12] J. Davalos, W.R. Anderson, R.E. Phelps, A.J. Kidnay, "Liquid-vapor equilibria at 250.00.deg.K for systems containing methane, ethane, and carbon dioxide", J. Chem. Eng. Data 21 (1976) 81-84.

[4.13] C. Hsi, B.C.-Y. Lu, "Vapor-liquid equilibria in the methane-ethylene-ethane system", Can. J. Chem. Eng. 49 (1971) 140-143.

[4.14] R.C. Miller, A.J. Kidnay, M.J. Hiza, "Liquid + vapor equilibria in methane + ethene and in methane + ethane from 150.00 to 190.00 K", J. Chem. Thermodyn. 9 (1977) 167-177.

[4.15] H. Sagara, Y. Arai, S. Saito, "Vapor-liquid equilibria of binary and ternary systems containing hydrogen and light hydrocarbons", J. Chem. Eng. Japan 5 (1972) 339-348.

[4.16] H. Kalra, H.-J. NG, R.D. Miranda, D.B. Robinson, "Equilibrium phase properties of the nitrogen-isobutane system", J. Chem. Eng. Data 23 (1978) 321-324.

[4.17] L. Grauso, A. Fredenslund, J. Mollerup, "Vapour-liquid equilibrium data for the systems C_2H_6 + N_2, C_2H_4 + N_2, C_3H_8 + N_2, and C_3H_6 + N_2", Fluid Phase Equilib. 1 (1977) 13-26.

[4.18] M. Yorizane, S. Yoshimura, H. Masuoka, A. Toyama, “Low temperature vapour-liquid equilibria of hydrogen-containing binaries”, Proc. 1st Int. Cryog. Eng. Conf. (1968) 57-62.

[4.19] F.A. Steckel, N.M. Zinn, “Investigation of the liquid-vapor phase behavior of the system methane-nitrogen–hydrogen”. Zurnal Chimiceskoj Promyslennosti, 16 (1939) 24-28.

Chapter 5

[5.1] D. Hendry, A. Miller, N. Wilkinson, M. Wickramathilaka, R. Espanani, W. Jacoby, “Exploration of high pressure equilibrium separations of nitrogen and carbon dioxide”. Journal of CO_2 Utilization 3-4 (2013) 37-43.

VITA

Reza Espanani was born and grew up in Rasht, Iran and graduated from Shahid Beheshti High School in 1992. He then attended Isfahan University of Technology and in 1997 earned a B.S. in Chemical Engineering with an emphasis in petrochemical industries. As an undergraduate, Reza spent internship during summer 1996 at Fiber Intermediate Products Co. in Isfahan, Iran as an engineer.

He continued his studies as a graduate student at Tarbiat Modares University in Tehran, Iran and earned his M.S. in Chemical Engineering with an emphasis in thermodynamics and kinetics in 2002. His paper about vapor-liquid equilibria of polymer mixtures was the hot paper of The J. Chemical Thermodynamics in Oct. to Dec. 2004. After graduation, Reza worked at Fajr Petrochemical Co. in Mahshahr (PETE ZONE), Iran. There, he worked as an engineer in water treatment and air separation units for two years, and later as a senior process engineer until 2010.

In December 2011, Reza flew to USA and started his Ph.D. in Bioengineering at University of Missouri in January 2012. He earned his Ph.D. in Bioengineering with an emphasis in bioprocess in 2016. His research includes biomass processing with supercritical water, thermodynamic modeling and separation of gaseous mixtures. He also worked as a research assistant and teaching assistant during the Ph.D. program. Reza succeeded in introducing a new dimensionless parameter, Espanani number (Es), and a new method for separation of N_2/CO_2 mixture.

As a process engineer, Reza has passed professional courses in energy management, advanced water treatment, pumps, compressors, and turbines.